Wang, Chui-Lin

COULOMB INTERACTIONS AND SOLITON MODEL DYNAMICS IN QUASI-ONE-DIMENSIONAL SYSTEMS

City University of New York PH.D. 1987

PLEASE NOTE:

In all cases this material has been filmed in the best possible way from the available copy. Problems encountered with this document have been identified here with a check mark ✓.

1. Glossy photographs or pages _____
2. Colored illustrations, paper or print _____
3. Photographs with dark background _____
4. Illustrations are poor copy _____
5. Pages with black marks, not original copy _____
6. Print shows through as there is text on both sides of page _____
7. Indistinct, broken or small print on several pages ✓
8. Print exceeds margin requirements _____
9. Tightly bound copy with print lost in spine _____
10. Computer printout pages with indistinct print _____
11. Page(s) _____ lacking when material received, and not available from school or author.
12. Page(s) _____ seem to be missing in numbering only as text follows.
13. Two pages numbered _____. Text follows.
14. Curling and wrinkled pages _____
15. Dissertation contains pages with print at a slant, filmed as received ✓
16. Other _____

_____

_____

University
Microfilms
International

COULOMB INTERACTIONS AND SOLITON MODEL DYNAMICS IN QUASI-ONE-DIMENSIONAL SYSTEMS

by

Chui-Lin Wang

A dissertation submitted to the Graduate Faculty in Physics
in partial fulfillment of the requirements for the degree of
Doctor of Philosophy, The City University of New York.

1987

This manuscript has been read and accepted for the Graduate Faculty in Physics in satisfaction of the dissertation requirement for the degree of Doctor of Philosophy.

October 16, 1986

Date

Melvin Lax

Chairman of Examining Committee

Oct 20, 1986

Date

Executive Officer

Supervisory Committee

The City University of New York

ABSTRACT

COULOMB INTERACTIONS
AND SOLITON MODEL DYNAMICS
IN QUASI-ONE-DIMENSIONAL SYSTEMS

by

Chui-Lin Wang

Advisors: Professor Frank Martino and Professor Melvin Lax

The Su-Schrieffer-Heeger (SSH) soliton model and its continuum version, the Takayama-Lin-liu-Maki (TLM) model, are presented and their solutions for both the dimerized ground states and the soliton excited states are discussed. The dynamical effects of the electron-electron Coulomb interaction in degenerate systems are studied by using the SSH-extended Hubbard model. We find from numerical simulation that two possible states may be photogenerated depending on the energy gained by the system. If the system energy is higher than a critical value, soliton-antisoliton pairs are photogenerated and are free to separate, leaving behind a central breather mode. If the system energy is lower than the critical value, the soliton-antisoliton pairs will bind and form a different central

oscillation: an exciton-breather. The critical energy is slightly above the soliton pair creation energy. We interpret this exciton-breather to be the origin of the observed infrared activity "pinning" mode at 500 cm^{-1} in *trans*-polyacetylene, and the cause of the disappearance of the photoconductivity at low temperature.

Nondegenerate conjugated polymers are also studied by means of a modified SSH-type model Hamiltonian. We present numerical solutions representing a bipolaron-breather mode, which oscillates between two stages (a kink-antikink pair and a bound polaron pair). We show that the creation of such a bipolaron can be energetically favorable in the case of either doping or photoexcitation. Our results compare well with the experimental photoluminescence spectrum of *cis*-$(CH)_x$.

Acknowledgment

It is a great pleasure to acknowledge my deep indebtedness to Prof. Frank Martino and Prof. Melvin Lax for their continued support, encouragement, instruction, and patient guidance during the course of this research.

I am extremely grateful to Prof. Zhao Bin Su for his collaboration and contribution to the bipolaron problem. I also benefited from discussions with Prof. Lu Yu.

I would like to thank all the members of the Lax research group for their encouragement and helpful discussions. They are Dr. Shirish Chitanvis, Dr. Wei Cai, Dr. M. Cristina Marchetti, Dr. Ya Qiu Jin, Mr. Boris Yudanin, Mr. Ting Fang Zheng, Mr. Feng Lin, and Mr. Buu Kao Chen. I also would like to thank Mrs. Evelyne Rosenstock for her encouragement.

It is my pleasure to thank the faculty of the Physics Department for its instruction and help, especially Profs. J. Birman, C. Yuan, H. Z. Cummins, N. Tzoar, K. Rubin, T. Boyer, and M. Sarachik. Special thanks also to my former advisor, Prof. H. Y. Tsu of the High Energy Institute of Academia Sinica.

I heartily thank Profs. T. D. Lee and N. P. Chang for their tremendous efforts to promote academic exchange between China and United States, which

enabled me to come to City College of New York to participate in the Ph. D. program in Physics.

This work was supported by the International foundation for Cancer Research and a grant from the U. S. Department of Energy (Office of Basic Energy Science, the Division of Material Sciences).

Dedication

I dedicate this thesis to my late father who died 2 months after my arrival in the U. S., as well as to my beloved mother for taking such good care of my two children in China during my stay here. I dedicate this thesis also to my wonderful wife, Xiao Xin, for her understanding of the many hours spent on this work both days and nights.

Table of Contents

Figure List

CHAPTER I

Introduction

In the past several years, quasi-one-dimensional organic polymers have been regarded as a new class of electronic materials[1-4] that have the properties of semiconductors or metals, depending upon doping mechanism or photoinduction. Recent progress[5,6] in polyacetylene and related conjugated polymers indicate that the electrical properties of this new class of organic conductors can be systematically varied through chemical or electrochemical doping to span the full range from insulator to semiconductor to metal. Thus they have potential use in a number of areas of future technology. Scientists believe[7] that they might be useful in such applications as (1) the replacement of increasingly scarce conventional conductors by synthetic metals; (2) the development of lightweight, high-energy-density batteries; and (3) low-cost solar photovoltaic materials.

The proposal[8,9,10,11] that kink solitons play a central role in determining the electronic properties of *trans*-$(CH)_x$ (polyacetylene) has provoked considerable theoretical and experimental study of the system. To provide a qualitative description of many experiments that have been performed on $(CH)_x$, Su, Shrieffer, and Heeger[8] proposed a simple and elegant model Hamiltonian (SSH model) in terms of coupled electrons and phonons which successfully interpreted

the magnetic, optical, transport, and electronic properties of pristine, photoinduced, and light-doped *trans*-polyacetylene. More recently, Takayama, Lin-Liu, and Maki[12] (TLM) took a continuum limit of the SSH discrete model and found a remarkable analytic solution for solitons. From this work most of the physical properties of solitons can be understood both quantitatively and qualitatively.

The research reported in this thesis extends the SSH model Hamiltonian to include the electron-electron Coulomb interaction, which is absent from the original model, and studies the dynamical properties of the system by means of numerical simulation. It is found that a photogenerated exciton-breather state exists in *trans*-$(CH)_x$, which can explain the observed infrared absorption peak[13] at about 500 cm^{-1}, as well as its temperature dependence[14,15] and associated photoconductivity.

The SSH model Hamiltonian was also modified to cover nearly degenerate ground state polymers. A bipolaron-breather mode was discovered, explaining the observed photoluminescence peak at $1.9eV$ in *cis*-$(CH)_x$.[16] The main results of this thesis have been published in Physical Review B.[17,18]

In the current work, we first review the general properties, physical concepts, and analytical solutions of the soliton model before presenting numerical results. In particular, we discuss the structural formulas of $(CH)_x$ and polythiophene, Peierls instability, and elemental excitations, such as solitons, polarons, bipolarons, excitons, and breathers, all of which have special characteristics in quasi-one-dimensional polymers, in this chapter.

1. Structure of Polyacetylene

Polyacetylene $(CH)_x$, a prototypical conducting polymer, is the simplest known conjugated polymer. It consists of weakly coupled chains of CH groups. The electronic structure of $(CH)_x$ can be described as follows: Each carbon has four valence electrons, three of which are in sp^2 hybridized orbitals and form σ-type bonds; two of the σ-type bonds are links in the backbones, whereas the third forms a bond with the hydrogen side group.[19] The remaining valence electron is in a $2p_z$ orbital and forms a π-type bond in which the charge density is perpendicular to the plane of the molecule. In the notation of band spectroscopists. σ refers to states with $m=0$, and π refers to states with $m=\pm 1$, where m is the quantum number of the component of angular momentum along the axis of the molecule.

In an energy band description, the σ electrons form low-lying completely filled bands (Fig. 1). Excitations from these bands cost an energy of order 10 eV, which is large compared to phonon and soliton energies, and hence we can treat the σ electrons in the adiabatic approximation. In this sense, the σ electrons can be considered as core electrons which contribute an effective interaction between ions. Similarly, the unoccupied antibonding σ orbitals lie at such a high energy that they can be ignored. Thus only one π electron per carbon needs to be treated explicitly. Because π orbitals on neighboring carbon atoms overlap substantially, a broad π band is formed and π electrons move preferentially along the chain. Because hopping between neighbor atoms depends on the orbital overlap, the probability of such hops depends strongly on the dis-

tance between neighboring sites. Note further that hopping between chains is strongly suppressed, and that this anisotropy renders such materials quasi-one-dimensional.

The three σ bonds make a 120° bond angle with each other. This leads to two possible arrangements of the carbon atoms, *trans*-polyacetylene, and *cis*-polyacetylene, with two and four CH monomers per unit cell. The schematic representations of *trans*-$(CH)_x$ and *cis*-$(CH)_x$ are shown in Fig. 2 and Fig. 3 respectively. Experimentally, *cis*-polyacetylene is synthesized by the method of Ito, Shirakawa, and Iketa,[20] and *trans*-polyacetylene is subsequently isomerized by heating *cis*-polyacetylene to 180°C for about 5 min. The new technique for synthesizing of polyacetylene involves applying a stress to the prepolymer film during the thermal conversion. Using this technique, it is possible to obtain highly crystalline films of $(CH)_x$ which are close to the theoretical density and have the $(CH)_x$ chain oriented parallel to the direction of stress. These highly ordered films of $(CH)_x$ are of great importance in resolving the problems associated with the characterization of polyacetylene. It is worthwhile to point out that some defects can be induced during isomerization. These defects are neutral solitons, which are mismatches (domain walls) between two different bond arrangements.

2. Peierls Instability

For simplicity, we take *trans*-polyacetylene as a typical example to discuss some basic concepts here. As mentioned before, each carbon has one electron in the π orbital, which can accommodate two electrons of opposite spin. Thus

the π band is only half filled. If the bond lengths in pure *trans*-polyacetylene were uniform (undimerized), the polymer would be a quasi-one-dimensional metal. But such a system is unstable with respect to the distortion induced by dimerization. This phenomenon is well known as the Peierls instability.

In his *Quantum Theory of Solids*, Peierls pointed out that for a one-dimensional metal with a partly filled band the regular chain structure will never be stable, since a distortion will always open a gap at or near the Fermi surface, and the system energy is thereby lowered. The argument can be illustrated as follows. If the atoms of a linear chain are equidistant, with a lattice constant a, the basic cell in reciprocal space is in the interval $-\frac{\pi}{a} < k \leqslant \frac{\pi}{a}$. Now assume the chain is distorted by moving every rth atom a given distance in a given direction. This immediately reduces the translational symmetry; the basic cell now contains r atoms and the cell in reciprocal space is in the interval $-\frac{\pi}{ra} < k \leqslant \frac{\pi}{ra}$. The energy curve $E(k)$ without the distortion, plotted in Fig. 4a, will be modified, as in Fig. 4b, which has gaps at $k_\rho = \rho\frac{\pi}{ra}$, $(\rho = 1,2,...,r-1)$. These gaps are called Peierls gaps. The size of the gap can be calculated by perturbation theory for nearly degenerate states. If such a break occurs exactly or very nearly at the Fermi surface, then the occupied states are lowered and the unoccupied states are raised, so that the electronic energy of the chains is reduced. Thus for a one-dimensional metal with a partly filled band, the equidistant structure will never be stable, because a distortion with a suitable r will always create a gap at or near the Fermi surface. In the case of polyacetylene, each CH group has one π electron; allowing for

spin, the Fermi surface ends at $k = \frac{\pi}{2a}$, and thus $r = 2$, so that every second atom is displaced, and the chain is dimerized. In the perfectly dimerized case, the lattice displacement u_n can expressed as $u_n = (-1)^{n-1}u$, where u is the displacement magnitude. Because dimerization raises the elastic energy between ions, there is a competition between the electron energy and the elastic energy of the system. This competition determines the dimerization distortion u_0 which minimizes the total energy of the system. In *trans*-polyacetylene, the experimental value of u_0 is equal to 0.03Å ± 0.01Å.

3. Degenerate Ground States and Concept of Solitons

If the chain is undimerized, the *trans* polymer has reflection symmetry with respect to a plane which passes through a carbon site and is perpendicular to the $(CH)_x$ chain. Dimerization breaks this symmetry spontaneously. This spontaneous symmetry breaking leads to degenerate vacua (ground states) and soliton formation. The soliton is a topological excited state which acts as a boundary between domains having different vacua. In *trans*-polyacetylene there is no energetic difference between two possible dimerizations. Each even site moves to the right, resulting in short-long-short bond sequences (corresponding to $u > 0$, A-phase), or it moves to the left, resulting in long-short-long bond sequences ($u < 0$, B-phase). In the chemical language, short and long bonds are called "double" and "single" bonds respectively. Solitons are domain walls connecting these two different ground state phases. As discussed, solitons are basic electronic excitations in degenerate ground state systems.

The concept of a solitary wave was introduced to science over a century

ago by Scott-Russell.[21] who observed "a rounded, smooth and well defined heap of water", which was "some thirty feet long and a foot to a foot and a half in height", and move "at a rate of eight or nine miles an hour", "assuming the form of a large solitary elevation". This solitary wave kept its shape and speed for one or two miles before disappearing in the windings of the channel.

The classic concept of a soliton is defined as a solitary wave solution of a nonlinear and dispersive wavefunction which asymptotically preserves its shape and velocity upon collision with other solitary waves.[22] A solitary wave $f(\zeta)$, where $\zeta = x - ut$ and u is the velocity, is a localized traveling wave, whose transition from one constant asymptotic state (in which $\zeta \rightarrow -\infty$) to another ($\zeta \rightarrow \infty$) is essentially localized in ζ. There are two types of solitary waves. A "pulse-like" solitary wave has the same asymptotic values at $\zeta = -\infty$ and $\zeta = \infty$, whereas a "kink-like" solitary wave has different asymptotic values at $\zeta = -\infty$ and $\zeta = \infty$. Solitary waves can be formed only in dispersion, nonlinearity conditions. The effect of introducing dispersion without nonlinearity is to destroy the possibility of solitary waves because their various Fourier components of any initial condition will propagate at different velocities. On the other hand, introducing nonlinearity without dispersion again makes solitary waves impossible because the pulse energy is continually injected (via harmonic generation) into higher frequency modes. The solitary wave is qualitatively understood as representing a balance between the contrasting effects of nonlinearity and dispersion.[23] To physicists, the most interesting solutions are the sine-Gorden equation and the ϕ^4 equation, which have analytical soliton (kink) solutions. These nonlinear phenomena appear to be common to all fields of phy-

sics, and have attracted many physicists to explore them. In polyacetylene, the two-fold degeneracy gives rise to the possibility of existing a kink-like soliton excitation (domain wall) connecting the two different phases. We will discuss it in detail in section 1.5.

4. Nearly Degenerate Polymers

As mentioned above, the two-fold degeneracy of the ground state of *trans*-polyacetylene is responsible for symmetry breaking in the system and leads to the formation of soliton-like excitations. Since ground state degeneracy is not a general property of quasi-one-dimensional conducting polymers, however, theoretical and experimental studies of the large class of nondegenerate conjugate polymers are necessary and interesting. An important subclass of these are polymers having nearly degenerate ground state structure. Some examples are *cis*-$(CH)_x$, polythiophene, polypyrrole, and polyparaphelene, of which *cis*-$(CH)_x$ has the simplest structure. Examining the chemical structures in Fig. 3, the configuration of *cis*-$(CH)_x$ is clearly different from that of *trans*-$(CH)_x$. There are two types of bonds in *cis*-$(CH)_x$. The type-I bonds are those parallel to the chain axis and the type-II bonds make an angle of about $\pi/3$ with the chain. Dimerization can thus occur in two different ways. If dimerization results in type-I bonds becoming short and type-II bonds becoming long, the configuration is called *cis*-transoid. On the other hand, the configuration with long type-I bonds and short type-II bonds is called *trans*-cisoid. From experiment, the *cis*-transoid configuration has lower energy than the *trans*-cisoid one, so the former is referred to as a ground state configuration and the latter is referred to as a metastable state configuration. Because of the tiny energy

difference between the two states, the system is called a nearly degenerate polymer.

In reality, experimentalists prefer to use polythiophene instead of *cis*-$(CH)_x$. Polythiophene is highly crystalline, with a simple backbone geometry similar to that of *cis*-$(CH)_x$. Its structure is stabilized by the sulfur atoms, whose covalent bonds to neighboring carbons form the heterocycle, and which only interact weakly with the π electrons of the backbone. Polythiophene may be thought of as a pseudopolyne.[24]

Because the sulfur atoms have little affect on the π band structure but stabilize the backbone structure, we can redraw the polythiophene backbone structure with the intentional omission of the sulfur heteroatom (Fig. 6). The resulting structure is that of an sp^2p_z polyne chain consisting of four carbon all-trans segments which are linked through a *cis*-like unit[25] that is analogue to *cis*-$(CH)_x$. Obviously the ground state in such a structure is not degenerate, but it is more nearly degenerate than that of *cis*-$(CH)_x$. This means that the energy difference between two configurations per carbon $\frac{\Delta E}{N}$ in polythiophene is greater than zero, as in *trans*-polyacetylene, but less than that of *cis*-$(CH)_x$.

5. Excitation in Quasi-one-dimensional Polymers.

The excitations in one-dimensional semiconductor polymers are quite different from traditional three-dimensional semiconductors. In the three-dimensional case, each atom has at least four or more than four-fold coordination and connects to its neighbors through covalent bonds. This leads to a rela-

tively rigid structure. In such systems the electronic excitations lead to the conventional concepts of electrons and holes as dominant excitations. However, in the quasi-one-dimensional case, which has only two-fold coordination, the structures are much less rigid, and therefore they are generally more susceptible to structural distortions from electronic excitations. As a result, the dominant electronic excitations inherently cause chain deformations through electron-phonon interaction. On the other hand, such chain distortions also affect electronic excitation structures. The reciprocating interaction must be self-consistent at each instant of time, and a requirement that makes the problem interesting and productive. (More than 2000 papers have been devoted to $(CH)_x$ since the SSH model was proposed).

Progress has been made in the case of *trans*-polyacetylene to the extent that an insulating polymer can be made to conduct by partial oxidation or reduction, which removes or adds enough electrons to facilitate conductivity. Polyacetylene is a π-bonded unsaturated polymer that can be readily oxidized or reduced and that forms a cation or an anion rather than undergoing other chemistry. In $(CH)_x$, the π electrons can be removed relatively easily to give a polymeric cation without breaking the σ bonds, which are primarily responsible for holding the polymer together.[26] The principles learned from polyacetylene have been successfully applied to an increasingly large number of other polymer systems. Conductivity is usually achieved by oxidation, but several polymer systems can also be reduced to produce conducting polymeric anions. It should be pointed out that photoexcitation causes conductivity as well and is therefore considered an important tool for investigation of mechanism of excitation.

Photogeneration provides us a "clean" means to examine the nature of quasi-particles, which is not the case for doping, in which the interaction of the electronic charges with the dopant ions can significantly affect the system energy.

The generation of charge carriers in nonintrinsically conducting polymers is not analogous to that in classical inorganic semiconductors, such as silicon or germanium. In inorganic semiconductors, such as silicon, the doping process involves removing a neutral atom of silicon and substituting for it another neutral atom, boron, for example, which fits into the lattice vacancy. Silicon has four valence electrons, but boron has only three; substituting the latter for the former leads to empty energy levels associated with the boron atoms which appear slightly above the top of the silicon valence band. Electrons can be thermally transferred from the silicon to the boron levels, producing holes in the silicon valence band and giving rise to unpaired electrons, which can be detected by electron spin resonance (ESR) techniques.

The situation is very different when it comes to generating of charge carriers by doping conjugated polymers. Doping polymers is more appropriately seen as a chemical modification that strongly perturbs the polymers. This is because of the dopant's large physical size, which does not allow it to fit substitutionally into the polymer lattice. The extensive charge transfer between the polymer chain and the dopant causes both to become ionic which in turn leads to changes in the chain's geometry. After doping, the electronic energy levels associated with the lattice distortion are removed from the top of the valence band and the bottom of the conduction band and brought into the gap. This process also changes the valence and conduction band structures.

6. Polarons

A polaron is defined as an elemental excitation entity of an extra electron (or a hole) plus its induced lattice deformation. Conventional discussions of polarons concentrate on adding a single electron to a deformable crystal, creating a single localized electronic level just below the conduction band. In our case, however, we must explicitly include the valence band electron effects, which makes these polarons rather complicated. Polarons can be produced in both degenerate and nearly degenerate ground state quasi-one-dimensional polymers. To describe the physics of polaronic excitation precisely, we introduce an ordeian parameter, a staggered lattice displacement, which is related to the real displacement by

$$\eta_n = (-1)^{n-1} u_n \ . \tag{1.1}$$

In the perfectly dimerized state (ground state with no polaron), η_n is equal to a constant u_0 (represented as straight line in Fig. 8), and all the valence bands are occupied whereas all the conduction bands are empty. If an electron is removed from the top of the valence band or added to the bottom of the conduction band, it is energetically favorable for the electron to move in a spatially localized level accompanied by a local distortion in the dimerized polymers. This lattice distortion involves changes in the band structure which increase the electronic energy. However, this increase in electronic energy is more than compensated for by the decline in elastic energy due to distorted forms of the chain --- resulting a net lower energy. Calculations from the TLM continuum model have shown that in *trans*-$(CH)_x$ the polaron creation energy is

equal to

$$E_p = \frac{2\sqrt{2}}{\pi} \Delta_0 , \tag{1.2}$$

where Δ_0 is a gap parameter equal to half of the Peierls gap energy E_g. Removing an electron from the bottom of the valence band or adding an electron to the top of the conduction band causes the system energy to rise by Δ_0. In Fig. 9, the curve of the order parameter η_n has a dip for the distorted lattice configuration forming a polaron. At the same time, two localized states, the bonding state ψ_+ and the antibonding state ψ_- are split off from the conduction and valence band edges. A positive polaron occurs when ψ_+ is occupied by one electron and ψ_- is unoccupied, whereas a negative polaron corresponds to the case of two electrons in ψ_+ and one electron in ψ_-.

7. Soliton-Antisoliton Pairs

In *trans*-$(CH)_x$, if a second electron is removed (added) from (to) the chain containing a positive (negative) polaron, calculations show that it is energetically favorable to remove (add) it from (to) the polaron to create a soliton-antisoliton pair rather than a second polaron. The creation energy of a soliton-antisoliton pair can be calculated from TLM continuum model,

$$E_{s\bar{s}} = \frac{4}{\pi} \Delta_0 . \tag{1.3}$$

which is less than the creation energy of two polarons $\frac{4\sqrt{2}}{\pi} \Delta_0$. In the process of formation of soliton-antisoliton pairs, the depth and the width of the small polaron dip in Fig. 9 become larger, and finally a distorted configuration will be

reached which connects the A-phase to the B-phase (soliton), and then the B-phase to the A-phase (antisoliton). See Fig. 10(a). At the same time, the two localized states ψ_+ and ψ_- in Fig. 9 move towards to the center of the gap, and finally become mid-gap states as the soliton and antisoliton are completely separated (see Fig. 10(c)-(e)).

From the above analysis, we can see that associated with soliton-antisoliton pairs are two mid-gap localized states whose spin degeneracy ensures that they can accommodate four electrons. Each of mid-gap state is associated with a single soliton and is formed from both the valence and conduction bands, each of which contributes one-half a state for each spin. the presence of a soliton effectively deprives the valence band of a total of one electron. (Precisely, one should say that two electrons are taken from the valence band during the creation of a soliton-antisoliton pair). If there is no doping involved in the process and the missing electron occupies the mid-gap state, the soliton is neutral. Because that the valence band remains spin paired while the electron in the mid-gap state is spin unpaired, a neutral soliton always has spin one-half. Removing the unpaired electron from the mid-gap state or adding a second electron to the mid-gap state results in the soliton becoming positively or negatively charged with a paired spin. Therefore, a charged soliton has spin zero. These novel spin-charge relations can be summarized as

$$Q_0 = 0\,, \qquad S_0 = \frac{1}{2}$$

$$Q_\pm = \pm e\,, \qquad S_\pm = 0\,. \tag{1.4}$$

Soliton-antisoliton pairs can also be produced by photoexcitations. Such photogeneration can occur in two different ways, direct process and indirect process. If the energy of an incident photon $\hbar\omega$ is equal to or greater than the gap energy E_g, an electron hole pair is generated before the formation of a soliton-antisoliton pair through a multi-phonon process (lattice relaxation). This is called an "indirect" process. If $\hbar\omega \geqslant E_{s\bar{s}}$, a soliton-antisoliton pair can also be directly photogenerated. From symmetry and parity considerations, photogeneration of neutral soliton-antisoliton pairs is forbidden in the direct process, whereas they may occur in the indirect process although with a small branch ratio (the rate of photoproduced neutral pairs to charged pairs) of 10^{-2}.[27,28,29] Detailed analysis of photogenerated $S\bar{S}$ pairs will be provided in the Chapter IV.

The soliton-antisoliton pairs generated in such a system can be freely separated. Because the two phases connected by a soliton (domain wall) have the same energy, solitons can move freely along the chain without expenditure of energy. This, in conjunction with the soliton's small mass (order of the electron mass), makes the soliton highly mobile and allows them to be charge carriers. which explains the system's conductivity after doping and photoexcitation.

8. Bipolarons

The situation is different in systems having nearly degenerate ground states. Although soliton-antisoliton pairs are free to separate in *trans*-$(CH)_x$, they are confined[30] in nearly degenerate polymers. Soliton-antisoliton pairs in *cis*-$(CH)_x$, to cite one example, connect the *cis*-transoid configuration through

the *trans*-cisoid back to the *cis*-transoid configuration. Separation of the pair therefore involves a higher energy configuration that costs extra energy. This confined soliton-antisoliton pair is called a bipolaron. The lattice configuration and electronic structure of neutral and charged bipolarons are presented in Fig. 11.

Charged bipolarons are spinless and highly mobile, and can be considered analogous to the BCS theory of superconductivity's cooper pairs, which consist of electron pairs coupled together through a phonon. These mobile bipolarons are the charge carriers in nearly degenerate systems and are responsible for the conductivity mechanism.

Recently, Brazovski, Kirova, and Yakovenko[31] have shown that such spinless bipolarons could exhibit Bose condensation in a novel charged superfluid state. Thus, investigation of such charged carriers in nearly degenerate conjugated polymers is of special importance.

9. Excitons

The description to the present has not taken into consideration the electron-electron Coulomb interaction. Both the theoretical calculations and experimental results indicate that in the presence of the Coulomb interaction the photogenerated solitons are no longer free to separate but form instead a bound excitonic complex.

Usually, in the conventional solid state, an exciton is an electronic excitation entity in nonmetallic solids consisting of an excited electron and a hole that

has left behind, They are bound by the Coulomb interaction into a hydrogen-like state. A loosely bound exciton with a radius much larger than the lattice constant is called a Wannier exciton, whereas one that is tightly bound is called a Frenkel exciton.

The "excitons" in a quasi-one-dimensional system are somewhat different from those in conventional solid states. When we refer to excitons in such a system, we also include the effect of the lattice distortions created by the bound electron-hole pair. An exciton in *trans*-$(CH)_x$ is a state in which oppositely charged solitons are bound by the Coulomb interaction; it is like a Wannier exciton. Alternately, the excitonic complex in *trans*-$(CH)_x$ can be treated as a bound pair of two oppositely charged polarons --- the proper nomenclature might be "polaron-exciton".

10. Breathers

A breather is a particle-like non-dispersive envelope with internal oscillatory motion, which represents an oscillatory standing wave solution of nonlinear wave equations. If a system has energy slightly greater than the creation energy of a particular low-lying excited state, the system will have kinetic energy and might oscillate around that low-lying excited state. There are two types of breather modes in *trans*-$(CH)_x$: a central breather mode, which is a separated soliton-antisoliton pair with a breather oscillated left behind; and an exciton breather mode, which is an exciton complex with a breather oscillating around it. In systems where the ground state degeneracy is lifted, the lattice configuration can oscillate around a bipolaron producing a bipolaron breather

mode. Owing to the electron-phonon coupling, the electron structure oscillates with the same frequency as the lattice configuration, which necessarily implies the nonlinearity of the breather phenomenon.

The remaining chapters are organized as follows. Chapter II describes the SSH model, extended Hubbard terms, and the modified SSH model, and discuss the ground state properties in terms of energy spectra and wavefunctions. In Chapter III, the static analytical solutions of solitons, polarons, and bipolarons in the TLM continuum model and their related properties are presented. In Chapter IV, the results of dynamical simulation of photogenerated exciton-breather in *trans*-$(CH)_x$ are compared to experiment. In Chapter V, we study bipolaron dynamics in a system where the ground state degeneracy is lifted, and find that the creation of such a bipolaron can be energetically favorable in the case of either doping or photoexcitation. Finally, the summary and conclusions are in Chapter VI.

CHAPTER II

Discrete Microscopic Model

Our numerical dynamical simulations are based on discrete microscopic soliton models. In this chapter, we discuss the model Hamiltonians, and the properties derived from the models as well.

1. SSH Discrete Model

To begin, we perform a detailed analysis of the model Hamiltonian proposed by Su, Schrieffer, and Heeger (SSH). In this model, interchain electron hybridization is neglected because the bandwidth W of the π electrons ($\approx 10eV$ in *trans*-$(CH)_x$) is large compared to interchain bandwidth $W_\perp$ ($\approx 0.1eV$). This leads to relatively weak interaction coupling, that is, quasi-one-dimensional behavior. The σ electrons are core electrons, which are treated as almost completely localized and are assumed to move adiabatically with the nuclei, forming a backbone. Their chief contribution is to modify the effective phonon potential. The π electrons are treated in a tight binding approximation, In which, each of their orbitals is localized on a particular atom, and their combination is represented as a state running throughout the chain. Because, as described in section 1.1, the π electrons hop preferentially along the chains, only hopping terms in that direction are used in this model. The phonon fields are treated classically, which means that the mean field approximation is used to

replace the phonon field operator by an unquantized c-number parameter, the mean value of the phonon field. There are six degrees of freedom for each CH group, of which three are for the hydrogens. They are neglected, because to first order they are not coupled to neighboring CH groups. The remaining three for carbon are the in-chain displacement u_n from the equilibrium position, which describes the translation of the group n along the symmetry axis (x-axis) of the chain; the displacement in the direction of the hydrogen (y-axis); and the out of plane displacement (z-axis). Since we are interested primarily in the dimerization structure of the polyene, and the latter two displacements have no effects on the changing the difference of the bond lengths between right and left bonds of site n, only x-axis u_n terms are kept in the Hamiltonian. (In calculations of local phonon modes around a soliton, Horovits[32] used all the three displacement parameters and got very good results.) Therefore we are left with only one ionic and one electronic degree of freedom per carbon. The resulting model Hamiltonian can be expressed as two parts: the bare lattice part H_{lat}, which includes the contribution of the core σ electrons, and the electronic part H_{el}, which is the sum of the π electron contribution. Hence,

$$H = H_{el} + H_{lat} \tag{2.1}$$

$$H_{el} = -\sum_{n,n',\sigma} t_{n',n}(c^{\dagger}_{n',\sigma}c_{n,\sigma}+h.c.) \tag{2.2}$$

$$H_{lat} = \frac{M}{2}\sum_{n} \dot{u}_n^2 + V(\{u\}) , \tag{2.3}$$

where $c^{\dagger}_{n,\sigma}(c_{n,\sigma})$ is the creation (annihilation) operator of a π electron with spin σ in the nth CH group, and M is the mass of CH group. It is assumed

that there is no relative motion between the hydrogen and the carbon. Both the hopping matrix $t_{n',n}$ and the lattice potential energy V are the functions of the lattice displacement $\{u\}$. The hopping matrix element $t_{n',n}$ gives the probability amplitude of an electron hopping from site n to n', which depends on the overlap between corresponding orbitals. Since the π electron orbital is exponentially localized, the hopping terms beyond nearest neighbor sites are quite small and can be neglected to the first order. This gives

$$t_{n',n} = 0 \qquad \text{for} \quad |n - n'| \geq 2 . \tag{2.4}$$

For the nearest neighbor term, $t_{n,n+1}$ depends on the distance between the sites n and $n+1$, which has average spacing a (lattice constant), so $t_{n,n+1}$ should be a function of $u_n - u_{n+1}$, where u_n is a bond length parameter. Because u_n is in general very small compared to the lattice constant a ($u_n \sim 0.03$ Å, and $a \sim 1.22$ Å in *trans*-$(CH)_x$), it is sufficient to keep $t_{n,n+1}$ to linear order,

$$t_{n,n+1} = t_0 + \alpha(u_n - u_{n+1}) , \tag{2.5}$$

where t_0 is the hopping matrix element between nearest neighbor sites in the undimerized case, and α is the electron-phonon coupling constant. In a k-space representation, this is just the famous Fröhlich coupling. Because $\alpha > 0$, when $(u_n - u_{n+1}) > 0$ the magnitude of $t_{n,n+1}$ becomes large. Thus, when two sites move closer to each other, the magnitude of probability amplitude for electron hopping rises.

The terms $t_{n,n}$ represent the π electron energy on site n , which might change as neighboring atoms squeeze in on it,[33] and hence it should depend on

the deviation of the lattice constant, Δa. Because in the dimerized system, all the even atoms move in one direction while all the odd atoms move in the opposite direction, this implies that Δa is proportional to $(u_{n-1} - u_{n+1})$. Therefore to the first order $t_{n,n}$ can be expanded as

$$t_{n,n} = \epsilon_0 + \beta (u_{n-1} - u_{n+1}) \tag{2.6}$$

If we define the center of the π band to be the zero of energy, ϵ_0 can be set to zero. The term proportional to β in Eq. (2.6) was ignored by SSH. Since, for the most part, we are interested in states that are approximately dimerized, $u_{n+1} \approx -u_n \approx u_{n-1}$, the factor of $(u_{n+1} - u_{n-1})$ which appears with β is always small compared with the factor of $(u_n - u_{n+1})$ which appears with α in Eq. (2.5). For instance, we shall see in this chapter that in the perfectly dimerized ground states $(u_{n-1} - u_{n+1}) \equiv 0$, whereas in the presence of a soliton $|u_{n-1} - u_{n+1}| \sim \frac{a}{\xi_0} |u_n - u_{n+1}|$, where ξ_0 is the electron correlation length ($\xi_0 \sim 13a$ in *trans*-$(CH)_x$).

The lattice potential energy V can be expanded as

$$V = V_0 + A \sum_n (u_n - u_{n+1}) + \frac{1}{2} K \sum_n (u_n - u_{n+1})^2 + \cdots \tag{2.7}$$

The first term V_0 affects only the origin of energy, so we can set V_0 to zero without loss of generality. The second term is linear in $(u_n - u_{n+1})$. If we expand the lattice displacements about the appropriate equilibrium position, the derivative $\left. \frac{\partial V_{tot}}{\partial (u_n - u_{n+1})} \right|_{u_n = 0}$ should be zero. Noticing that V_{tot} consists of

two parts, an electron part and a lattice part, with the electron part of the potential energy implicitly containing a linear term of $(u_n - u_{n+1})$, due to the electron phonon coupling. This implies that the coefficient A of the linear term in Eq. (2.7) is not an independent physical parameter, but is a Lagrange multiplier determined by the condition

$$\frac{\partial V_{tot}}{\partial(u_n - u_{n+1})}\Bigg|_{\{u_n\}=0} = 0 , \tag{2.8}$$

which can be rewritten as

$$A = -\frac{\partial V_{el}}{\partial(u_n - u_{n+1})}\Bigg|_{\{u_n\}=0} . \tag{2.9}$$

This term is necessary to fix the total length of the chain in the dynamical simulation, because $\sum_n (u_n - u_{n+1}) = u_1 - u_N = \Delta L$, where ΔL is the overall change in the length of the molecule and N is the number of sites. Making use of a quadratic approximation, the SSH analysis ignores the higher order terms.

The coefficient K of the second order term is the effective stiffness constant, which is determined by both the direct ion-ion interactions and the σ electron interactions. The resulting Hamiltonian H_{SSH} can be written as

$$H_{SSH} = -\sum_{n,\sigma} [t_0 + \alpha(u_n - u_{n+1})](c^{\dagger}_{n+1,\sigma} c_{n,\sigma} + h.c.)$$

$$+ \frac{K}{2}\sum_n (u_n - u_{n+1})^2 + \frac{M}{2}\sum_n \dot{u}_n^2 + A\sum_n (u_n - u_{n+1}) , \tag{2.10}$$

where for $(CH)_x$, the parameters entered in the above Hamiltonian are

$$t_0 = 2.5eV,$$

$$\alpha = 4.1eV/\text{ Å},$$

$$K = 21eV/\text{ Å}^2,$$

$$M = 13 \text{ atomic mass unit} = 1.34\times10^{-27}\ eV\cdot sec^2/\text{ Å}^2, \tag{2.11}$$

and

$$A \approx \frac{4\alpha}{\pi}, \tag{2.12}$$

which will be proved in the next section.

This Hamiltonian is based on a one electron theory in which each π electron is treated as an independent particle moving in a well defined effective potential. Because the ionic mass M is very large compared to the electron mass, the motion of the ion is slow. The Born-Oppenheimer (adiabatic) approximation is expected to be hold in this model. Therefore we can separate the equation of motion into two parts, an electron part and a lattice part. Assuming that the lattice distribution is static at any given moment, the equation for electron part can be solved at this moment. Then the electron energy, which is a sum over all the occupied states of the one electron energy, can be regarded as a part of the ion potential energy to solve the equation of motion for the nuclei. This approximation assumes the electrons will require no time to rearrange themselves according to the lattice distribution at each instance, and also assumes there is no electronic transition between two electron states. It has been shown formally by Brazovskii and Dzyaloshinskii[34] that the adiabatic approximation is

valid if $\frac{\hbar\omega_0}{\Delta_0}$ is less less than one, where ω_0 is a typical optical phonon frequency. For $(CH)_x$, $\hbar\omega_0 \sim 1400\ cm^{-1} \sim 0.17eV$ and $\Delta_0 \sim 1.4eV$, so $\frac{\hbar\omega_0}{\Delta_0} \sim 0.12$, and the adiabatic approximation is justified. This approximation will be used to perform our numerical simulations.

2. Ground State Properties

In this section we discuss the properties of the perfectly dimerized ground state. The discussion only involves the static properties, so the kinetic term of H_{SSH} is omitted.

In the perfectly dimerized chain, the lattice chain displacement u_n are constrained to be

$$u_n = (-1)^{n-1} u \ . \tag{2.13}$$

The SSH Hamiltonian of the dimerized case for fixed u becomes

$$H^d = -\sum_{n,\sigma} (t_0 - (-1)^n \ 2\alpha u)(c^{\dagger}_{n+1,\sigma} c_{n,\sigma} + h.c.) + 2NKu^2 \tag{2.14}$$

where N here is the number of CH groups and is chosen to be even. Since each CH group has only one π electron, N is also the number of π electrons. In the case of undimerization ($u = 0$), each unit cell contains one atom, and the wave vector $k = \frac{2\pi}{L} m$, where $m = -\frac{N}{2}, \cdots, 0, \cdots, \frac{N}{2}$ and the molecule length $L = Na$ runs within the first Brillouin zone $(-\frac{\pi}{a}, \frac{\pi}{a}]$.

The electron spectrum in undistorted chains is given by

$$\epsilon_k = -2t_0 \cos ka \ , \qquad -\frac{\pi}{a} < k \leqslant \frac{\pi}{a} \ . \tag{2.15}$$

In the case of dimerization, each unit cell contains two atoms, the hopping potential has a periodicity of $2a$, and the first Brillouin zone is reduced to an interval of $(-\frac{\pi}{2a}, \frac{\pi}{2a}]$. The reduced zone scheme is used to label electron states,

$$c^v_{k,\sigma} = \frac{1}{\sqrt{N}} \sum_n e^{ikan} \ c_{n,\sigma}$$

$$c^c_{k,\sigma} = \frac{1}{\sqrt{N}} \sum_n e^{ikan} \ (-1)^n c_{n,\sigma} \qquad -\frac{\pi}{2a} < k \leqslant \frac{\pi}{2a} \ , \tag{2.16}$$

where $c^v_{k,\sigma}$ ($c^c_{k,\sigma}$) annihilates an electron with wave vector k and spin σ in the valence (conduction) band for zero-order bands ($u = 0$).

The transformation can be inverted into

$$c_{n,\sigma} = \frac{1}{\sqrt{N}} \sum_k (e^{-ikan} \ c^v_{k,\sigma} + e^{-ikan} \ (-1)^n \ c^c_{k,\sigma}) \ . \tag{2.17}$$

Substituting Eq. (2.17) into Eq. (2.14), H^d can be expressed in the k representation,

$$H^d = \sum_k \Big\{ \epsilon_k \ (\ c^{c\dagger}_{k,\sigma} \ c^c_{k,\sigma} - c^{v\dagger}_{k,\sigma} \ c^v_{k,\sigma}) \Big.$$

$$\Big. + i \ \Delta_k \ (\ c^{c\dagger}_{k,\sigma} \ c^v_{k,\sigma} - c^{v\dagger}_{k,\sigma} \ c^c_{k,\sigma}) \Big\} + 2KNu^2 \ , \tag{2.18}$$

with

$$\epsilon_k = 2t_0 \cos ka \ , \qquad \Delta_k = 4\alpha u \sin ka \ . \tag{2.19}$$

H^d can be reexpressed as

$$H^d = \sum_k C^{\dagger}_{k,\sigma} \ B \ C_{k,\sigma} + 2kNu^2 \tag{2.20}$$

for diagonalization, where

$$B = \begin{pmatrix} \epsilon_k & i\Delta_k \\ -i\Delta_k & -\epsilon_k \end{pmatrix}$$

and

$$C_{k,\sigma} = \begin{pmatrix} c^c_{k,\sigma} \\ c^v_{k,\sigma} \end{pmatrix} . \tag{2.21}$$

After diagonalizing of the matrix B, Eq. (2.20) becomes

$$H^d = \sum_k E_k \ (\ a^{c\dagger}_{k,\sigma} \ a^c_{k,\sigma} - a^{v\dagger}_{k,\sigma} \ a^v_{k,\sigma}) + 2NKu^2 \ , \tag{2.22}$$

where

$$E_k = \sqrt{\epsilon_k^2 + \Delta_k^2} \tag{2.23}$$

and

$$a^c_{k,\sigma} = \mu \ c^c_{k,\sigma} - i \ \mathrm{sgn}k \ \ \nu \ c^v_{k,\sigma}$$

$$a^v_{k,\sigma} = \mu \ c^v_{k,\sigma} - i \ \mathrm{sgn}k \ \ \nu \ c^c_{k,\sigma} \tag{2.24}$$

here $\mu = \left(\frac{E_k + \epsilon_k}{2E_k} \right)^{\frac{1}{2}}$, $\nu = \left(\frac{E_k - \epsilon_k}{2E_k} \right)^{\frac{1}{2}}$, sgn k is the sign function of k, and the phases are chosen in such a way that $a^c_{k,\sigma} \to c^c_{k,\sigma}$, $a^v_{k,\sigma} \to c^v_{k,\sigma}$ as $u \to 0$.

It is evident to see from Eq. (2.22) that $a^{c\dagger}_{k,\sigma} \ a^c_{k,\sigma}$ is the occupation

number operator of state k with energy E_k in the conduction band, and that $a^{v\dagger}_{k,\sigma}\, a^{v}_{k,\sigma}$ is the occupation number operator of state k with energy $-E_k$ in the valence band. The dispersion relation of Eq. (2.23) shows that dimerization opens a Peierls energy gap $E_g = 2\,\Delta_0 = 8\alpha u$ at the edge of the first Brillouin zone. Moreover, the energy spectrum is little changed, which is useful for the further approximation needed to convert the discrete model to a continuous one.

There are N π electrons in the chain, and $\frac{N}{2}$ states in the valence band (N is even). Because of spin degeneracy, each state can accommodate two electrons, so that all the states in the valence band are occupied and all the states in the conduction band are unoccupied. From Eq. (2.22), the system energy of the dimerized chain is given by

$$E_0 = -2 \sum_k E_k + 2NKu^2 , \tag{2.25}$$

where the factor of 2 in the first term of the r.h.s is due to spin. To sum over k, one must recall that k is constrained in the first Brillouin zone of $-\frac{\pi}{2a} < k \leqslant \frac{\pi}{2a}$ and that N has two possible values, $N = 4m$ and $N = 4m+2$ (m is an integer). When we replace the sum in Eq. (2.25) with an integral, we should take account of these circumstances. For $N = 4m$, the system energy of dimerized case is,

$$E_0(u) = -\frac{2L}{\pi} \int_0^{\frac{\pi}{2a}} \left| (2t_0 \cos ka)^2 + (4\alpha u \sin ka)^2 \right|^{\frac{1}{2}} dk + 2NKu^2$$

$$= -\frac{4Nt_0}{\pi} \left\{ E(1-z^2) - \frac{1}{2\lambda} z^2 \right\}, \tag{2.26}$$

where

$$z = \frac{2\alpha u}{t_0} \tag{2.27}$$

and the dimensionless coupling constant

$$\lambda = \frac{4\alpha^2}{\pi K t_0} . \tag{2.28}$$

For the typical value of parameters for $(CH)_x$ given in Eq. (2.11), $\lambda = 0.408$. The complete elliptic integral $E(1-z^2)$ of the second kind can be expanded for small z as,

$$E(1-z^2) = 1 + \frac{1}{2}(\ln\frac{4}{|z|} - \frac{1}{2})z^2 + \frac{3}{16}(\ln\frac{4}{|z|} - \frac{11}{12})z^4 + \cdots \tag{2.29}$$

From Eqs. (2.26) and (2.29), it is clear that, because of the logarithm term, for the values of z near zero, the π-electron energy is always more negative than the elastic energy. Therefore, a small deviation of z from zero will bring the system to a lower energy state. This corresponds to the theorem by Peierls described in section 1.2. Differentiating Eq. (2.26) with respect to z gives one local maximum at $z = 0$ and two equal stable minima at

$$z_0 = \pm e^{-(\frac{1}{\lambda} + 1)} \tag{2.30}$$

Given the value of λ from Eq. (2.28), yields $z_0 = \pm 0.127$, which corresponds to $u_0 = \pm 0.0386$Å, in good agreement with experiment.[35]

The condensation energy per site in eV is

$$-\frac{\Delta E_0}{N} = \frac{1}{N}[\, E_0(u_0) - E_0\,(0)\,] = -\frac{t_0 z_0^2}{\pi} = -0.013 \qquad (2.31)$$

and the density of states per spin of the perfectly dimerized state [using Eq. (2.23)] is

$$\rho_0(E) = \frac{L}{2\pi\left|\frac{dE_k}{dk}\right|} = \begin{cases} \frac{N}{\pi}|E|/[(4t_0^2 - E^2)(E^2 - \Delta_0^2)]^{\frac{1}{2}} & \Delta_0 < |E| < 2t_0 \\ 0 & \text{otherwise} \end{cases} \qquad (2.32)$$

From the above discussion, we can see that the excitation spectrum about zero energy (Fermi energy) determines many of the properties of the system. In the previous derivation of Eq. (2.26), we used a linear chain of $N = 4m$ CH groups. For $N = 4m$, k runs from $-\frac{\pi}{2ma}(m-1)$ through $\frac{\pi}{2a}$, whereas for $N = 4m+2$, k runs from $-\frac{\pi}{(2m+1)a}m$ through $\frac{\pi}{(2m+1)a}m$. The former has states at the Fermi level, half of which are occupied, which leads to an absolute Peierls instability of the system with respect to dimerization. The latter has an intrinsic gap of width $4t_0\sin\frac{\pi}{N}$ at the Fermi level even in the undimerized case, and therefore the system will be dimerized only if $\frac{\alpha^2}{Kt_0}$ exceeds an N-dependent critical value.[36] These differences vanish in the thermodynamical limit $N \to \infty$.

Because the perfectly dimerized state is a ground state, the energy of this state is an absolute minimum. A more restrictive condition is to require that the derivative of this ground state energy with respect to $y_n = u_n - u_{n+1}$ be

equal to zero for all n,

$$\frac{\partial}{\partial y_n} <G \mid H \mid G> =$$

$$-\alpha <G \mid c^{\dagger}_{n+1,\sigma} c_{n,\sigma} + c^{\dagger}_{n,\sigma} c_{n+1,\sigma} \mid G> + K y_n + A = 0 . \qquad (2.33)$$

From this condition, the coefficient A of the linear term can be determined. This linear term, as shown in Eqs. (2.7-2.9), depends on fixing the chain length as a boundary condition. Using the results of Eq. (2.17) through Eq. (2.24), the first term of r.h.s of Eq. (2.33) can be rewritten as

$$W = <G \mid c^{\dagger}_{n+1,\sigma} c_{n,\sigma} + c^{\dagger}_{n,\sigma} c_{n+1,\sigma} \mid G>$$

$$= \frac{1}{N} \sum_k e^{-ika(n+1)} (\mu^* + (-1)^{n+1} i \,\mathrm{sgn} k \, \nu^*) \, e^{ikan} \, (\mu - (-1)^n i \,\mathrm{sgn} k \, \nu) + h.c. . \qquad (2.34)$$

After some algebra, Eq. (2.34) becomes

$$W = -\frac{2}{N} \sum_k \left| \frac{4 t_0 \cos^2 ka + (-1)^n 8 \alpha u \sin^2 ka}{E_k} \right| , \qquad (2.35)$$

and can be replaced by the complete elliptic integrals for the first and second kind,

$$W = \frac{4}{\pi} \left| \frac{1}{1-z^2} (E(1-z^2) - z^2 K(1-z^2)) - (-1)^n \frac{z}{1-z^2} (K(1-z^2) - E(1-z^2)) \right| , \qquad (2.36)$$

where $z = \frac{2\alpha u}{t_0}$, as in Eq. (2.27). Comparing Eqs. (2.33) and (2.36), we obtain

$$A = \frac{4\alpha}{\pi}\left[1 + z^2\left(-\frac{1}{2}\ln\frac{4}{|z|} + \frac{3}{4}\right)\right] \tag{2.37}$$

$$\frac{Kt_0}{\alpha^2} = \frac{4}{\pi}\left[\left(\ln\frac{4}{|z|} - 1\right) + z^2\left(\frac{3}{4}\ln\frac{4}{|z|} - 1\right)\right] \tag{2.38}$$

Eq. (2.38) is nothing new but a reexpression of Eq. (2.30). In deriving Eqs. (2.37) and (2.38), we expanded $K(1-z^2)$ for small z,

$$K(1-z^2) = \ln\frac{4}{|z|} + \frac{I}{4}\left(\ln\frac{4}{|z|} - 1\right)z^2 + \cdots$$

It should be noted that the above derivation does not constitute a proof that the ground state is perfectly dimerized. Indeed, the use of Eq. (2.24) to obtain Eq. (2.34) implies that we have already assumed $u_n = (-1)^{n-1}u$ in Eq. (2.13), which means that the ground state is defined to have a dimerized structure. A restricted proof must begin with an arbitrary configuration of u_n. It has been suggested[33] that in the strong coupling limit (λ is very large), the true ground state configuration may have lower symmetry than the dimerized state. However, for weak or moderate coupling, the numerical results show that the ground state is the simple dimerized state.[37]

3. Charge Conjugation Symmetry

The SSH discrete model has charge conjugation symmetry, which means that if there is an eigenstate of H with eigen-energy ϵ, there is also a corresponding eigenstate with eigen-energy $-\epsilon$. This can be seen from following discussion: First, we construct an unitary one-particle charge conjugation operator[33]

$$V = \exp(i \sum_n \pi c_n^\dagger c_n) , \tag{2.39}$$

where c_n is used as in Eq. (2.2) above. The operator V satisfies the following relations,

$$V^\dagger c_{2n} V = c_{2n}$$

$$V^\dagger c_{2n+1} V = -c_{2n+1} . \tag{2.40}$$

Applying Eq. (2.40) to the electron part H^{el} of the SSH Hamiltonian, we obtain,

$$V^\dagger H^{el} V = - H^{el} . \tag{2.41}$$

If $|k>$ is a single-electron eigenstate of H with eigenvalue ϵ_k, then

$$H^{el} |k> = \epsilon_k |k> \tag{2.42}$$

and, $V^\dagger |k>$ and $-\epsilon_k$ should be another set of eigenstates and eigenvalues,

$$H^{el} (V^\dagger |k>) = -\epsilon_k (V^\dagger |k>) . \tag{2.43}$$

It is worthwhile to point out that from Eqs. (2.16) and (2.24), $c^v_{k,\sigma}$ and $a^v_{k,\sigma}$ can be transformed to $c^c_{k,\sigma}$ and $a^c_{k,\sigma}$ through the charge conjugation operator V,

$$V^\dagger c^v_{k,\sigma} V = c^c_{k,\sigma}$$

$$V^\dagger a^v_{k,\sigma} V = a^c_{k,\sigma} . \tag{2.44}$$

4. The Nature of the Localized Gap State Associated with a Soliton

The SSH Hamiltonian does not have an analytical solution for a soliton, but the nature of the localized gap state associated with a single soliton can be determined by consideration of charge conjugation symmetry.[38] As pointed out in Chapter I, each isolated soliton introduces only one localized electronic state. From the argument of section 2.3, this localized state must lie at the gap center and have an energy value of zero.

To determine the profile of $|\psi_0(n)\rangle$, the wavefunction of the mid-gap state, we write

$$|\psi_0(n)\rangle = \sum_n a_n^0 c_n^\dagger \, |0\rangle . \tag{2.45}$$

From the Eq. (2.10), we have

$$H^{el} \, |\psi_0(n)\rangle = - \left\{ \sum_{n'} t_{n'} \, (c_{n'+1}^\dagger c_{n'} + c_{n'}^\dagger c_{n'+1}) \right\} \sum_n a_n^0 c_n^\dagger \, |0\rangle$$

$$= - \sum_n t_n a_n^0 c_{n+1}^\dagger + t_{n-1} a_n^0 c_{n-1}^\dagger \, |0\rangle , \tag{2.46}$$

which leads to

$$t_n a_n^0 + t_{n+1} a_{n+2}^0 = 0 . \tag{2.47}$$

Note that even-n and odd-n terms of a_n^0 are not coupled in Eq. (2.47). If a soliton centered near $n = 0$ approaches $\eta_n = u_0$ (A -phase) when $n \to \infty$ and it approaches $\eta_n = -u_0$ (B-phase) when $n \to -\infty$ then from the expression $t_n = t_0 + (-1)^{n-1}\alpha(\eta_n + \eta_{n+1})$, we get

$$\frac{t_{2m}}{t_{2m-1}} = \begin{cases} < 1 & m \to \infty \\ > 1 & m \to -\infty \end{cases} \tag{2.48}$$

$$\frac{t_{2m+1}}{t_{2m}} = \begin{cases} > 1 & m \to \infty \\ < 1 & m \to -\infty \end{cases} . \tag{2.49}$$

It turns out that a^0_{2m} falls exponentially for both $m \to \infty$ and $m \to -\infty$, whereas a^0_{2m+1} is unbounded because of the conditions in Eq. (2.49). Therefore

$$a^0_{2m+1} = 0 \qquad \text{for all } m \tag{2.50}$$

and

$$a^0_{2m} \sim (-1)^m \, e^{-\left|2m\frac{a}{\xi_0}\right|} , \tag{2.51}$$

where $\left(\frac{\xi_0}{a}\right)^{-1} = \tanh^{-1}\frac{\Delta_0}{2t_0}$. This relation can be easily derived from Eq. (2.47) by assuming that a^0_{2m} has a form of $(-1)^m e^{-2mx}$ for large m.

In Fig. 12, we plot a schematic diagram of the probability density function $(a^0_n)^2$ contributed by the gap state of a neutral soliton.

5. Reversed Spin-Charge Relations and Fractional Charge

From the last two sections, the reversed spin-charge relations of solitons described qualitatively in section 1.7 can be found explicitly. Firstly, we consider the dimerized case, where the completeness of one particle wavefunctions for each spin can be expressed as

$$1 = \sum_{k \in v.b.} \langle k | c^\dagger_{n,\sigma} c_{n,\sigma} | k \rangle + \sum_{k \in c.b.} \langle k | c^\dagger_{n,\sigma} c_{n,\sigma} | k \rangle . \tag{2.52}$$

Because of the charge conjugation symmetry, the first term on the r.h.s of Eq. (2.52), which is summed over all the valence band, is equal to the second term, which is summed over all the conduction band, and both are equal to one-half the total value. Recalling that the valence band states are entirely occupied whereas those of the conduction band are completely empty, and assuming that there is a uniform background positive charge which makes the system both neutral and spin-free in the dimerized system, the density function on each site can be defined as

$$\rho_\sigma(n) = \sum_{k \in occ.} < k \mid c^\dagger_{n,\sigma} c_{n,\sigma} \mid k > - \frac{1}{2} , \tag{2.53}$$

which is, of course, equal to zero in the absence of solitons.

In the presence of a soliton, Eq. (2.52) becomes

$$1 = \sum_{k \in v.b.} < k \mid c^\dagger_{n,\sigma} c_{n,\sigma} \mid k > + \mid a^0_{n,\sigma} \mid^2 + \sum_{k \in c.b.} < k \mid c^\dagger_{n,\sigma} c_{n,\sigma} \mid k > , \tag{2.54}$$

where $a^0_{n,\sigma}$ was implicitly defined in Eq. (2.45) as representing the gap state ($\mid a^0_{n\downarrow} \mid = \mid a^0_{n\uparrow} \mid$). Again resorting to the charge conjugation symmetry, Eq. (2.54) becomes

$$\frac{1}{2} = \sum_{k \in v.b.} < k \mid c^\dagger_{n,\sigma} c_{n,\sigma} \mid k > + \frac{1}{2} \mid a^0_{n,\sigma} \mid^2 . \tag{2.55}$$

Combining the Eqs. (2.53) and (2.55), we obtain

$$\rho_\sigma(n) = (f_\sigma - \frac{1}{2}) \mid a^0_{n,\sigma} \mid^2 , \tag{2.56}$$

where f_σ is the electron occupation number of the mid-gap state for spin σ.

Since $\sum_n |a^0_{n,\sigma}|^2 = 1$ and $|a^0_{n,\sigma}|^2$ is localized over the width of a soliton (see section 2.4), the charge borne by a single soliton for each spin is equal to

$$Q_\sigma = e \sum_n \rho_\sigma(n) = \left(f_\sigma - \frac{1}{2} \right) e \ . \tag{2.57}$$

From Eq. (2.57), $Q_\sigma = \frac{1}{2} e$ when $f_\sigma = 1$, but $Q_\sigma = -\frac{1}{2} e$, when $f_\sigma = 0$, resulting in an apparently anomalous fractional charge. However, this fractional charge cannot be observed, because electrons of both spin orientations in $(CH)_x$ enter symmetrically in the Fermi sea, so that the charge $Q_\sigma = \pm \frac{e}{2}$ is "spin masked".[39] Thus instead of fractional charge, the conventional spin-charge relations are reversed. From Eq. (2.56),

$$S = \frac{1}{2} \sum_n \left| \rho_\uparrow(n) - \rho_\downarrow(n) \right| = \frac{1}{2} \left(f_\uparrow - f_\downarrow \right)$$

$$Q = e \sum_n \left| \rho_\uparrow(n) + \rho_\downarrow(n) \right| = e \left(f_\uparrow + f_\downarrow - 1 \right) \ . \tag{2.58}$$

This is just a reexpression of Eq. (1.4). The schematic diagrams in Fig. 13 clearly demonstrate these novel spin-charge relations. It has been pointed out[40] however, that spin no longer masks fractional charge for trimerized chains, in which only one-third band are filled by electrons, and that the fractional charge should be observed in that case.

In addition, Kivelson and Schrieffer[41] have shown that the spin and charge associated with the solitons are sharp quantum observable.

6. Extended SSH-Hubbard Model

Experiment indicates that the electron-electron Coulomb interaction has an important role in the formation of solitons. The electron-nuclear double resonance (ENDOR)[42,43] studies of the hyperfine interaction associated with the neutral defect in $(CH)_x$ imply that there are two discrete carbon sites which correspond to spin densities of |0.02| and |0.06|. Triple resonance studies furthermore confirm that the two spin densities have opposite signs. These results cannot be obtained from the SSH model Hamiltonian [see Eqs. (2.50), (2.51) and (2.56)], but can be obtained within inclusion of electron-electron Coulomb interaction[38,44]

The extended SSH (Peierls)-Hubbard model Hamiltonian can be written as,

$$H = H_0 + H_1 , \tag{2.59}$$

where H_0 is the standard SSH Hamiltonian in Eq. (2.10), and

$$H_1 = U \sum_n c_{n\uparrow}^{\dagger} c_{n\uparrow} c_{n\downarrow}^{\dagger} c_{n\downarrow}$$

$$+ V' \sum_{n,\sigma,\sigma'} c_{n,\sigma}^{\dagger} c_{n,\sigma} c_{n+1,\sigma'}^{\dagger} c_{n+1,\sigma'} , \tag{2.60}$$

where the coefficients U and V represent the effective strengths of the Coulomb interaction. In writing the extended Hubbard terms, we assume that the Coulomb interaction is strongly screened ($\epsilon \sim 10$ in $(CH)_x$) and only very short range effective interactions are considered. We also assume that only the nearest neighbor V'-term is essential to the description of Coulomb binding.

Many authors[45,46,47,48] have investigated the static effects on dimerization and solitons of this model by using Monte-Carlo method and unrestricted Hartree-Fock approximation, which treats energy spectra and wavefunctions of different spin separately. The main results can be summarized as follows,

(a) The Hartree-Fock approximation is justifiable when U and V are small compared with bandwidth $W = 4t_0$;

(b) Dimerization occurs only when U is less than a critical value (4.66 eV for *trans*-$(CH)_x$), and $V = 0$;

(c) The neutral and charged soliton creation energies are split and the soliton profiles are changed, with the width of neutral soliton being narrower and the width of charged soliton being broader than the case for $U = 0$, $V = 0$;

(d) For a neutral soliton, the spin densities on the even-numbered sites, increase as U increases and, in compensation, the spin densities on the odd-numbered sites decrease such that the total spin of a neutral soliton keeps its value of one-half.

From measurements of soliton creation energy[49] and the ratio of two opposite-sign spin densities which is obtained from ENDOR experiment[42,43] the coefficient U of the Hubbard term is estimated to be $3 \sim 4$ eV, which implies that the Hartree-Fock approximation can be used in $(CH)_x$.

7. Modified SSH Model and Its Properties of Dimerization

The two-fold degeneracy of the ground state of *trans*-polyacetylene is responsible for symmetry breaking in the system and leads to the formation of solitonlike excitations. The SSH model successfully interpreted the magnetic,

optical, and electronic properties of pristine and lightly doped *trans*-polyacetylene. Since ground state degeneracy is not a general property of quasi one dimensional conducting polymers, however, theoretical and experimental studies of the large class of nondegenerate conjugated polymers are necessary. An important subclass of these are polymers having a nearly degenerate ground state structure. Some examples are *cis*-$(CH)_x$, polypyrrole, poly(paraphenylene), and poly(thiophene). It has been recognized[50] that despite the lack of solitons in non-degenerate systems, the notion can be readily generalized to cases of near degeneracy. When such a system is photoexcited, oxidized, or reduced, the creation of a kink-antikink-like pair, or bipolarons, can be energetically favored. Once a kink-antikink pair is created in those systems, they may be 'confined', if separating them requires extra energy.[30] Such "confined" kink-like excitations may be charged, but they have zero spin. This is consistent with the magnetic susceptibility measurements[51,52] in doped polyparaphenylene and polypyrrole.

Wang, Su and Martino[53] investigated the nearly degenerate ground state case by proposing a modified SSH-type model Hamiltonian of the following form:

$$H = -\sum_{n,\sigma}\Big\{(t_1 + \alpha_1(u_{2n}-u_{2n+1}))\,(c^{\dagger}_{2n+1}c_{2n}+h.c.)$$

$$+ (t_2 + \alpha_2(u_{2n+1}-u_{2n+2}))\,(c^{\dagger}_{2n+2}c_{2n+1}+h.c.)\Big\}$$

$$+ \frac{K}{2}\sum_i (u_i-u_{i+1})^2 + \frac{M}{2}\sum_i \dot{u}_i^2\,, \qquad (2.61)$$

where it is assumed that the transfer integrals and electron-phonon coupling constants have different values t_1, t_2 and α_1, α_2, corresponding to the alternative bonds. As before, K is the effective stiffness constant for the undimerized system and M is the mass of the CH group. Fig. 3 illustrates a prototype non-degenerate polymer, *cis*-$(CH)_x$, which can be described by this Hamiltonian. The *cis*-transoid configuration has lower energy than the *trans*-cisoid configuration. The configuration coordinates u_i are the displacements from the site position of the undimerized state.

In the perfectly dimerized chain, the configuration coordinates u_i are constrained by $u_i = (-1)^i u$. The ground state of the chain has exactly one π electron per site on average. The Hamiltonian in Eq. (2.61) for the dimerized case can be rewritten as,

$$H = -\sum_{i,\sigma} \left| (t_0 + u\ \Delta\alpha) + (-1)^{i-1} \left(2\alpha_0 u + \frac{\Delta t}{2}\right) \right| (c_{i+1,\sigma}^{\dagger}\ c_{i,\sigma} + h.c.)$$

$$+ 2NKu^2 \qquad (2.62)$$

where for convenience we define $t_0 = (t_2+t_1)/2$, $\Delta t = t_2-t_1$, $\alpha_0 = (\alpha_2+\alpha_1)/2$, and $\Delta\alpha = \alpha_2-\alpha_1$. Comparing Eq. (2.62) with Eq. (2.14), we can see that all the formulas in section 2.2 that were derived from Eq. (2.14) can be directly used here if t_0 is replaced by $t_0 + u\ \Delta\alpha$, and $2\alpha u$ by $2\alpha_0 u + \frac{\Delta t}{2}$.

Therefore, the single electron spectrum can be obtained from Eq. (2.23),

$$E_{\pm} = \pm \sqrt{(2t_0 + 2u\Delta\alpha)^2\cos^2 ka + (4\alpha_0 + \Delta t)^2\sin^2 ka} \quad . \tag{2.63}$$

From this expression, we can see that in the undistorted case $u = 0$, the energy spectrum becomes,

$$E_{\pm} = \pm \sqrt{(2t_0 \cos ka)^2 + (\Delta t \sin ka)^2} \tag{2.64}$$

This implies the existence of an extrinsic gap Δt which occurs in the rigid undimerized polymer skeleton of the system because of the σ electron interaction. The total static energy for this nearly dimerized system is

$$\frac{E_0(z)}{N} = -\frac{4t_0}{\pi}\left[\left[1-\nu\left(\frac{z-\mu}{1-\nu z}\right)\right] E(1-z^2) - \frac{1}{2\lambda}\left(\frac{z-\mu}{1-\nu z}\right)^2\right], \tag{2.65}$$

where λ was defined in Eq. (2.28), and the dimensionless parameters z, μ, and ν are defined respectively as,

$$z = \frac{4\alpha_0 u + \Delta t}{2t_0 + 2u\Delta\alpha}$$

$$\mu = \frac{\Delta t}{2t_0}, \quad \text{and} \quad \nu = \frac{\Delta\alpha}{2\alpha_0}. \tag{2.66}$$

This function has one local maximum near $u = 0$ and two unequal minima. The minimum values can be found by solving the equation $\frac{dE_0(z)}{dz} = 0$. Although this equation cannot be solved exactly, it can be simplified by noting that μ and ν are of order 10^{-3}, whereas z and λ are of order 10^{-1}, and that the second and higher orders of μ and ν terms, and the third and higher orders of z terms can be disregarded. It then reads as,

$$(2z + 3\nu z^2)\left(\ln 2 - \frac{1}{2} - \frac{1}{2\lambda} - \frac{1}{4}\ln z^2\right) + \left(\nu + \frac{\mu}{\lambda}\right) = 0 , \tag{2.67}$$

which can be solved approximately by perturbation method. If we assume $\pm z_0$ are the solutions of

$$\ln 2 - \frac{1}{2} - \frac{1}{2\lambda} - \frac{1}{4}\ln z^2 = 0 \tag{2.68}$$

then the solutions of Eq. (2.67) can be written as $z_\pm = \pm z_0 + \Delta z_\pm$, where $\Delta z_\pm$ can be expressed in terms of z_0, μ and ν,

$$\Delta z_\pm = \frac{\nu + \frac{\mu}{\lambda}}{1 \pm \frac{3\nu}{2} z_0}$$

$$\approx \nu + \frac{\mu}{\lambda} \tag{2.69}$$

The energy values at these two minimum points are

$$\frac{E_0(z_\pm)}{N} \approx -\frac{4t_0}{\pi}\left|1 + \frac{z_0^2}{4} \pm \left(\nu + \frac{\mu}{\lambda}\right)z_0 + \frac{1}{4}\left(\nu + \frac{\mu}{\lambda}\right)^2 - \frac{\mu^2}{2\lambda}\right| . \tag{2.70}$$

The energy difference per site of these two local minimum energy states are

$$\frac{\Delta E_0}{N} = \frac{E(z_+) - E(z_-)}{N} = -\frac{8t_0}{\pi}\left(\nu + \frac{\mu}{\lambda}\right)z_0 , \tag{2.71}$$

where $z_0 = 4e^{-\left(\frac{1}{\lambda} + 1\right)}$ is obtained from Eq. (2.68).

The degenerate ground state system corresponds to the case in which $\mu = \nu = 0$. If one of them has value other than zero, the degeneracy is lifted. It is interesting to note that from Eq. (2.71) for fixed parameters K, t_0, α_0, a

negative value of $\Delta\alpha$ can compensate for the contribution to ΔE by a positive value of Δt. This implies that if we let $\nu = -\frac{\mu}{\lambda}$, a degenerate system could be produced. However, this system is not the same as *trans*-$(CH)_x$, because despite the total system energy's degeneracy, the two configurations have different energy spectra. This can be understood from Eq. (2.63), wherein Δt explicitly changes the width of the gap, and $\Delta\alpha$ explicitly changes the density of energy levels. We believe this case is worth further study.

The above description tells us that for small values ν and μ, the energy difference between the two local minima is small. It is in this sense that we define "nearly degenerate". For weak coupling limits, the lower minimum state is a ground state and the higher one is a metastable state. The metastability vanishes for large enough values of μ and ν. The condition that vanishing metastability can be obtained by investigating the behavior of $\frac{dE_0(z)}{dz}$. If the function has only one root, the metastability disappears. The function $\frac{dE_0(z)}{dz}$ will have but one root if it satisfies the following inequality, which is obtained through the calculation of extremum values of $\frac{dE_0(z)}{dz}$,

$$2\,e^{-(\frac{1}{\lambda}+2)} < \nu + \frac{\mu}{\lambda} \tag{2.72}$$

For the typical parameter values in Eqs. (2.11), and (2.28), $\lambda = 0.4$. Given these, the critical values for $\nu + \frac{\mu}{\lambda}$ is 0.023, which corresponds to $\Delta t = 0.12$ eV when $\Delta\alpha = 0$, or $\Delta\alpha = 0.075$ eV / Å when $\Delta t = 0$.

CHAPTER III

Continuum Model

In the weak coupling limit, it is possible to make use of the continuum approximation of the SSH discrete model.[12] Because in that limit onlythe electron states near the Fermi surface are strongly affected by the lattice distortions, we can linearize the energy spectrum to reduce the problem to Bogoliubov-de Gennes-like (BdG) equation.[54] The benefit of the continuum Takayama-Lin-liu-Maki (TLM) model is that almost all the physical properties of the soliton can be expressed by the parameters used in the SSH model and that the internal relations between the physical quantities can be well understood. In this chapter, we first introduce the TLM continuum model and discuss the boundary conditions; we then present solutions for a single soliton and for a soliton pair, which are also solutions for a polaron and a bipolaron, depending on the electronic configuration and the system degeneracy. Finally, we adapt a two polaron solution which is used in Chapter V.

I. TLM Model

The fact that the dimerization only changes the band structure near the Fermi level can be seen by comparison of Eqs. (2.15) and (2.23). If we let $k' = k - k_F$ for $k > 0$, and $k' = k + k_F$ for $k < 0$ ($k_F = \frac{\pi}{2a}$), and note

that $\cos ka \approx \mp k'a$ and $\sin ka \approx \pm 1$ for small $|k'a|$, Eq (2.23) reduces to the approximation

$$\epsilon(k') = \pm \sqrt{(k'V_F)^2 + \Delta_i^2}\,, \tag{3.1}$$

where $V_F = 2t_0 a$ is the Fermi velocity ($\hbar = 1$).

When the energy spectrum is expanded near $\pm k_F$, the band structure is split into two branches, a right-going branch with $\epsilon_k \approx V_F(k - k_F)$ and a left going branch with $\epsilon \approx V_F(k + k_F)$, where Δ_0 is set to 0. This recalls the two particle Luttinger model for one dimensional interacting electron gas.[55] The electronic wave function therefore can be described by a two-component field $\psi_{j,\sigma}(x)$ ($j = 1,2$), which is related to the discrete electron operators by[56]

$$\psi_{1,\sigma}(x_n) = \frac{1}{2\sqrt{a}} \left(e^{-i\pi n} c_{2n,\sigma} + e^{-i\pi(n+\frac{1}{2})} c_{2n+1,\sigma}\right)$$

$$\psi_{2,\sigma}(x_n) = \frac{-i}{2\sqrt{a}} \left(e^{i\pi n} c_{2n,\sigma} + e^{i\pi(n+\frac{1}{2})} c_{2n+1,\sigma}\right) \tag{3.2}$$

and the inverse transformations,

$$c_{2n,\sigma} = \sqrt{a}\left(e^{i\pi n}\psi_{1,\sigma}(x_n) + ie^{-i\pi n}\psi_{2,\sigma}(x_n)\right)$$

$$c_{2n+1,\sigma} = i\sqrt{a}\left(e^{i\pi n}\psi_{1,\sigma}(x_{n+\frac{1}{2}}) - ie^{-i\pi n}\psi_{2,\sigma}(x_{n+\frac{1}{2}})\right) \tag{3.3}$$

where $x_n = (2n + \frac{1}{2})a$ is a lattice site coordinate in the dimerized case. By treating the slowly varying field in space defined in Eq. (3.2) as continuous, the SSH Hamiltonian becomes (up to order $\frac{\xi}{a}$, where ξ is the electronice correlation length $\xi = \frac{V_F}{\Delta_0}$)

$$H_{\mathrm{TLM}} = \sum_{\sigma} \int_{-\frac{L}{2}}^{\frac{L}{2}} dx \;\; \Psi_{\sigma}^{\dagger}(x) \left[-iV_{\mathrm{F}} \frac{\partial}{\partial x} \tau_3 + \Delta(x) \tau_1 \right] \Psi_{\sigma}(x)$$

$$+ \frac{1}{\lambda \pi V_{\mathrm{F}}} \int_{-\frac{L}{2}}^{\frac{L}{2}} dx \, \Delta^2(x) \, , \tag{3.4}$$

where the real lattice pattern parameters

$$\Delta(x_n) = (-1)^{2n-1} 2\alpha \, (u_{2n} - u_{2n+1})$$

$$\Delta(x_{n+\frac{1}{2}}) = (-1)^{2n} 2\alpha \, (u_{2n+1} - u_{2n+2}) \, , \tag{3.5}$$

the τ_i are the Pauli matrices,

$$\tau_1 = \begin{bmatrix} 0 & 1 \\ 1 & 0 \end{bmatrix} \quad \tau_2 = \begin{bmatrix} 0 & -i \\ i & 0 \end{bmatrix} \quad \tau_3 = \begin{bmatrix} 1 & 0 \\ 0 & -1 \end{bmatrix} \tag{3.6}$$

and $\Psi_{\sigma}(x) = \begin{bmatrix} \psi_{1,\sigma}(x) \\ \psi_{2,\sigma}(x) \end{bmatrix}$. The kinetic term is absent from Eq. (3.4) because the discussion for the moment concerns only the static properties of solitons. The second term of the r.h.s in Eq. (3.4) represents the coupling of the electron gas and the phonon field, which causes scattering from one branch field (one side of the Fermi surface) to another, because the dimerization has wave number $2k_{\mathrm{F}}$.

If we expand the electron field $\Psi_{\sigma}(x)$ in k-space,

$$\Psi_{\sigma}(x) = \sum_{k} \Psi_{\sigma}^{k}(x) c_k \, , \tag{3.7}$$

The electron eigenvalue equation

$$H_{\mathrm{TLM}}|k> = \epsilon_k |k> \tag{3.8}$$

is written as

$$(-iV_F \frac{\partial}{\partial x}\tau_3 + \Delta(x)\tau_1)\ \Psi^k(x) = \epsilon_k \Psi^k(x) \tag{3.9}$$

This is a BdG equation[54] which satisfies the self-consistent equation (gap equation),

$$\frac{\delta}{\delta\ \Delta(x)} <\Phi| H_{\mathrm{TLM}} |\Phi> = 0\ ,$$

where $|\Phi>$ is a Slater determinant, and $|\Phi> = \prod_{k,\sigma} c_{k,\sigma}\dagger |0>$ include all occupied states. The gap equation reads

$$\Delta(x) = -\frac{\pi\lambda V_F}{2} \sum_{k,\sigma} \left[\Psi^k_\sigma(x)\right]\dagger \tau_1 \Psi^k_\sigma(x) \tag{3.10}$$

where the summation is over all the occupied states. Equation (3.9) is analogue to the Dirac equation, if we view $\Delta(x)$ as a position-dependent mass, so that the electronic spectrum is unbounded below. In order to reflect the real physics of polyacetylene, we should artificially cut off the spectrum at the actual π-band width $E = -W \approx -2t_0$. From Eq. (3.5), $\Delta(x)$ represents the optical phonon part. The coupling term of electrons and acoustic phonons is omitted in the TLM model, because it is used only to discuss dimerization. The resulting model can describe many properties of $(CH)_x$ to a good approximation. As in the SSH model, charge conjugation symmetry holds in the TLM model.

Eq. (3.9) accompanied with Eq. (3.10) can be solved exactly for the cases of perfect dimerization, solitons and polarons. In order to get solutions whith physical meaning, we must first discuss the boundary conditions.

2. Boundary Conditions

Incorrect boundary conditions produce spurious results which mislead the calculations of real physical quantities, such as, the optical absorption coefficient. The correct boundary conditions should reflect the topological changes that occur in the presence of a soliton. They can be derived from the corresponding parts of the discrete model.[56]

In dimerization, the cyclic boundary condition applies to the real order parameter $\Delta(x)$, resulting in $\Delta(x-\frac{L}{2}) = \Delta(x+\frac{L}{2})$ for a chain of length L. However, for a system with one soliton the topological constraint of in the boundary condition should reflect the phase changes across the soliton, $\Delta(x-\frac{L}{2}) = -\Delta(x+\frac{L}{2})$. In general, if a chain contains M solitons, then

$$\Delta(x-\frac{L}{2}) = (-1)^M \Delta(x+\frac{L}{2}) . \tag{3.11}$$

The boundary conditions for the electronic wave function are more complicated, having to be consistent with the real order parameter $\Delta(x)$. There are two other physical quantities whose periodicity determines the boundary conditions: the charge density and the current density. Suppose the wave functions obey the relation

$$\Psi(x+\frac{L}{2}) = B\,\Psi(x-\frac{L}{2}) \tag{3.12}$$

where B is a 2×2 unitary matrix to be determined. Requiring the charge density to be periodic gives

$$\Psi\dagger(x+\frac{L}{2})\Psi(x+\frac{L}{2}) = \Psi\dagger(x-\frac{L}{2})\Psi(x-\frac{L}{2}) \ . \tag{3.13}$$

The current density in the continuum model is derived by analogy to the discrete model.

$$j = J_0\sum_\sigma (c_{n,\sigma}\dagger c_{n+1,\sigma} - \text{h.c.})$$

$$= J_0\sum_\sigma \Psi_\sigma\dagger(x)\tau_3\Psi_\sigma(x) \ ,$$

where $J_0 = eV_F$ and e is the electron charge. So periodicity also requires

$$\Psi\dagger(x+\frac{L}{2})\tau_3\Psi(x+\frac{L}{2}) = \Psi\dagger(x-\frac{L}{2})\tau_3\Psi(x-\frac{L}{2}) \ . \tag{3.14}$$

The consequence of the boundary condition on $\Delta(x)$ from Eq. (3.11) creates further constraints on $\Psi(x)$ through Eq. (3.10),

$$\Psi\dagger(x+\frac{L}{2})\tau_1\Psi(x+\frac{L}{2}) = (-1)^M\Psi\dagger(x-\frac{L}{2})\tau_1\Psi(x-\frac{L}{2}) \ . \tag{3.15}$$

Combining Eqs. (3.13), (3.14) and (3.15), B obeys the relations,

$$\begin{aligned} B\dagger B &= 1 \\ B\dagger\tau_3 B &= \tau_3 \\ B\dagger\tau_1 B &= (-1)^M\tau_1 \end{aligned} \tag{3.16}$$

Thus B has the form

$$B = e^{i\alpha_1}I \qquad \text{for } M \text{ even}$$

$$B = e^{i\alpha_2\tau_3} \qquad \text{for } M \text{ odd}, \tag{3.17}$$

where the phases α_1 and α_2 can be determined from the discrete model, $\alpha_1 = 0, \pi$ and $\alpha_2 = \frac{\pi}{2}, \frac{2\pi}{2}$. The values of α make no difference in the thermodynamic limit $L \to \infty$, and all the physical quantities are independent[56] of α. In the following, we take $\alpha_1 = 0$ and $\alpha_2 = \frac{\pi}{2}$.

3. Soliton Solution

For convenience, Eq. (3.9) will be rewritten by the first defining

$$f(x) = \begin{pmatrix} f_-(x) \\ f_+(x) \end{pmatrix} = \sqrt{2}U\ \Psi(x) \tag{3.18}$$

where the transformation matrix

$$U = \frac{1}{\sqrt{2}} \begin{pmatrix} 1 & -i \\ 1 & i \end{pmatrix} \tag{3.19}$$

It is easy to check that

$$U\tau_1 U\dagger = \tau_2\,, \quad U\tau_2 U\dagger = \tau_3\,, \quad U\tau_3 U\dagger = \tau_1\,. \tag{3.20}$$

Then, Eqs. (3.9) and (3.10) become

$$[-iV_F \frac{\partial}{\partial x}\tau_1 + \Delta(x)\tau_2]\ f^k(x) = \epsilon_k\, f^k(x) \tag{3.21}$$

$$\Delta(x) = -\frac{\pi\lambda V_F}{4} \sum_{k,\sigma} \left[f^k_\sigma(x)\right]\dagger \tau_2 f^k_\sigma(x) \tag{3.22}$$

which can be cast as a Schrödinger-like equation,

$$\left[-V_F^2 \frac{\partial^2}{\partial x^2} + V(x)\right] f^k(x) = \epsilon^k f^k(x) \tag{3.23}$$

where $V(x) = \Delta^2(x) + \tau_3 V_F \frac{\partial}{\partial x}\Delta(x)$.

We first discuss the dimerization solution, where the real order parameter is a constant, $\Delta(x) = \Delta_0$. Thus, Eq. (3.23) becomes,

$$\left[-V_F^2 \frac{\partial^2}{\partial x^2} + \Delta_0^2 - \epsilon_k^2\right] f_-^k(x) = 0$$

$$i\,\epsilon_k\, f_-^k(x) = \left[V_F \frac{\partial}{\partial x} + \Delta_0\right] f_+^k(x) \tag{3.24}$$

The solutions which satisfy the boundary condition

$$f_+(\frac{L}{2}) = f_+(-\frac{L}{2}), \qquad f_-(\frac{L}{2}) = f_-(-\frac{L}{2}) \tag{3.25}$$

and the normalization condition

$$\int_{-\frac{L}{2}}^{\frac{L}{2}} \left[|f_+(x)|^2 + |f_-(x)|^2\right] dx = 2 \tag{3.26}$$

can be written as

$$f_+^k(x) = \frac{\mathrm{sgn}(\epsilon_k)}{\sqrt{L}}\, e^{i(kx + \frac{\pi}{2} - \phi_k)}$$

$$f_-^k(x) = \frac{1}{\sqrt{L}}\, e^{ikx}\ , \tag{3.27}$$

where $\phi_k = \tan^{-1}(k\,\xi)$, and

$$\epsilon_k = \pm\sqrt{V_F^2 k^2 + \Delta_0^2} \tag{3.28}$$

for

$$kL = 2n\pi, \qquad -\frac{\pi}{2a} < k < \frac{\pi}{2a}. \tag{3.29}$$

The value of the dimerization parameter Δ_0 is determined using the gap equation (3.22),

$$\Delta_0 = \frac{\pi\lambda V_F}{4}\frac{2}{L}\sum_{k,\sigma}\frac{\Delta}{\sqrt{\Delta_0^2 + (V_F k)^2}}. \tag{3.30}$$

Replacing the summation by an integral

$$\Delta_0 = We^{-\frac{1}{\lambda}}, \tag{3.31}$$

where W is the bandwidth. Comparing Eq. (3.31) with Eq. (2.30) for the discrete model, we find that the results obtained from the two models are in good agreement.

The soliton solutions are obtained similarly. In a single soliton case, which has topological charge +1,

$$\Delta(x) = \Delta_0 \tanh\frac{x}{\xi}, \tag{3.32}$$

where the correlation length $\xi = \frac{V_F}{\Delta_0}$ is also the soliton half width and the soliton is centered at $x_0 = 0$. Then, Eq. (3.23) is expressed as,

$$\left[-V_F^2\frac{\partial^2}{\partial x^2} + \Delta_0^2 - \epsilon_k^2\right] f_{\pm}^{k}(x) = 0$$

$$i\,\epsilon_k\, f_-^k(x) = \left(V_F\frac{\partial}{\partial x}+\Delta(x)\right) f_+^k(x) \tag{3.33}$$

which has one bound state solution

$$f_-^0(x) = 0$$

$$f_+^0(x) = \xi^{-\frac{1}{2}}\mathrm{sech}\frac{x}{\xi} \tag{3.34}$$

whith energy $\epsilon_0 = 0$. The extended state solutions are

$$f_-^k(x) = A_k e^{ikx}$$

$$f_+^k(x) = A_k\,\mathrm{sgn}(\epsilon_k)[\sin\phi_k + i\cos\phi_k\tanh\frac{x}{\xi}]e^{ikx} \tag{3.35}$$

with the energy spectrum,

$$\epsilon = \pm\sqrt{(V_F k)^2 + \Delta_0^2}\,. \tag{3.36}$$

The normalization factor A_k is calculated from the condition (3.26),

$$A_k = [L - \xi\cos^2\phi_k]^{-\frac{1}{2}} \tag{3.37}$$

where

$$\phi_k = \tan^{-1} k\,\xi\,, \quad \text{and} \quad -\frac{\pi}{2} < \phi_k \leqslant \frac{\pi}{2} \tag{3.38}$$

The wave vectors are determined through the boundary conditions (3.17),

$$f_-(\frac{L}{2}) = i f_+(-\frac{L}{2})$$

$$f_+(\frac{L}{2}) = i f_-(-\frac{L}{2}) \tag{3.39}$$

and we find

$$kL = 2n\pi + \phi_k \qquad \text{for} \quad \epsilon_k > 0$$

$$kL = (2n+1)\pi + \phi_k \qquad \text{for} \quad \epsilon_k < 0 . \tag{3.40}$$

Comparing Eq. (3.36) with Eq. (3.28) and Eq. (3.40) with Eq. (3.29), we find that the soliton and dimerized solutions have similar dispersion relations, but that the wave vectors are shifted in the presence of a soliton. We should take account of this fact when we calculate the formation energy of a soliton.

The solutions of Eqs. (3.34) and (3.35) also satisfy the gap equation, which can be verified by noting that the bound state has zero contribution to the summation of the r.h.s in Eq. (3.22) and that the contribution of the extended states is expressed as,

$$\sum_{k,\sigma} (f_\sigma^k(x))^\dagger \tau_2 f_\sigma^k(x) = 2\sum_{k,\sigma} \mathrm{Im}\left\{ f_-^k(x))^* f_+^k(x) \right\}$$

$$= -\frac{8}{2\pi}\int_0^{\frac{\pi}{2a}} dk \frac{\Delta(x)}{\sqrt{(V_F k)^2 + \Delta_0^2}} . \tag{3.41}$$

From Eq. (3.41), Δ_0 obeys the same relation in the single soliton case as it does in the dimerization case, Eq. (3.31). This means the presence of a soliton changes neither the gap parameter nor the gap energy.

We now discuss the effective mass of a soliton. The effective mass associated with the soliton motion is defined as the coefficient of $\frac{1}{2}V^2$ in the expression for the soliton kinetic energy, where V is the soliton velocity. Thus, by

making use of the Galilean boost $x \rightarrow x - Vt$ in Eq. (3.32), the effective mass is expressed as

$$M_s = \frac{1}{\lambda \pi V_F \omega^2} \int dx \left[\frac{\partial}{\partial t}\Delta(x)\right]^2 / \frac{1}{2}V^2$$

$$= \frac{4}{3} M_{CH} \left[\frac{u_0}{a}\right]^2 \left(\frac{a}{\xi}\right)$$

$$\approx 4m_e \tag{3.42}$$

which is of the order of the electron mass. Here M_{CH} is the mass of the CH group. In the above expression, the optical phonon frequency $\omega^2 = \frac{4K}{M_{CH}}$. The reasons for the smallness of M_s can be understood by rewriting Eq. (3.42) as

$$M_s \xi^2 \sim \left[M_{CH} \frac{\xi}{a}\right] u_0^2 \ . \tag{3.43}$$

Because ξ is the half width of a soliton, moving a soliton by a distance ξ can be accomplished by simply shifting each of the $\left[\frac{\xi}{a}\right]$ ions by a distance u_0. As a result of this light mass, we can use the equipartition theorem to estimate that in the range of interesting temperatures ($100 \sim 300°K$) the soliton velocity is of the order of the speed of sound.

4. The Modified Continuum Model

From the modified SSH discrete model of Eq. (2.61), which is used to describe nondegenerate quasi-one-dimensional systems, we use the same procedure employed in Section 2.1 to obtain a modified continuum model, which is

written as the action integral[17]

$$I = \int dt \int_{-\frac{L}{2}}^{\frac{L}{2}} dx \left\{ -\frac{1}{\lambda \pi V_F} \Delta^2(x,t) + \right.$$

$$\psi\dagger(x) \left| i\hbar \frac{\partial}{\partial t} + i(V_F + \frac{\Delta\alpha}{2\alpha_0} a\, \Delta(x))\tau_3 \frac{\partial}{\partial x} \right.$$

$$\left. \left. + i\frac{\Delta\alpha}{4\alpha_0} a \frac{\partial \Delta(x)}{\partial x} \tau_3 - \tau_1(\Delta(x) + \Delta_e) \right| \psi(x) \right\}, \tag{3.44}$$

with $\lambda = \frac{4\alpha_0^2}{\pi K t_0}$, $V_F = 2t_0 a$, $\Delta\alpha = \alpha_1 - \alpha_2$, and $\Delta_e = \Delta t = t_1 - t_2$. The parameters α_0, t_0, Δt, and $\Delta\alpha$ were defined in Eq. (2.62), and the corresponding Hamiltonian form is

$$H = \frac{1}{2} \int_{-\frac{L}{2}}^{\frac{L}{2}} dx \left\{ \Psi_\sigma\dagger(x)[-i(V_F + \mu a\, \Delta(x))\tau_3 \frac{\partial}{\partial x} + (\Delta(x) + \Delta_e)\tau_1]\Psi_\sigma(x) + h.c \right\}$$

$$+ \frac{1}{\lambda \pi V_F} \int_{-\frac{L}{2}}^{\frac{L}{2}} dx\, \Delta^2(x), \tag{3.45}$$

where $\mu = \frac{\Delta\alpha}{2\alpha_0}$.

If we let $\Delta t = 0$ and $\Delta\alpha = 0$, Eq. (3.45) will give the familiar TLM Hamiltonian. If we let only $\Delta\alpha = 0$ and keep the transfer integral t alternating, the corresponding Hamiltonian becomes exactly the same as those proposed by

Brazovskii and Kirova,[57] and Fesser, Bishop and Campbell.[58] The electron eigenvalue equation is written as

$$\left\{-i(V_F + \mu a\,\Delta(x))\frac{\partial}{\partial x}\tau_3 - i\frac{\mu a}{2}\frac{\partial \Delta(x)}{\partial x}\tau_3 - (\Delta(x)+\Delta_e)\tau_1\right\}\Psi(x) = \epsilon_k\,\Psi(x) \tag{3.46}$$

and the self-consistent equation is

$$\Delta(x) = -\frac{\lambda\pi V_F}{2}\left\{\sum_{k,\sigma}(\Psi_\sigma^k(x))^\dagger\tau_1\Psi_\sigma^k(x) - i\,\mu a\sum_{k,\sigma}(\Psi_\sigma^k(x))^\dagger\tau_3\frac{\partial}{\partial x}\Psi_\sigma^k(x)\right\}. \tag{3.47}$$

For the dimerized ground state $\Delta(x) = \Delta_0$, the equation is exactly solvable. The one-electron energy spectrum is

$$\epsilon_k = \pm\left|k^2(V_F + \mu a\,\Delta_0)^2 + (\Delta_0 + \Delta_e)^2\right|^{\frac{1}{2}} \tag{3.48}$$

and the gap parameter Δ_0 satisfies the following equation

$$\Delta_0 = \lambda\left\{\left[(\Delta_0 + \Delta_e) - \mu\frac{(\Delta_0+\Delta_e)^2}{4|t_0^*|^2}\right]\ln\frac{W^*}{|\Delta_0+\Delta_e|} + \mu t_0^*\right\} \tag{3.49}$$

where $W^* = 4t_0^*$ and $t_0^* = t_0(1 + \mu\nu)$, $\nu = \frac{\Delta t}{2t_0}$. The lowest order perturbation solution of Eq. (3.49) is

$$\Delta_0 = \pm We^{-\frac{1}{\lambda}} + \mu t_0 + (\frac{1}{\lambda} - 1)\Delta_e\ . \tag{3.50}$$

The local minima of the system energy occur at the values shown in Eq. (3.50). The energy difference between these two unequal minima per unit site is

$$\frac{\Delta E}{N} = -\frac{4}{\pi}\left[\frac{\mu}{\lambda} + \frac{\nu}{2}\right]We^{-\frac{1}{\lambda}}, \tag{3.51}$$

which is similar to that obtained in the modified SSH model (Eq. (2.71)), except that here the factor $(\frac{\mu}{\lambda} + \frac{\nu}{2})$ replaces $(\frac{\mu}{\lambda} + \nu)$ in the discrete model.

From Eqs. (3.48) and (3.49), it is easy to verify an inherent symmetry for the nondegenerate system: changing the signs of both Δt and $\Delta\alpha$ results in Δ_0 changing sign accordingly, but the electron spectrum remains invariant. This is obvious since changing the signs of both Δt and $\Delta\alpha$ is equivalent to interchanging type-I and type-II bonds, and all the physical properties should therfore remain the same.

For systems in which both ν and μ are not equal to zero, there are no known analytical solutions for polarons and bipolarons, but there are solutions for systems with $\mu = 0$, and $\nu \neq 0$. Examining the Eqs. (3.50) and (3.51), we find that $\frac{\mu}{\lambda}$ has the same effect as $\frac{\nu}{2}$ in the dimerized case, so we can discuss such a system qualitatively even if we set $\mu = 0$.

5. Solutions for Polarons, Soliton Pairs and Bipolarons

In this section we will use the equations obtained in section 2.4 (with $\mu = 0$ and $\nu \neq 0$) to discuss general solutions for polarons, bipolarons and soliton pairs. The solutions depend on both the electron occupation of the gap states and the values of ν, where we recall $\nu = \frac{\Delta_e}{2t_0}$. If there is an extra electron or a hole in the system, there exists a polaron solution in both degenerate ($\nu = 0$) and nondegenerate ($\nu \neq 0$) systems. If there are two extra electrons, or two holes, or an electron-hole pair in the system, the resulting solutions will be

fo soliton pairs in the degenerate system ($\nu = 0$), or bipolarons in the nondegenerate system ($\nu \neq 0$).

The lattice displacement pattern $\Delta(x)$ for all of these solutions is commonly described by[59]

$$\Delta(x) = \Delta_0+\chi(\Delta_0+\Delta_e)\left|\tanh\frac{\chi}{\xi}(x-x_0) - \tanh\frac{\chi}{\xi}(x+x_0)\right|, \tag{3.52}$$

where in this model the coherence length $\xi = \frac{V_F}{(\Delta_0+\Delta_e)}$ and $2x_0$ is the characteristic width of the distortion range. The dimensionless shape parameter χ, which depends on the type of solutions, will be determined later. The potential of the Schrödinger-like equation, Eq. (3.23), is related to $\Delta(x)$ by

$$V(x) = [\Delta(x)+\Delta_e]^2 + \tau_3 V_F\frac{\partial\Delta(x)}{\partial x} .$$

$V(X)$ is required to be "reflectionless", a condition arising from minimization of the total energy with respect to the electron reflection coefficients.[60,61] Such a potential and its corresponding wave functions are constructed by means of the inverse scattering method.[62] To satisfy the reflectionless-ness, condition, the following relation should be obeyed for $\Delta(x)$ defined in Eq. (3.52),

$$\chi = \tanh\frac{\chi}{\xi}2x_0 . \tag{3.53}$$

Then, the reflectionless potential $V(x)$ has the following form:

$$V(x) = (\Delta_0+\Delta_e)^2\left\{1 - 2\chi^2\begin{bmatrix}\operatorname{sech}^2\frac{\chi}{\xi}(x+x_0) & 0\\ 0 & \operatorname{sech}^2\frac{\chi}{\xi}(x-x_0)\end{bmatrix}\right\}. \tag{3.54}$$

For this potential, the eigenvalue problem in Eq (3.46) allows two localized levels with energy

$$\epsilon_0 = (\Delta_0 + \Delta_e)(1-\chi^2)^{\frac{1}{2}} \tag{3.55}$$

and the wave functions

$$f_-(x) = \sqrt{\frac{\chi}{2\xi}}\operatorname{sech}\frac{\chi}{\xi}(x+x_0)$$

$$f_+(x) = \sqrt{\frac{\chi}{2\xi}}C_0\operatorname{sech}\frac{\chi}{\xi}(x-x_0) \tag{3.56}$$

with $C_0 = i\,\mathrm{sgn}(\epsilon_k)$. The energy spectrum for the conduction and valence bands has the same form as that of the dimerized case

$$\epsilon_k = \pm(V_F^2 k^2 + (\Delta_0 + \Delta_e)^2)^{\frac{1}{2}} . \tag{3.57}$$

The wave functions of the former, however, are distorted in the presence of the lattice distortion,

$$f_-(x) = A_k[\frac{\chi}{\xi}\tanh\frac{\chi}{\xi}(x+x_0) - ik\,]e^{ikx}$$

$$f_+(x) = A_k C_k[\frac{\chi}{\xi}\tanh\frac{\chi}{\xi}(x-x_0) - ik\,]e^{ikx} \tag{3.58}$$

where the normalization factor A_k is obtained from Eq. (3.26),

$$A_k = \left|(k^2 + \left[\frac{\chi}{\xi}\right]^2)(L + \frac{d\,\delta(k)}{dk})\right|^{-\frac{1}{2}} \tag{3.59}$$

with

$$\delta(k) = 2\cot^{-1}\left|\frac{k\xi}{\chi}\right| \tag{3.60}$$

and the phase factor C_k is written as

$$C_k = \mathrm{sgn}(\epsilon k)e^{i\phi(k)} \tag{3.61}$$

with

$$\phi(k) = \cot^{-1}(k\xi) . \tag{3.62}$$

The values of the wave vectors are determined from the boundary condition of Eq (3.17), with $M = 2$ in the present situation,

$$kL + \delta(x) = 2n\pi \qquad -\frac{\pi}{2a} \leqslant k < \frac{\pi}{2a} . \tag{3.63}$$

By substituting of the wave functions in Eqs. (3.56) and (3.58) into Eq. (3.47) and noting that $\mu \equiv 0$ in the present discussion, we obtain the self-consistency condition,

$$\frac{\pi}{4}(n_+ - n_-) + \cos^{-1}\chi = \gamma\frac{\chi}{\sqrt{1-\chi^2}} , \tag{3.64}$$

where the confinement parameter $\gamma \equiv \dfrac{\Delta_e}{\lambda(\Delta_0 + \Delta_e)}$, and n_+ and n_- are the electron occupation numbers of the discrete levels with energy $+\epsilon_0$ and $-\epsilon_0$, respectively. As in the dimerized case, the gap parameter Δ_0 satisfies

$$\frac{1}{\lambda} = -\ln\frac{|\Delta_0 + \Delta_e|}{W} + \gamma . \tag{3.65}$$

Eq. (3.64) is important in using the electron configuration to calculate the shape parameter χ, which in turn determines the shape of distortion. For the cases of a negative polaron with an extra electron located at the $+\epsilon_0$ level and a positive

polaron with a hole at the $-\epsilon_0$ level (see Fig. 9),

$$n_+ - n_- = -1 \tag{3.66}$$

For the case of a soliton pair or a bipolaron (see Figs. 10 and 11), there are three kinds of electron configuration in the gap states: double negatively charged, double positively charged and neutral, all obeying the relation,

$$n_+ - n_- = 0 \, . \tag{3.67}$$

In the following situations, χ can be calculated:

(a). Degenerate system ($\gamma = 0$)

(1). polaron case ($n_+ - n_- = -1$)

$$\chi = \frac{\sqrt{2}}{2} \tag{3.68}$$

(2). soliton pair ($n_+ - n_- = 0$)

$$\chi = 1 \tag{3.67}$$

(b). Nearly degenerate systems ($\gamma \neq 0$) use $\gamma = 0.13$, which is estimated from experiment for polythiophene[63]

(1). polaron case ($n_+ - n_- = -1$)

$$\chi = 0.629 \tag{3.70}$$

(2). bipolaron case ($n_+ - n_- = 0$)

$$\chi = 0.938 \tag{3.71}$$

It is worthwhile to point out that from Eq. (2.72), Δt must be less

than $0.12eV$ (for $\lambda = 0.4$) to produce near degeneracy, which corresponds to $\gamma < 0.46$. Previous estimations γ are too large to represent the physical case.[58,64]

In summary, we find that the shape parameter χ plays an important role in determining the type of solutions. When $\chi = 0$, $\Delta(x) = \Delta_0$, $x_0 = 0$, and $\epsilon_0 = \pm(\Delta_0 + \Delta_e)$, which implies a dimerized solution. On the other hand, when $\chi \to 1$, $x_0 \to \infty$ and $\epsilon_0 \to 0$, which implies the existence of the solution for two infinitely separated solitons.

6. Formation Energy

In this section we calculate the formation energy of a polaron, a bipolaron, or a soliton pair, which are the lowest excited states of the system for the different electronic configurations. The formation energy is defined as the energy difference between the system containing a quasiparticle and the ground state system (i.e. dimerized state). The calculation is divided into three sections: the lattice part, the electronic part of extended states and the electronic part of localized states.

The contribution of the lattice part is directly calculated,

$$\delta E_{\text{lat.}} = \frac{1}{\pi\lambda V_F} \int_{-\frac{L}{2}}^{\frac{L}{2}} dx\,(\Delta^2(x) - \Delta_0^2)$$

$$= \frac{4(\Delta_0 + \Delta_e)}{\pi} \left[-\frac{\chi}{\lambda} + \gamma \frac{2\chi(\Delta_0 + \Delta_e)x_0}{V_F} \right] \tag{3.72}$$

The contribution of the localized states depends on the electron occupation,

$$\delta E_{\text{loc.}} = (\Delta_0 + \Delta_e)\sqrt{1-\chi^2}(n_+ - n_-) \tag{3.73}$$

where n_+ and n_- are defined as in Eq. (3.64). When we deal with the extended states, we should notice that one-half state disappears from the conduction band and one-half from the valence band, and as a result the disappeared state becomes a localized state. Hence the valence band in the dimerized case has two more electrons than it does in the presence of a polaron or a soliton pair (a bipolaron). Furthermore, the wave vectors of the two cases satisfy different relations:

$$kL = 2\pi m \tag{3.74}$$

for the dimerized case, whereas

$$kL + 2\cot^{-1}\frac{k\xi}{\chi} = 2\pi m \tag{3.75}$$

for polaron, soliton pair, or bipolaron, where $\cot^{-1}\frac{k\xi}{\chi}$ is $(-\pi, \pi]$. The contribution to the formation energy from the extended states is written as

$$\delta E_{\text{ext.}} = 2\left\{\sum_k E_q - \sum_k E_d - [-(\Delta_0 + \Delta_e)]\right\}, \tag{3.76}$$

where the first two summations have exactly the same items and the last term accounts for the extra state in the dimerized case. To compute the first two terms, the phase shifts of the wave function solutions must be determined by comparing their asymptotic behavior for large x (i.e. $|x| \gg \xi$) with the

solutions in the dimerized state.[12] We obtain

$$k'L + \delta(k') = 2\pi m = kL \tag{3.77}$$

where k' is the wave number for the state bearing the quasi-particle, and k is for the dimerized state. By comparing Eqs. (3.75) and (3.74), we find $\delta(k') = 2\cot^{-1}(\frac{k'}{\chi})$, $-\pi < \delta(k') \leqslant \pi$. The contribution from the first two terms of Eq. (3.76) for the extended states is

$$\sum_{k'} E_q(k') - \sum_{k} E_d(k) = \sum_{k} \frac{dE}{dk} \frac{\delta(k)}{L}$$

$$= \frac{4(\Delta_0+\Delta_e)}{\pi}\left[-\frac{\pi}{2} + \chi + \chi\ln\frac{W}{|\Delta_0+\Delta_e|} + \sqrt{1-\chi^2}\cos^{-1}\chi\right]. \tag{3.78}$$

Combining Eqs. (3.72), (3.73), (3.76) and Eq. (3.78), the formation energy is seen as the sum of its three constituent parts,

$$\delta E = \delta E_{\text{ext.}} + \delta E_{\text{loc.}} + \delta E_{\text{lat.}}$$

$$= \frac{4(\Delta_0+\Delta_e)}{\pi}\left[\chi(1-\frac{1}{\lambda} + \ln\frac{W}{|\Delta_0+\Delta_e|}) + \sqrt{1-\chi^2}\cos^{-1}\chi\right.$$

$$\left. + 2\gamma\frac{\chi(\Delta_0 + \Delta_e)x_0}{V_F} + \frac{\pi}{4}(n_+ - n_-)\sqrt{1-\chi^2}\right]. \tag{3.79}$$

Two conditions obtained from Eq. (3.79) by setting $\frac{\partial}{\partial\Delta_0}\Delta E = 0$ and $\frac{\partial}{\partial\chi}\Delta E = 0$ are

$$\frac{\sqrt{1-\chi^2}}{\chi}\left[-\frac{1}{\lambda} + \ln\frac{W}{|\Delta_0+\Delta_e|} + \frac{1}{1-\chi^2}\gamma\right] - \left[\cos^{-1}\chi + \frac{\pi}{4}(n_+ - n_-)\right] = 0 \tag{3.80}$$

and

$$\left[-\frac{1}{\lambda} + \ln\frac{W}{|\Delta_0+\Delta_e|}\right]\frac{\chi}{\sqrt{1-\chi^2}} + \cos^{-1}\chi + \frac{\pi}{4}(n_+ - n_-) = 0 . \qquad (3.81)$$

From Eqs. (3.80) and (3.81), we again obtain the self consistency condition (3.64) and the gap equation (3.65).

Using Eqs. (3.64) and (3.65), Eq. (3.79) for the total excitation energy becomes,

$$\Delta E = \frac{4(\Delta_0 + \Delta_e)}{4}\left[\chi(1 - \gamma) + 2\gamma\frac{\chi(\Delta_0 + \Delta_e)x_0}{V_F}\right.$$

$$\left. + \sqrt{1-\chi^2}\cos^{-1}\chi + \frac{\pi}{4}(n_+ - n_-)\sqrt{1-\chi^2}\right]$$

$$= 4(\Delta_0 + \Delta_e)\left[\chi + 2\gamma\frac{\chi(\Delta_0 + \Delta_e)x_0}{V_F}\right] . \qquad (3.82)$$

From the above derivation, we see that the lattice part of the formation energy is reduced by the distortion whereas the electronic part is increased, resulting in a positive net energy gain. In the degenerate system where $\Delta_e = 0$ and $\gamma = 0$, we obtain the formation energy

$$\Delta E = \frac{2\sqrt{2}}{\pi}\Delta_0$$

for a polaron, and

$$\Delta E = \frac{4}{\pi}\Delta_0 \qquad (3.84)$$

for a soliton-antisoliton pair. The formation energy for a polaron or a bipolaron in the nearly degenerate system depends on the value of γ determined

from Eq. (3.64) supplemented by the conditions Eqs. (3.70) and (3.71). The relations of the formation energy ΔE and the confinement parameter γ is plotted in Fig. 15.

From the above description, we see that the polaron creation energy in the degenerate system is $\frac{2\sqrt{2}}{\pi}\Delta_0$, which is less than the energy needed to add one charge to perfectly dimerized system ($E = \Delta_0$), so it is always energetically favorable for an electron or a hole to self-trap and form a polaron in this quasi-one dimensional system. Adding a second charge to the chain may form a second polaron, however, and the two polaron state is unstable. Because the creation energy of a soliton pair $\frac{4}{\pi}\Delta_0$ is less than two polaron energy ($2E_p = \frac{4\sqrt{2}}{\pi}\Delta_0$), it is energetically favorable to produce a soliton pair instead of two polarons. Similar situations happen for the optical absorption of a photon, which leads to dynamical soliton pair generation.

7. Two Polaron Solution

In this section, part of two polaron solution is presented; it compared later with the results obtained in the Chapter V. The displacement pattern of the two-polaron solution is written as [59,65]

$$\Delta(x) = \Delta_0 + (\Delta_0 + \Delta_e)\left[\frac{\chi_1^2 - \chi_2^2}{\chi_1 \coth(\frac{\chi_1}{\xi}x - \beta_1) - \chi_2 \coth(\frac{\chi_2}{\xi}x - \beta_2)}\right.$$

$$\left. - \frac{\chi_1^2 - \chi_2^2}{\chi_1 \coth(\frac{\chi_1}{\xi}x + \beta_1) - \chi_2 \coth(\frac{\chi_2}{\xi}x + \beta_2)}\right] \qquad (3.85)$$

where

$$\tanh 2\beta_j = \chi_j \qquad j = 1, 2 \tag{3.86}$$

and the energies ϵ_1 and ϵ_2 of the localized states are related to the parameters χ_1 and χ_2 by

$$\epsilon_j = (\Delta_0 + \Delta_e)\sqrt{1 - \chi_j}\ . \tag{3.87}$$

The distance between these two polarons is given approximately by

$$d = \frac{\xi}{\chi_1 + \chi_2} \ln \left| \frac{\chi_1^{\frac{1}{2}} + \chi_2^{\frac{1}{2}}}{\chi_1^{\frac{1}{2}} - \chi_2^{\frac{1}{2}}} \right| \tag{3.88}$$

For the infinitely separated polaron pair, the difference $\chi_1 - \chi_2$ is equal to zero, corresponding to two independent polarons, each of which admits two discrete states. When the polarons approach to each other, the difference $\chi_1 - \chi_2$ appears and the two degenerate discrete states of these two polarons are split into four discrete states. The separation can approach zero only when χ_2 is equal to zero, which implies that the discrete state ϵ_2 is returned to the valence band and only two localized states are left inside the gap. This indicates that a bipolaron (or a soliton pair) is produced to carry the charges of the two polarons.

The creation energy of two polarons is

$$E_{2p} = \frac{4(\Delta_0 + \Delta_e)}{\pi} \sum_{j=1,2} \left\{ \chi_j(1-\gamma) + 2\gamma\beta_j \right.$$

$$+ \sqrt{1 - \chi_j}(\cos^{-1}\chi_j + \frac{\pi}{4}(n_{+,j} - n_{-,j}))\Big\}, \qquad (3.89)$$

which from Eq. (3.82) is always more than the creation energy of a bipolaron (or a soliton pair). Thus, it is energetically favorable to form a bipolaron (or a soliton pair in the degenerate system) from two polarons. Fig. 14 depicts a picture for two polarons, where the four localized gap states are located symmetrically around the mid-gap; and the electron configuration of these states plays an essential role in determining the properties of the polarons.

CHAPTER IV

Photogenerated Exciton-Breather State in *Trans*-Polyacetylene

In this chapter, we perform a dynamical simulation of photogenerated excitations in *trans*-polyacetylene by using the SSH-extended Hubbard model. We find that depending on the energy gained by the system two possible excited states may be photogenerated. If the system energy is higher than a critical value, the photogenerated soliton-antisoliton pairs and are free to separate, leaving behind a central breather mode. If the system energy is lower than the critical value, the soliton-antisoliton pairs will bind and form a different central oscillation: an exciton-breather. The critical energy is slightly above the soliton pair creation energy. These results are then discussed and compared with experiment.

1. Introduction

It is well known[42,43,66,67] that the Coulomb interaction plays an important role in the formation of the soliton in *trans*-polyacetylene $(CH)_x$. Many authors[44,45,68,69] have discussed the static effects of electron-electron Coulomb interaction in the framework of the SSH Hamiltonian,[8] but the dynamical effects have not yet been considered. Recently, Rice and Howard[10,36] performed a semi-

phenomenological calculation which suggested that photogenerated solitons will bind and form a solitonic exciton. Grabowski, Hone and Schrieffer[69] used a first-order perturbation treatment to prove the existence of an excitonic bound state which has lower potential energy than a well-separated soliton-antisoliton pair, and they concluded that oppositely charged soliton-antisoliton pairs do form excitonlike bound states.

Recent experimental findings[14,15,13,70] support these conclusions. The strong temperature dependence of the photoconductivity and the absorption peak observed at 1.35*ev* suggest that the photoexcited electron-hole pairs decay into different excited states at different temperatures. The infrared absorption peaks at about 500 cm^{-1} in $trans-(CH)_x$ and at 400 cm^{-1} in $trans-(CD)_x$, which were previously assigned to the "pinned" translation mode of the soliton by comparison with infrared spectra of chemically doped samples, may be more appropriately interpreted as vibrational modes around the excitonlike bound state.

Many numerical dynamical simulations[71,72,73,74] have been performed using the pure SSH model to explore the dynamical features of soliton formation. Perhaps the most interesting of these was done by Bishop, *et al*.[74] They found that the soliton has a maximum velocity on the order speed of the sound. Because the kinetic energy has this upper limit, the excess energy of the system forms a breather, leaving behind well-separated photogenerated solitons. Bishop, *et al* claim this breather to be responsible for the 1.35*ev* absorption peak. However, since there is no essential difference between photogeneration and doping in the pure SSH model calculation, and the 1.35*eV* absorption peak is absent

in the case of doping, it is necessary to include the effect of electron-electron interactions in order to test this claim adequately.

This chapter presents a dynamical simulation of photogeneration in the presence of electron-electron interactions in *trans*-polyacetylene. We find that a photoinduced electron-hole pair may decay into an exciton-breather state if the system energy is less than the creation energy of a well-separated soliton pair and greater than that of the excitonic bound state. (The system energy is measured with respect to that of the perfectly dimerized ground state in this paper.) It is necessary here to draw a clear distinction between this "exciton-breather state" and the central breather found by Bishop *et al*[74]. The exciton-breather is a symmetric oscillation of the bound soliton pair along the chain about the exciton center. Such a mode is also found in photoexcited states of non-degenerate linear chains[17]. If the system energy is above the threshold for soliton pair creation, both the soliton pairs and the central breather mode of the separated soliton antisoliton pair are produced. The soliton pairs are not free to separate, however, unless the system energy is large enough. In the following sections we discuss the photogenerated state, the perturbative calculation, the numerical technique and the main results.

2. Photogenerated Soliton State

The model Hamiltonian employed for our calculation is the standard SSH Hamiltonian with the added extended Hubbard terms, presented in Section 2.6. Dimerization owing to Peierls instability opens a gap in the π energy band structure at the Fermi surface. The number of π electrons of the system is

equal to that of the sites, and all the π electrons are in the valence band below the gap in the ground state. The ground state is degenerate, and this degeneracy is not destroyed by the Coulomb interaction. Thus solitons can still be generated. After an electron-hole pair is photogenerated, the single electron spectrum is changed by the lattice distortion. The potential energy of the system is lowered and a charged soliton-antisoliton pair is formed. The single electron energy spectrum in the presence of soliton pairs has two localized levels that have been shifted from the top of the valence band and the bottom of the conduction band and now located symmetrically with respect to the gap center. The two levels are singly occupied and have opposite spins.

First, we describe the dynamical process of photogeneration of a soliton-antisoliton pair. Upon absorption of a photon with energy $\hbar\omega \sim E_g = 2\Delta_0$, the system is excited, and an electron is transited from the top of the valence band to the bottom of the conduction band. Since the transition time is short compared to the lattice relaxation time, the lattice is assumed to remain in its original dimerized state (the Franck - Condon approximation). This excited state with an electron-hole pair is unstable against the formation of a soliton-antisoliton pair. It is taken as the initial condition in the dynamical simulation.

Two possible soliton-antisoliton states can be photogenerated; neutral or oppositely charged. But according to experiment and theoretical analysis [27,28,75], the photogeneration of neutral soliton pairs is forbidden in the direct process and is almost forbidden in the indirect process with a neutral-to-charged branching ratio of about the order 10^{-2}. This fact can be understood by the resource to inversion symmetry and the Pauli exclusion principle.

Because the valence band plays no essential role, we focus on the gap states (bonding state ψ_+ and antibonding state ψ_- with energy ϵ_+ and ϵ_- respectively, $\epsilon_+ < \epsilon_-$), which are split from the conduction and valence bands during the dynamical process. The photogeneration of the gap states is analogous to the photodissociation of molecular hydrogen.

Initially, the system is in its ground state, in which the bonding state ψ_+ is doubly occupied and the electronic wave function is

$$\psi_0(1,2) = \psi_+(r_1)\psi_+(r_2)\chi_{12} , \tag{4.1}$$

where

$$\chi_{12} = (\alpha_1\beta_2 - \alpha_2\beta_2)/\sqrt{2} \tag{4.2}$$

is the singlet spin function. Upon absorbing a photon of energy $\hbar\omega = \epsilon_- - \epsilon_+$, an electron is transited from the ψ_+ state to the ψ_- state, and an electron-hole pair is created. Because the spin-flip time in $(CH)_x$ is longer than the soliton generation time of 10^{-13} sec,[71] the photo-produced pair is always in the singlet state.[76] Its wave function is

$$\psi_x(1,2) = [\psi_-(r_1)\psi_+(r_2) + \psi_+(r_1)\psi_-(r_2)]\chi_{12}/\sqrt{2} , \tag{4.3}$$

where the spatial part of $\psi_x(1,2)$ is even because χ_{12} is odd and the Pauli principle requires $\psi_x(1,2)$ to be antisymmetric in the exchange of 1 and 2. Assuming that the electrons follow the nuclear motion adiabatically, $\psi_x(1,2)$ determines the charges born by solitons as their separation approaches infinity. In the limit of large separation,

$$\psi_{\pm}(r) = [\phi_s(r) \pm \phi_{\bar{s}}(r)]/\sqrt{2} \tag{4.4}$$

where $\phi_s(r)$ is the bound state localized on the soliton and $\phi_{\bar{s}}(r)$ is the bound state localized on the antisoliton. Thus,

$$\psi_x(1,2) = [\psi_s(r_1)\phi_s(r_2) - \phi_{\bar{s}}(r_1)\phi_{\bar{s}}(r_2)]\chi_{12}/\sqrt{2}\,, \tag{4.5}$$

which means that two electrons have an equal possibility either of doubly occupying the bound state localized on the soliton or the bound state localized on the antisoliton. Thus the soliton is negatively charged and the antisoliton is positively charged in the former case, and vice versa in the latter case. Because ψ_x does not contain a term like $\phi_s(r_1)\phi_{\bar{s}}(r_2)$, it is not possible for the bound states localized on soliton and antisoliton to be both singly occupied at the same time, and therefore photogeneration of a neutral soliton pair is forbidden.

In polyacetylene, oppositely charged soliton-antisoliton pairs can be described using the spin-singlet state,[28,69]

$$\Psi_x = (\Psi_{+-} + \Psi_{-+})/\sqrt{2}, \tag{4.6}$$

with

$$\Psi_{\alpha\beta} = c^{\dagger}_{\alpha\uparrow} c^{\dagger}_{\beta\downarrow} |V\rangle, \tag{4.7}$$

and

$$|V\rangle = \prod c^{\dagger}_{k\uparrow} c^{\dagger}_{k\downarrow} |0\rangle\,. \tag{4.8}$$

Here $c^{\dagger}_{+\sigma}$ ($c^{\dagger}_{-\sigma}$) is the creation operator of an electron with spin σ in a bonding (antibonding) localized state with the energy lower (higher) than the gap center, and the operator $c^{\dagger}_{k\sigma}$ creates an electron with spin σ in the molecular orbital k inside the valence band. The valence band is fully occupied by N - 2 spin-paired

electrons, where N is the number of π electrons of the system and is even.

Following Ref. 8, we first transform the site electron operators $c_{n\sigma}$ into molecular orbital operators $c_{k\sigma}$. They have the relation

$$c_{n\sigma} = \sum_{k'} a_{n\sigma}^{k'} c_{k'\sigma} , \tag{4.9}$$

with k' summed over the entire electron spectrum. Since the electron distributions for each spin are the same in this case, the spin degeneracy of the single electron energy is maintained. We will drop the spin subscript σ below. The electron part of the system energy of the excited state Ψ_x can be obtained directly,

$$E^{el} = \langle \Psi_x | H^{el} | \Psi_x \rangle = \epsilon_0 + \epsilon_c , \tag{4.10}$$

with the Hartree-Fock part ϵ_0 written as

$$\epsilon_0 = \frac{1}{2}(\langle \Psi_{+-} | H^{el} | \Psi_{+-} \rangle + \langle \Psi_{-+} | H^{el} | \Psi_{-+} \rangle) , \tag{4.11}$$

and the correlation part ϵ_c written as

$$\epsilon_c = \frac{1}{2}(\langle \Psi_{+-} | H^{el} | \Psi_{-+} \rangle + \langle \Psi_{-+} | H^{el} | \Psi_{+-} \rangle) . \tag{4.12}$$

To write the explicit results in a short form, we define charge density parameters and bond parameters at each site as

$$D_n^v = \sum_k | a_n^k |^2$$

$$D_n^+ = D_n^v + | a_n^+ |^2 , \tag{4.13}$$

$$D_n^- = D_n^v + |a_n^-|^2,$$

$$P_n^v = \sum_k (a_n^k)^* a_{n+1}^k,$$

$$P_n^+ = P_n^v + (a_n^+)^* a_{n+1}^+, \tag{4.14}$$

$$P_n^- = P_n^v + (a_n^-)^* a_{n+1}^-,$$

where k is summed over the valence band. The Hartree-Fock part and the correlation part of the electron energies can be expressed as

$$\epsilon_0 = \left| -\sum_n t_n (P_n^+ + P_n^-) + \text{c.c} \right| + U \sum_n D_n^+ D_n^-$$

$$+ V \sum_n \left\{ D_n^+ D_{n+1}^- + D_n^- D_{n+1}^+ + D_n^+ D_{n+1}^+ + D_n^- D_{n+1}^- \right.$$

$$\left. - |P_n^+|^2 - |P_n^-|^2 \right\} \tag{4.15}$$

$$\epsilon_c = U \sum_n |a_n^+|^2 |a_n^-|^2 + 2V \sum_n (a_n^-)^* a_n^+ (a_{n+1}^+)^* a_{n+1}^-. \tag{4.16}$$

In order to calculate the single electron energy spectrum, we make use of the mean field approximation to get the effective one electron Hamiltonian,

$$H_{\text{eff}}^{\text{el}} = \sum_{n,\sigma} \left\{ -t_n - V \frac{P_n^+ + P_n^-}{2} \right) c_{n+1,\sigma}^{\dagger} c_{n,\sigma} \Big| + h.c.$$

$$+ \sum_{n,\sigma} \left\{ U \frac{D_n^+ + D_n^-}{2} \right.$$

$$+ V\ (D_{n+1}^{+} + D_{n+1}^{-} + D_{n-1}^{+} + D_{n-1}^{-})\Big] c_{n',\sigma}^{\dagger} c_{n,\sigma} \tag{4.17}$$

To eliminate end effects the periodical boundary conditions are used, $D_{N+1}^{\pm} = D_1^{\pm}$, $D_0^{\pm} = D_N^{\pm}$. The matrix form of H_{eff}^{el} is Hermitian and tridiagonal; it can be diagonalized by a unitary matrix A, whose elements a_n^k are defined in Eq. (4.9). Because the elements of the matrix $h_{n',n} \equiv <0|c_{n'} H_{\text{eff}}^{\text{el}} c_n^{\dagger}|0>$ contain a_n^k, the matrix equation can be iterated to obtain selfconsistency. In practice, a selfconsistent result can be obtained if by assuming the matrix is real and symmetric. This means that the $P_n^{\pm}$ are real and the transformation matrix A is real orthogonal, which is consistent with the original assumptions. We also find that charge conjugation symmetry is not broken in this particular case if the Coulomb terms are included, as can be seen from Eq. (4.17). If we assume $D_n^{+} = D_n^{-} = 1/2$ in the H_{eff}^{el}, all the diagonal elements of $h_{n,n}$ become equal. Recalling that the matrix form of $H_{\text{eff}}^{\text{el}}$ is real symmetric tridiagonal, if $\{a_n^k\}$ $(n = 1,...,N)$ is an eigenvector of the matrix, then $\{(-1)^n a_n^k\}$ $(n = 1,...,N)$ should be another eigenvector of the same matrix. This immediately implies that $a_n^{+} = (-1)^n a_n^{-} \equiv a_n^0$, $D_n^{+} = D_n^{-} = 1/2$, and $\frac{P_n^{+} + P_n^{-}}{2} = P_n^{v}$, from which selfconsistency is obtained. The constant charge density is a result of Eq. (4.6), where the soliton (antisoliton) has an equal probability of being positively (negatively) charged or negatively (positively) charged. The above analysis allows us to simplify our computation procedure. Moreover, because the equal constant elements of $h_{n,n}$ have no effect on the calculation except to shift the energy scale, we can drop all the constant terms and set all the $h_{n,n} = 0$ in the computation.

Using all the simplifications in the analysis above, Eqs. (4.15), (4.16) and (4.17) become

$$\epsilon_0 = -2\sum_n t_n (P_n^v + (P_n^v)^*)$$

$$- 2V \sum_n \left\{ |P_n^v|^2 + |a_n^0|^2 |a_{n+1} su\, 0|^2 \right\} \tag{4.18}$$

$$\epsilon_c = U \sum_n |a_n^0|^4 - 2V \sum_n |a_n^0|^2 |a_{n+1}^0|^2 \tag{4.19}$$

and

$$H_{\text{eff}}^{el} = \sum_{n,\sigma} \left\{ -t_n - V P_n^0 \right) c_{n+1,\sigma}^{\dagger} c_{n,\sigma} + h.c. \Big\} \tag{4.20}$$

3. Perturbation Results

There are no exact solutions for Eqs. (4.18) and (4.19) in the presence of the Coulomb interaction, but we can make use of the analytical solution of the TLM model shown in Eq. (3.52), and treat the extended Hubbard terms as perturbation terms. This is justifiable when U and V are small compared with the bandwidth $4t_0$, which is the case in polyacetylene. The results given in section 2.4 can be applied straightforwardly here if we set $\Delta_e = 0$, which implies $\gamma = 0$, except that in the presence of the Coulomb interaction, we have two independent parameters Δ_g and Δ_0 whereas in the absence of the Coulomb interaction there is but a single parameter Δ_0. The gap parameter Δ_g represents half of the Peierls gap and the dimerization parameter Δ_0 is related to u_0, the magnitude of the uniform dimerization, through the relation $\Delta_0 = 4\alpha u_0$. The

coherence length ξ is related to the gap parameter through $\xi = \frac{V_F}{\Delta_g}$.

To proceed, we transform Eqs. (4.18) and (4.19) to continuum form by using the relations

$$a^k_{2n} = (-1)^n \sqrt{a}\, f^k_+(x)$$

$$a^k_{2n+1} = (-1)^n i \sqrt{a}\, f^k_-(x) \tag{4.21}$$

which are easily obtained from Eqs. (3.3) and (3.18). Thus, if

$$\epsilon = \epsilon_0 + \epsilon_c \tag{4.22}$$

then

$$\epsilon_0 = \int dx \sum_k \left[f^k(x)\right]^\dagger \left\{-iV_F \frac{\partial}{\partial x}\tau_1 + \Delta(x)\tau_2\right\} f^k(x) + \frac{1}{\lambda \pi V_F}\int \Delta^2(x)dx$$

$$-2Va\int dx \left|\sum_k \left[f^k_+(x)\right]^* f^k_-(x)\right|^2 + \left|f^0_+(x)\right|^2 \left|f^0_-(x)\right|^2 \tag{4.23}$$

$$\epsilon_c = \int dx \left\{\frac{1}{2}Ua\left[\left|f^0_+(x)\right|^4 + \left|f^0_-(x)\right|^4\right] - 2Va\left|f^0_+(x)\right|^2 \left|f^0_-(x)\right|^2\right\}. \tag{4.24}$$

In the dimerized case, the energy calculated from Eqs. (4.21), (4.22) and (4.23) is

$$\epsilon = \frac{L}{\pi V_F}\left\{-W\sqrt{W^2+\Delta_g^2} + (\Delta_g^2 - 2\Delta_0\Delta_g)\ln\frac{W}{\Delta_g}\right.$$

$$\left. + \frac{1}{\lambda}\Delta_0^2 - v\,\Delta_g^2 \ln\frac{W}{\Delta_g}\right\}, \tag{4.25}$$

where the dimensionless Coulomb strength $v = \frac{V}{\pi t_0}$, and $u = \frac{U}{\pi t_0}$ (definitions

that will be used later).

The parameters Δ_0 and Δ_g are determined from the equations $\frac{\partial \epsilon}{\partial \Delta_0} = 0$ and $\frac{\partial \epsilon}{\partial \Delta_g} = 0$, which give

$$\Delta_0 = \lambda \Delta_g \ln \frac{W}{\Delta_g} \tag{4.26}$$

and

$$\ln \frac{W}{\Delta_g} = \frac{1}{\lambda + \nu} \tag{4.27}$$

The creation energy of the photogenerated soliton pair state is obtained through a procedure similar to that described in Section 3.5,

$$\epsilon(\chi) = \epsilon_0(\chi) + \epsilon_c(\xi) \tag{4.28}$$

$$\epsilon_0(\chi) = \frac{4\Delta_0}{\pi}\left[\chi + \sqrt{1-\chi^2}\cos^{-1}\chi - \nu\left(\frac{\pi^2}{4} + (\cos^{-1}\chi)^2\right)(\tanh^{-1}\chi - \chi)\frac{(1-\chi^2)}{\chi^2}\right] \tag{4.29}$$

$$\epsilon_c(\chi) = \frac{4\Delta_0}{\pi}\left[\mu\frac{\pi^2}{24}\chi - \nu\frac{\pi^2}{4}(\tanh^{-1}\chi - \chi)\frac{1-\chi^2}{\chi^2}\right] \tag{4.30}$$

Eq. (4.27) has a minimum value related to the coulomb interaction strengths U and V. For instance, $\chi = 0.9184$ when $U = 4.0\ eV$ and $V = 1.5\ eV$. For values of χ other than 1, the soliton separation $2x_0 = \frac{\xi}{\chi}\tanh^{-1}\chi$ (see Eq. (3.53)) is finite. Thus, the existence of a minimum energy value suggests that the soliton pair is bounded and forms an "excitonic" state.

4. Numerical Technique

The equation of motion is integrated within the adiabatic (Born-Oppenheimer) approximation. According to Monte Carlo simulations and quantum fluctuation studies of polyacetylene, this approximation is justified if the Coulomb interaction strength U is less than $2t_0$.[77,78] This is reasonable because the ion mass is much greater than the electron mass and the Peierls gap is less than the typical optical phonon energy.[34]

For convenience we define η_n, the staggered displacement order parameter, in terms of the real displacement u_n such that

$$\eta_n = (-1)^{n-1} u_n . \tag{4.31}$$

The equation of motion reads

$$M\ddot{\eta}_n = -K(2\eta_n + \eta_{n+1} + \eta_{n-1}) + F_n^{el}, \tag{4.32}$$

with

$$F_n^{el} = -\frac{\partial}{\partial \eta_n} \langle \Psi_x \mid H^{el} \mid \Psi_x \rangle. \tag{4.33}$$

The major numerical problem is the calculation of the electron force term F_n^{el}. We use the matrix form to illustrate our method. Suppose H is a real symmetric matrix, whose elements are functions of η_n and a_i^k, which are the elements of the transformation matrix A. If A is real orthogonal, and Λ is the diagonalized matrix, with elements λ_k, we have

$$\Lambda = A^{t} H A, \tag{4.34}$$

with

$$A'A = AA' = 1, \tag{4.35}$$

and A' is the transpose matrix of A. Differentiating both sides of Eq. (4.34) with respect to η_n, we have

$$\frac{\partial \Lambda}{\partial \eta_n} = A' \frac{\partial H}{\partial \eta_n} A + G, \tag{4.36}$$

where the elements of G have the following form,

$$g_{k,p} = \sum_s \frac{\partial a_s^k}{\partial \eta_n} a_s^p (\lambda_p - \lambda_k). \tag{4.37}$$

Using Eqs. (4.16) and (4.35) and noticing that the off-diagonal terms of $\frac{\partial \Lambda}{\partial \eta_n}$ and the diagonal terms of G are all equal to zero, we derive the following expression for $\frac{\partial P_n^v}{\partial \eta_m}$:

$$\frac{\partial P_n^v}{\partial \eta_m} = \sum_l K_{n,l} \left(-\frac{\partial t_l}{\partial \eta_m} - V \frac{\partial P_l^v}{\partial \eta_m} \right), \tag{4.38}$$

with

$$K_{n,l} = \sum_{k,p} (a_n^k a_{n+1}^p + a_n^k a_{n+1}^p) \frac{1}{\lambda_k - \lambda_p} (a_l^k a_{l+1}^p + a_l^k a_{l+1}^p), \tag{4.39}$$

where the k-sum is over all the occupied states and the p-sum is over all the unoccupied states. From Eq. (4.39), it is clear that the $K_{n,l}$ are symmetric about n and l and only depend on the eigenvalues and the eigenvectors obtained from Eq. (4.17). Hence we need only calculate them once for each time interval before solving for the derivative. Then the derivatives of P_n^v with respect to different η_m can be obtained through a simple iteration method or by solving a system of linear equations. We should point out that the formulations of Eq.

(4.38) are similar to the formulas from first order perturbation theory, except that the expressions here for $\frac{\partial P_n^v}{\partial \eta_m}$ are exact. $\frac{\partial u_n^0}{\partial \eta_m}$ can be calculated similarly. The use of Eq. (4.38) greatly reduces the necessary CPU time and makes the present simulation possible.

As pointed by Kivelson, *et al*,[45] the Hamiltonian in Eq. (2.59) is unstable with respect to a shrinking of the chain length in the presence of soliton pairs. We add an extra term in addition to the usual linear term[71] to avoid length shrinking:

$$H' = A\left\{ \sum_n (u_n - u_{n+1}) + S(u_1 - u_0)^2 + S(u_N + u_0)^2 \right\}, \tag{4.40}$$

where the parameter A is determined by minimizing the energy with respect to the lattice constant in the perfectly dimerized ground state, and the parameter S is chosen to be 0.1 here. Adding this extra S term is equivalent to attaching a spring to each end of the chain. These terms do not affect the lattice distortion patterns in the calculation.

5. Numerical Results

We first study the potential energy in the presence of a soliton pair. In the continuum model[12] there is a solution for the lattice displacement patterns corresponding to a soliton-antisoliton pair which can be used approximately here,[60]

$$\eta(x) = u_0(1 + \chi\{\tanh[\frac{\chi}{\xi}(x - x_0)] - \tanh[\frac{\chi}{\xi}(x + x_0)]\}), \tag{4.41}$$

where (to repeat)

$$\xi_0 = \frac{2t_0 a}{\Delta_0}, \qquad \tanh(2\frac{\chi}{\xi}x_0) = \chi, \tag{4.42}$$

ξ_0 is the coherence length; a is the lattice constant; Δ_0 is the gap parameter for the perfectly dimerized chain; u_0 is the magnitude of the uniform dimerization; $2x_0$ is the soliton-antisoliton separation.

In Fig. 16, the potential energy is plotted against the separation, $2x_0$, of the soliton-antisoliton pair. The curve can be fitted approximately by the function $V(x_0) = -\frac{c}{x_0} + \frac{d}{x_0^2}$. As in classical mechanics, lattice relaxation after photoexcitation depends on the total energy gain. If the total energy is below the height of the potential well, the excitation will be locally trapped. Our simulation is performed for different total system energies.

The basic excitation in each simulation was the transfer of an electron from the top of the valence band to the bottom of the conduction band, with an energy difference of $2\Delta_0$. (Owing to the Coulomb interaction, the total energy gain is actually smaller than $2\Delta_0$. For example, $E_t = 1.963\Delta_0$, when $U = 4.0ev$, and $V = 1.5ev$). Two methods can be used to consider lowering total system energies. We can set all the velocities to zero after several time intervals, or, we can begin not with the perfectly dimerized case, but other lattice configuration by means of Eq. (4.41). The first method may be interpreted as the emission of phonons during the relaxation process, and the latter can be related to the instanton approach,[79] wherein the lattice fluctuates owing to quantum effects before it absorbs a photon whose energy is less than $2\Delta_0$. The two methods are equivalent in the numerical calculation.

The simulations have been performed for different sets of U and V in a chain of 40 atoms. We focus on a typical situation, $U = 4.0eV$, $V = 1.5ev$. The other parameters used here are $t_0 = 2.5eV$, $\alpha = 4.82eV/\text{Å}$, $u_0 = 0.1\text{Å}$, and $K = 18.17eV/\text{Å}^2$. The calculated gap parameter $\Delta_0 = 2.52eV$, which is enlarged by the V term. The creation energy of a well separated soliton-antisoliton pair is about $1.42\Delta_0$, and the creation energy of an excitonic bound state is about $1.37\Delta_0$. For these parameters the dynamical simulations were performed under the following sets of system energies: (a) $E_t = 1.963\Delta_0$(initialized from the dimerized state), (b) $E_t = 1.7693\Delta_0$, (c) $E_t = 1.5311\Delta_0$, (d) $E_t = 1.4526\Delta_0$, (e) $E_t = 1.4458\Delta_0$, (f) $E_t = 1.4389\Delta_0$, (g) $E_t = 1.4325\Delta_0$, (h) $E_t = 1.4265\Delta_0$, (i) $E_t = 1.4210\Delta_0$, (j) $E_t = 1.4157\Delta_0$, and (k) $E_t = 1.4110\Delta_0$.

Because the dynamics are very sensitive to the system energy, it is necessary to ensure that this energy is conserved precisely during the calculation. We use milne's multistep method[80] to integrate the equation of motion so that the calculated system energy fluctuates within $10^{-4}\ \Delta_0$ (i.e., the relative error of the energy is less than 10^{-6}). The time evolution of the system potential energy has different features in each case, (see Fig. 17 and Fig. 18). Fig. 17 has two curves representing case (a) and case (b). The ordinate represents the potential energy and ranges from $1.3\Delta_0$ to $2.0\Delta_0$ for each interval. Fig. 18 has nine curves corresponding to case (c) through case (k) from the top to the bottom respectively. The system energy for each case is stepped down from the top to the bottom. Each interval of the ordinate is scaled from $1.35\Delta_0$ to $1.45\Delta_0$, except for case (c), which is scaled from $1.35\Delta_0$ to $1.55\Delta_0$.

We first consider the lower energy curves (i), (j), and (k). The system energies of these three cases are near or lower than the soliton pair energy. They clearly exhibit a periodic breather behavior. To see this in detail, we display the time evolution in (j) for a typical cycle of the optical components of the staggered displacement order parameters,[74] which are defined as $y_n = \frac{(2\eta_n + \eta_{n+1} + \eta_{n-1})}{4}$ (see Fig. 19 and Fig. 20). In Fig. 19, the exciton-breather expands from time $T = 116$, through $T = 125$ and $T = 137$ to $T = 144$ (in units of 1.25×10^{-15}sec), while the system potential energy goes from a local maximum through a local minimum, another local maximum, and then to a shallow local minimum. In Fig. 20, the breather shrinks from $T = 144$ to $T = 170$, while the system potential energy goes through a similar sequence. The periodicity is about 53 for case (k), about 54 for case (j), and about 55 for case (i), corresponding to $\hbar\omega \approx 500\ cm^{-1}$, in agreement with the observed $500\ cm^{-1}$ mode in the infrared.[15] (When $U = 4.0\ ev$, $V = 3.0\ ev$, the average periodicity is about 49). It is also interesting to note from Figs. 19 and 20 that there exists a small central breather feature around the local minimum energy configuration ($T = 144$).

For cases (c) and (d) in Fig. 17, the time evolution of the potential energy of these two curves has different features than it does for curves (i), (j), and (k) in Fig. 18. There is no exciton-breather feature in this energy region. Rather, a separated soliton-antisoliton pair forms and a central breather appears between the soliton-antisoliton pair. Diagrams of the process at different times for (c) and (d) are plotted in Figs. 21 and 22respectively. The three curves in

Fig. 21 represent the lattice configurations at $T = 209$, $T = 216$ and $T = 223$ with the potential energy reaching a local minimum at $T = 216$. The soliton-antisoliton is quite static; in a period of nearly 200 time steps the pair remains in the same positions, and only the central breather between them oscillates. Fig. 22 corresponds case (c), which has higher system energy than that of case (d). We can see from the figure that the soliton-antisoliton pair now has large separation, tough it is still confined, and has a large scale vibration along the chain with a much longer period than that of the central breather. The confinement is partially due to the Coulomb attraction and is partially due to the the central breather's consumption of excess energy, which would otherwise appear as kinetic energy in the solitons.

The salient difference between the low energy (Figs. 19 and 20) and high energy (Figs. 21 and 22) cases is that the former depicts an exciton oscillating about the center of the chain whereas the latter depicts a fully formed soliton pair with an oscillating breather state superimposed upon them. It is clear that in the low energy cases, the oscillation is in the width of the distortion but in the high energy cases the separation of the solitons may either remain fairly constant (Fig. 20) or may increase (Fig. 21). And the oscillation occurs only the central atoms of the chain.

In Figs. 23 and 24, the time evolutions of the single electron spectra of cases (j) and (d) are compared by plotting the top three levels below the gap center. In Fig. 29, the top state of case (d) becomes a mid-gap state because the appearance of the soliton-antisoliton pairs. The next state in the valence band is shifted into the gap and oscillates with the same frequency as the central

breather. In Fig. 23, the top state for case (j) oscillates near the gap center with the same frequency as the exciton-breather. From the above descriptions, we can conclude that the two types of breathers have different origins. It is also interesting to note that the next state in the valence band for case (j) oscillates near the gap edge, but has a higher frequency than that of the exciton-breather.

Higher system energies are encountered in cases (a) and (b), (see Fig. 17). Here the soliton-antisoliton pairs are no longer confined, but are free to separate, leaving behind a central-breather oscillation. The breather amplitude and the soliton velocity in case (a) are larger than those in case (b). In Fig. 17, the energy oscillations become weak at times near $T = 160$ in (a) and at times near $T = 220$ in (b) because of the collisions of the soliton pairs. This also implies that the soliton velocity is higher in (a) than in (b).

Cases (e), (f), (g) and (h) are in a transition region with a mixture of the properties of cases (d) and (j). The vibration of the exciton-breather slows and a central breather begins appear as the system energy becomes large. These cases will not be described here in detail.

6. Summary and Discussion

In summary, there are three major regions of different dynamical behavior in *trans*-polyacetylene, depending on the total system energy. An exciton-breather appears if the system energy is between the soliton pair creation energy and the low-energy exciton state. As the system energy increases, it is energetically favorable for the exciton-breather to dissociate into a soliton-antisoliton pair. In this energy region the soliton-antisoliton pair forms, but it

is confined. It oscillates along the chain with a large periodicity, and a central breather mode appears between the soliton and antisoliton. At higher system energies, the soliton-antisoliton pair starts to separate, but the central breather still exists. Because this last feature is also found in the pure SSH model simulation,[74] the main effect of including the Coulomb interaction in the analysis is to introduce the possibility of photogenerating an exciton-breather state.

It is worthwhile to point out that a similar result of finding it energetically possible to split the breather into a soliton-antisoliton pair has also been obtained in the driven sine-Gordon system by Lomdahl *et al.*[76] They concluded that large driving forces cause the breather to split into a kink-antikink pair whereas small driving forces cause the breather to go into a stationary mode. This similarity gives reason to believe that the exciton-breather state is an essential excitation in the SSH-extended Hubbard model, and one would be able to obtain an explicit expression of the thresholds for the three regions described above if an analytical solution for the exciton-breather is available.

The agreement between the calculated exciton-breather vibration frequency and the observed infrared activity "pinning" mode at 500 cm^{-1} in *trans*-polyacetylene is one of the principle results of this paper. Moreover, the weak dependence of the exciton-breather frequency on the system energy suggests that the interpretation will survive the quantization of the exciton-breather energy. The dissociation temperature of the exciton into oppositely charged soliton-antisoliton pairs has been estimated to be 120K° by calculating the exciton binding energy.[69] We are unable to estimate this temperature from our dynamical simulations but we believe that the dissociation temperature can

be obtained through quantization of the breather energy. The temperature dependency of the 500 cm^{-1} infrared mode and photoconductivity are further evidence of the existence of the exciton-breather. The overall neutral exciton-breather is not able to produce photoconductivity, but it is the cause of the "pinning" mode, which is why the 500 cm^{-1} mode and photoconductivity can't "coexist" at the same temperature (see Fig. 2 of Ref. 13).

The strong temperature-dependent absorption peak (high-energy peak) at $\sim 1.35eV$ in the photoexcitation[49,81] has been a puzzle for long time. Because the exciton-breather dissociates at high temperature and also because both the second top level in the valence band and the second bottom level in the conduction band shift into the gap and oscillate (see Fig. 23), a natural interpretation would be to attribute this peak to the electronic transition between these two states. This peak has also been interpreted as the electronic transition between the corresponding states in the presence of the central breather[74] (see Fig. 24). A possible solution is some sort of combination of the two interpretations. Examining experiment [49,81], and noticing that the average energy difference between two gap edge states in the exciton-breather case is about $1.82\Delta_0$, which is smaller than that for the central breather case (about $1.88\Delta_0$); that the decay time of the exciton breather is expected to be short; and that the exciton-breather is strongly temperature dependent; we conclude that the exciton-breather plays a major role for the high-energy peak at low temperatures and at short time intervals whereas the central breather is responsible for the bleaching peak at high temperatures and at long time intervals.

CHAPTER V

Bipolaron Dynamics in Nearly Degenerate Quasi One-Dimensional Polymers

In this chapter, we study a nondegenerate conjugated polymer by means of a modified SSH-type model Hamiltonian. Analytical solutions for the ground state were presented in Chapter II. Dynamic equations are solved numerically. We present solutions representing a bipolaron oscillating between two stages (a kink-antikink pair and a bound polaron pair). We show that the creation of such a bipolaron can be energetically favorable in the case of either doping or photoexcitation. Our results compare well with the experimental photoluminescence spectrum of $cis-(CH)_x$.

1. Introduction

The two-fold degeneracy of the ground state[8,82] of $trans-(CH)_x$ (polyacetylene) is responsible for symmetry breaking in the system and leads to the formation of soliton-like excitations. The elegant SSH Hamiltonian successfully interpreted the magnetic, optical, and electronic properties of pristine and lightly doped *trans*−polyacetylene. Because ground state degeneracy is not a general property of quasi one dimensional conducting polymers, however, theoretical and experimental studies of the large class of nondegenerate

conjugated polymers are necessary and interesting. An important subclass of these are polymers having nearly degenerate ground state structure. Some examples are $cis-(CH)_x$, polypyrrole, poly(paraphenylene), and poly(thiophene). It has been recognized[83] that despite the lack of solitons in non-degenerate systems, the ideas underlying the SSH model can be readily generalized to cases of near degeneracy. When such a system is photoexcited, oxidized, or reduced, the creation of a kink-antikink-like pair, or bipolarons, can be energetically favorable. In such systems, a kink-antikink pair may be "confined", if extra energy is required to separate them.[30] A "confined" kink-like excitation may be charged, but has zero spin. This is consistent with the magnetic susceptibility measurements[51,52] in doped polyparaphenylene and polypyrrole.

We use the slightly modified SSH-type model Hamiltonian of Eq. (2.61) to investigate the nearly degenerate ground state case, and to calculate the dynamics of this model. The motivation of our investigation is to explore the nature of bipolarons, and to explain some experimental data related to them. Since the bipolarons have a higher energy configuration than the ground state, it was expected that the pairs would quickly recombine. Quick recombination, however, seems inconsistent with some experimental evidence from the time-resolved absorption spectra measurements.[84] Our numerical dynamic simulation shows that instead of a static bipolaron the nearly degenerate one-dimensional system has a relatively stable oscillating bipolaron solution. The bipolaron oscillates back and forth stably between a kink-antikink like pair stage (stage I) and a bound polaron pair stage (stage II). The localized electronic energy level associated with the bipolaron oscillates in a similar way and has the same time

period as the bipolaron.

The creation energy of an oscillating bipolaron is about 1.8 times the gap parameter Δ, from our numerical simulations, which is lower than the creation energies of an electron-hole pair or a free polaron pair. Therefore the creation of the bipolaron is energetically favored in the case of either doping or photoexcitation. This is in good agreement with the excitation spectrum of the photoluminescence peak in $cis-(CH)_x$.[16] The luminescence excitation has a threshold at $2.05eV$, which is the energy gap of $cis-(CH)_x$. and the luminescence peak occurs at $1.9eV$ (about 1.85Δ) and is independent of the excitation frequencies. Our interpretation of this data is that an oscillating bipolaron is photoexcited before luminescence occurs, and luminescence then takes place from the bipolaron state. The Stokes shift of 0.15Δ is thus regarded as the energy difference between a free electron-hole pair and an oscillating bipolaron. This mechanism also explains the independence of the luminescence intensity and the peak energy on the excitation frequency. Because the relative motion of the internal degrees of freedom will not effect the translational invariance of the bipolaron as a whole, we also expect that this oscillating bipolaron is responsible for the conductivity found in some nondegenerate polymers.[52]

2. Numerical Results

There have been many numerical calculations done in the framework of the mean field approximation.[71,72,74] The numerical technique used here is similar, but, as in the last chapter, the code is written with the methods developed by milne,[80] so that the total system energy is conserved during integration of

the differential equations. We present here the results of our calculation on a 40 atom chain with the periodic boundary condition within the Born-Oppenheimer approximation. The parameters are $K = 18.2eV/\text{Å}^2$, α_0=4.82$eV/$ Å, $t_0 = 2.5eV$,$\Delta t = 0.08eV$, $\Delta\alpha = 0.2eV/$ Å; Using these values, the soliton width $\xi_0 \approx 2.7a$ and the energy gap $E_g = 2\Delta \approx 4eV$. The energy difference per CH group between the two configurations is $\Delta E_0 = 0.05\Delta$ from the calculation. A stable oscillating bipolaron solution was found within the simulation time period.

The calculation is for a doped system. Two electrons are placed at the bottom of the conduction band in the ground state (lower energy configuration), adding a total energy 2Δ to the system. The whole calculation runs over 1000 time steps of 1.25×10^{-15}sec. After about 300 time steps ($\approx 3.75\times10^{-13}$sec), the bipolaron oscillation stabilizes. Fig. 25 uses the staggered displacement parameter ($\psi_n \equiv (-1)^n u_n / u_0$) at the midpoint of the chain (ψ_{20} in our case) as a characteristic parameter to describe the time dependency of the bipolaron. We find that ψ_{20} oscillates with a period of about 40 time steps (0.5×10^{-13}sec, of the same order as the reciprocal of an optical phonon frequency). When ψ_{20} reaches its local minimum value, the bipolaron is in a stage (stage I), corresponding to a kink-antikink pair, and when ψ_{20} goes to its local maximum, the system is in a stage (stage II), corresponding to a bound polaron pair. To more closely examine the oscillating bipolaron, the time evolution of the staggered order parameters and charge densities of the system during a typical cycle is plotted in Fig. 26. The bipolaron goes from stage I, to stage II, and back to stage I. While at the corresponding times the charge densities of the system at

the corresponding times display a related oscillation. This represents a charge density, localized at any given time, but redistributed itself on an oscillating manner along the chain. One can picture the bipolaron as being composed of two bound polarons, vibrating around the bipolaron center. Stage I, a kink-antikink pair, is simply the combination of two such polarons. Fig. 27 show the topmost four single electronic energy levels below the mid-gap as functions of time (compare with Fig. 3 in Ref. 74). The top one, ϵ_{20}, which is associated with the bipolaron, oscillates inside the gap with the same frequency. The next level, ϵ_{19}, is also shifted into the gap and exhibits large-scale oscillation.

When Fig. 27 is compared with Fig. 11 and Fig. 14, a clear picture emerges. After a bipolaron is formed, the top level, ϵ_{20}, reaches its maximum position, while the next level, ϵ_{19}, returns to the valence band (see Fig. 11). After that, ϵ_{19} is split into the gap, and there are four localized gap states, that is a two-polaron configuration (see Fig. 14). Finally, as the two polaron separate, the two localized levels ϵ_{20} and ϵ_{19} join together and become nearly degenerate.

It is interesting to note that, from Fig. 25, at time steps about 330 and 490 the amplitude ψ_{20} has a smaller value, corresponding to a greater bipolaron width, while at time steps about 410 and 570 ψ_{20} has a larger value corresponding to a narrower bipolaron width. This implies the bipolaron's width is modulating in a time period for times the period of the bipolaron's vibration.

3. Discussion

The picture described in the last section is well understood from the analytical results obtained in Chapter III. In section 3.7, we concluded that because the creation energy of two polarons (Eq. (3.89)) is always less than that of a bipolaron (Eq. (3.79)), it is energetically favorable to form a bipolaron from two polarons. However, after a bipolaron configuration is reached, the potential energy difference between the two configurations (two polarons and one bipolaron) is converted to kinetic energy. This amount of kinetic energy cannot disappear. Instead, the system oscillates between the lower energy configuration (a bipolaron) and the higher energy configuration (two polarons).

This entire calculation has, of course, been performed within the framework of the Born-Oppenheimer approximation. Within this framework and taking into account charge conjugation symmetry the calculation should apply equally well to the photogeneration of an electron-hole pair. In both cases the presumption is that the electronic states are sufficiently stable to make the approximation physically meaningful, and hence the above results (except for charge density) can be taken to apply equally to the case of photoexcitation.

The energy required to create a bipolaron has been suggested to be[64] $E_{\text{bip.}} = 2E_s + n\,\Delta\,E_0$, where E_s is the creation energy for a single soliton (analogous to the degenerate case), and n is the number of sites separating two kinks (defined as the bipolaron width). This formula is fitted very well in our model by using a trial function for a kink-antikink pair. We found $2E_s \approx \Delta_0$ (compared with $2\,E_s = 4\Delta_0/\,\pi$ in the degenerate case) and $\Delta\,E_0 \approx 0.05\,\Delta$ for the

parameters given above. Our dynamical calculation gives $E_{bip.} \approx 1.8\Delta$ and $n \approx 7$, in fair agreement with this expression.

As a final remark, our discussion is limited to the mean field approximation, where the quantum fluctuations have been neglected. Furthermore, we have not taken into account the Coulomb interaction, which can be an important factor. We are at present considering the effect of the Coulomb interaction on the bipolaron.

CHAPTER VI

Conclusion and Discussion

We have studied the dynamical evolutions of both degenerate and nearly degenerate quasi-one-dimensional systems. In degenerate systems, such as *trans*-polyacetylene, we examined the Coulomb effects on the dynamical evolution of a soliton-antisoliton pair. In nearly degenerate systems, such as *cis*-polyacetylene and polythiophene, we modified the SSH model to lift the degeneracy and studied bipolaron dynamics.

Because the electron-electron Coulomb interaction does not lift the degeneracy in *trans*-polyacetylene, the condition to have a soliton excitation is still valid. The electron-electron Coulomb interaction produces an attractive force between two oppositely charged photoproduced solitons, whereas the lattice distortion due to electron-phonon interaction produces a short-range repulsive force between these two solitons. The overall effect is to form a potential well as shown in Fig. 16. If the system energy level is right at the bottom of this potential well, the soliton-antisoliton pair is bounded and forms a static "excitonic" complex with an overall charge of zero. If the system has greater energy, an oscillating motion is produced inside the potential well. The soliton and antisoliton oscillate around the exciton center, moving in opposite directions along the chain and forming an exciton-breather mode. However, this oscillation

feature disappears when the system has energy beyond the height of the potential well, and the soliton pair is free to separate.

One of the soliton model's main experimental supports has been the observation of infrared activity modes. Three major infrared lines have been observed in *trans*-$(CH)_x$; 900, 1260, and 1370 cm^{-1} for doping induced absorption,[85,86] and 500, 1260, and 1370 cm^{-1} for photoinduced absorption.[13,15,87]

Because the TLM model is translationally invariant, and the soliton breaks the translational symmetry, it should produce a zero-frequency phonon mode, the Goldstone mode. The remaining localized phonon in the presence of a soliton can be calculated by using the "amplitude mode" formalism developed by Horovitz[32] and others[88,89].

In the doping case, in which there is a impurity potential, the soliton translation mode becomes pinned and this mode is shifted to a finite frequency. Thus, the 900 cm^{-1} mode in the doping case is interpreted as a pinning Goldstone mode[32]. However, the situation is different in photoinduced absorption, for which there is no impurity present. In comparison with the infrared spectra of chemically doped samples, we find that the second and third mode have the same peak positions in both cases but the first one is shifted from 900 cm^{-1} to 500 cm^{-1}. This implies that the 500 cm^{-1} mode is essentially a "pinning" Goldstone mode, but the pinning mechanism is different from that in the doping case. From the calculation demonstrated in Chapter IV, this mode is interpreted as an exciton-breather mode.

The temperature dependence [15] of the 500 cm^{-1} mode and photoconductivity also supports our interpretation. The 500 cm^{-1} photoinduced signal is strong at low temperature, falls slightly up to about 150 K, and then decreases abruptly until it is essentially unobservable around 250 K. In contrast, the photoconductive gain falls with decreasing temperature until it becomes very small below 200 K. These results suggest that at low temperature, the photogenerated soliton pair is bound into an exciton-breather, which is overall neutral and is unable to give photoconductivity, but is the origin of 500 cm^{-1} infrared mode. However, as the temperature increases, the exciton-breather dissociates and the bounded soliton pair is released to become free charge carriers, therefore, to contribute to photoconductivity.

The oscillation between a bipolaron and two polarons in nearly degenerate systems as explained in Chapter V can be also interpreted as a bipolaron plus a breather mode. Although the oscillation is the same as that in the degenerate case described above, the origins are different. In the degenerate system, the soliton pair is bounded by the electron-electron interaction whereas in the nearly degenerate system the soliton pair is confined by the higher energy configuration. If the Hubbard terms are added to the calculation of photogenerated bipolaron dynamics, we expect that at low temperatures photoexcitation of such a system should produce an exciton plus a breather mode, whereas at high temperature, the product should be a bipolaron plus a breather mode.

The numerical simulations performed in this thesis are essentially based on a simple model. Many ingredients are missing from this model, and up to

now some interpretations of experimental data are still in question and must be considered further. In the following paragraphs, we list those missing factors which might have profound effects.

The dynamics of the lattice is treated in the classical approximation, and quantum effects of phonons have been neglected. Substantial lattice quantum fluctuations may complicate the description of the perfectly dimerized state and affect the calculated physical quantities of solitons as well. For instance, the quantum correction to the soliton creation energy has been calculated[90] to be $\delta E_S = -\frac{1}{4}E_S$, which is not a negligible amount.

The interchain coupling is also of importance and has not been taken into account in this model. Although the interchain bandwidth ($W_\perp \sim 0.1eV$)[91] is small compared to the π bandwidth ($W_0 \sim 10eV$), the three-dimensional effects may modify predictions based on the simple SSH model. X-ray scattering experiment suggest that the dimerization pattern exhibits three-dimensional order[92]. The interchain interaction arises from two factors, the interchain π-electron transfer and the electrostatic interaction between chains. It has been shown that an antiferromagnetic order between neighboring chains is favored and leads to soliton confinement.[93,94,95] Furthermore, soliton-antisoliton pair hopping between chains could play a role in the conduction process when the concentration of solitons is small.[96]

Because the electron-electron Coulomb interaction is essentially long-range and three-dimensional, the use of short range Hubbard terms is justified for $(CH)_x$, in which the Coulomb interaction is effectively screened[97,98]. Actually

most quantitative effects produced by the Coulomb interaction can be absorbed into the non-interacting SSH model by redefining the effective parameter, so that only the qualitative effects of the interaction need be studied extensively. The effective interaction strengths U and V are very difficult to estimate from first principles, and can only be deduced from experiment[49,67], which suggests $U = 3 \sim 4eV$. In this range, the electron-electron interactions in $(CH)_x$ are "weak", and the perturbation theory and Hartree-Fock approximation are valid. Thus, we conclude that our numerical results are qualitatively reliable. Recently a more general model has been proposed that combines the SSH and Solyom[99] models and uses six independent parameters to describe interactions. This model requires further study.

It is worthwhile to point out that, despite success of the SSH model, there still exists some discrepancy between theory and experiment in explaining the two main peaks observed in the photoinduced optical absorption measurement, i.e. the low energy peak $\hbar\omega_L = 0.5eV$ and the high energy peak $\hbar\omega_H = 1.4eV$. Satisfactory explanations are needed not only for the peak positions, but also the time resolved studies and the temperature dependence behaviors of the peaks as well. These peaks could be caused by the electronic transitions between different excitation states, such as a negative soliton going to a neutral soliton plus an electron, or a neutral soliton going to a positive soliton plus an electron.[98]

In addition, the band structure derived from the SSH model is far from "realistic". Developing such a theory requires further knowledge of the sample structures and more advanced experimental techniques. For instance, physical

parameters (e.g., the electron-phonon coupling constant, α) entered into the model should be determined more directly from experiment measurements. It is also necessary to determine whether polyacetylene has a planar structure or a helical structure.[100]

As a final remark, conducting polymers represents a new class of electronic materials that offer exciting opportunities to both theorists and experimentalists in condensed matter physics.[101] Studies of polyacetylene and other polyenes have developed new concepts in the theory of quasi-one-dimensional systems, and demonstrated the importance of the coupling between electron excitation and lattice conformation in one-dimensional polymers, which renders the excitations non-linear. The generalization of these concepts to a broad class of conjugated structures is of special interest.

Figure Captions

FIG. 1. Representation of one electron density of states in ground state configuration of *trans*-$(CH)_x$. The band structures are symmetric about the gap center which is set to be zero point in energy measurement. All the negative energy states are occupied whereas all the positive energy states are unoccupied.

FIG. 2. Structural formulas of perfectly dimerized *trans*-$(CH)_x$ for the two degenerate ground states, A-phase and B-phase. u_n is lattice displacement from undimerized place of n-th CH group. the double lines represent short bonds whereas the single lines represent long bonds.

FIG. 3. The two different configurations of *cis*-$(CH)_x$, cis-transoid configuration has lower energy than that in trans-cisoid configuration. There are two types of bonds, the type-I bonds make an angle of about $\pi/3$ with the chain and the type-II bonds are those parallel to the chain. The parameters t_1 and α_1 correspond to the type-I bonds while t_2 and α_2 correspond to the type-II bonds. Here we assume $t_2 > t_1$, and $\alpha_2 > \alpha_1$.

FIG. 4. (a), The energy curve $E(k)$ for an electron in the potential of the undimerized chain (without distortion).
(b), The modified energy curve $E(k)$ for an electron in the potential of the distorted chain (trimerized in this case, $r = 3$). Because of the reduction in the symmetry, the curve represents now three different bands and opens gaps at $\frac{\pi}{3a}$ and $\frac{2\pi}{3a}$ with the reduced reciprocal cell $(-\frac{\pi}{3a} < k < \frac{\pi}{3a})$. The broken lines show this reduction.

FIG. 5. Structural formulas of polythiophene. The two inequivalent thiophene heterocycles in polythiophene make the polymer two different phases with different energies. The sulfur stabilizes the structure but only weakly interacts with π-electrons of backbone.

FIG. 6. Schematic representation of polythiophene backbone structure leaving out the sulfur atoms (compare with Fig. 5), which is more analogue to that in *cis*-$(CH)_x$ (see Fig. 3). The two configurations are nearly degenerate which can also be described by our modified SSH Hamiltonian.

FIG. 7. The diagrams of energy versus the distortion parameter u ($u = 0$ corresponds to undimerized case where the bond length are equal). (a), degenerate ground state system (e.g. *trans*-$(CH)_x$) where there are two minima at $u = -u_0$ and $u = u_0$ which have same energy representing the two different phases of dimerization. (b), nearly degenerate ground state system (e.g. *cis*-$(CH)_x$ or polythiophene) where the two minima have different values resulting in A-phase being a ground state whereas B-phase being a metastable state.

FIG. 8. (a), the staggered lattice displacement η_n and (b), the structural formulas and (c), the electron band structure of the perfectly dimerized system. All the valence band are occupied with spin paired whereas all the conduction band are unoccupied.

FIG. 9. Diagrammatic representation of a polaron.
(a), the distorted configuration in the representation of staggered displacement η_n.
(b), chemical structure diagram in the presence of a negative polaron, the parallel solid and dash double lines represent distorted bonds whose length are between double and single bonds. The full dot represents an extra electron.
(c-d), the two localized gap states are formed in the presence of a negative polaron (c) and a negative polaron (d).

FIG. 10. Diagrammatic representation of a soliton-antisoliton pair.
(a), the distorted configuration in the representation of staggered displacement parameters η_n, where $\eta_n = u_0$ means configuration in A-phase while $\eta_n = -u_0$ in B-phase.
(b), chemical structure diagram in the presence of a negatively charged soliton-antisoliton pair.
(c-e), energy structures in the presence of positively charged (c), neutral (d) and negatively charged soliton pairs (e), respectively, depending on the occupation of the mid-gap states.

FIG. 11. Diagrammatic representation of a bipolaron.
(a), the distorted configuration η_n, where the bipolaron connects two energetically different configurations.
(b), chemical structure of a negative bipolaron.
(c-e), the energy structures of a positive (c), a neutral (d) and a negative bipolaron (e), respectively.

FIG. 12. The probability density distribution contributed by the mid-gap state of a neutral soliton in the absence of Coulomb interaction. The density on even numbered sites goes to zero exponentially on both sides, whereas the densities on the odd numbered sites are equal to zero.

FIG. 13. Schematic representation of the novel charge-spin relations. The lower curves of each diagram represent the probability density of the Fermi sea for each spin in the vicinity of a soliton while the upper ones represent that of the mid-gap state. the Fermi sea contributes charge of $+\frac{e}{2}$ for each spin to the soliton, being doubled to $Q = +e$. So if there is no electron occupied in the mid-gap state (a), the soliton has charge $+e$ and spin zero; if there is one electron in the mid-gap state (b), the soliton has charge zero and spin one-half; if there are two electrons in the mid-gap state (c), the soliton has charge $-e$ and spin zero.

FIG. 14. Diagrammatic representation of two polarons.
(a), the distorted configuration in the representation of staggered displacement η_n.
(b), the four localized gap states are formed in the presence of two polarons with finite separation. Here the electron configuration represents two positively charged polarons.

FIG. 15. The relations of the formation energy (units of Δ_0) and the confinement parameter γ. Solid line: the formation energy of a bipolaron vs. γ; dashed line: the formation energy of a polaron vs. γ.

FIG. 16. Potential energy (in unit of Δ_0) vs. the separation of the soliton-antisoliton pairs, $2x_0$ (in units of the lattice constance a). The small potential well makes the vibration of an exciton possible.

FIG. 17. Time Evolution of the potential energy. The total energy of the curve (a): $E_t = 1.963\Delta_0$ (initialized from the dimerized state); the curve (b): $E_t = 1.7693\Delta_0$. For each curve the ranges of the ordinate is from $1.3\Delta_0$ to $2.0\Delta_0$.

FIG. 18. As in Fig. 17. The curve (c): $E_t = 1.5311\Delta_0$, (d): $E_t = 1.4526\Delta_0$, (d): $E_t = 1.4526\Delta_0$, (e): $E_t = 1.4458\Delta_0$, (f): $E_t = 1.4389\Delta_0$, (g): $E_t = 1.4325\Delta_0$, (h): $E_t = 1.4265\Delta_0$, (i): $E_t = 1.4210\Delta_0$, (j): $E_t = 1.4157\Delta_0$, and (k): $E_t = 1.4110\Delta_0$. The range of the ordinate in each curve is from $1.35\Delta_0$ to $1.45\Delta_0$, except for the top one, which ranges from $1.35\Delta_0$ to $1.55\Delta_0$.

FIG. 19. Typical exciton-breather expansion cycle, for case (j) in Fig. 18 ($E_t = 1.4157\Delta_0$). The abscissa is the site index n, and the ordinate is the optical components of the staggered displacement order parameters, y_n. The solid line, $T = 116$ (in units of 1.25×10^{-15}); the dotted line, $T = 125$, the broken line, $T = 137$, and the dot-dash line, $T = 144$. The dotted line represents a lattice configuration which has a local minimum of the potential energy.

FIG. 20. (Follows Fig. 19). The exciton breather in contraction. The solid line $T = 144$, the broken line $T = 150$, the dotted line $T = 161$ (a local minimum potential energy configuration), and the dot-dash line $T = 170$.

FIG. 21. A central type breather is located between a quite static soliton-antisoliton pair. This is case (d) in Fig. 18 ($E_t = 1.4526\Delta_0$). The solid line $T = 209$; the dotted line $T = 216$ (a local minimum potential energy configuration) and the broken line $T = 223$.

FIG. 22. A central type breather is located between a well-separate soliton-antisolion pair, which vibrates along the chain with a long periodicity. ($E_t = 1.5311\Delta_0$, corresponding to case (c) in Fig. 18). The solid line $T = 203$; the dotted line $T = 210$ (a local minimum potential energy distribution) and the broken line $T = 217$.

FIG. 23. Time dependence of the single electron energy spectrum for case (j) ($E_t = 1.4157\Delta_0$). Only top three levels below the gap center are plotted. The top level oscillates with the same frequency as that of the exciton breather. the second top level oscillates with a higher frequency than that of the top one.

FIG. 24. (As in Fig. 23) Time dependence of the single electron energy spectrum for case (c) ($E_t = 1.5311\Delta_0$). The top level becomes a mid gap state owing to the soliton-antisoliton pair, and the second top one oscillates near the gap edge with the central breather frequency.

FIG. 25. Oscillating feature of ψ_{20}. When ψ_{20} reaches its local minimum value, the bipolaron is in a stage (stage I), corresponding to a kink-antikink pair, and when ψ_{20} goes to its local maximum, the system is in a stage (stage II), corresponding to a bound polaron pair.

FIG. 26. The normalized staggered parameter ψ_n and charge density relative to the sites. (a) time = 401 (in units of 1.25×10^{-15}sec); (b) time = 419 and (c) time = 440. (a) and (c) are in stage I ; (b) is in stage II.

FIG. 27. Time dependence of single electronic levels: The first 4 levels below the mid gap are plotted. They are ϵ_{20}(solid line), ϵ_{19}(broken line), ϵ_{18} and ϵ_{17} respectively. When ϵ_{20} has its maximum value, ϵ_{19} returns to the valence band, corresponding to stage I. When ϵ_{20} reaches its minimum value, ϵ_{19} has its maximum value, at this moment there are 4 localized states (2 below the mid-gap and another 2 symmetric counterparts above the mid-gap), which corresponds to stage II.

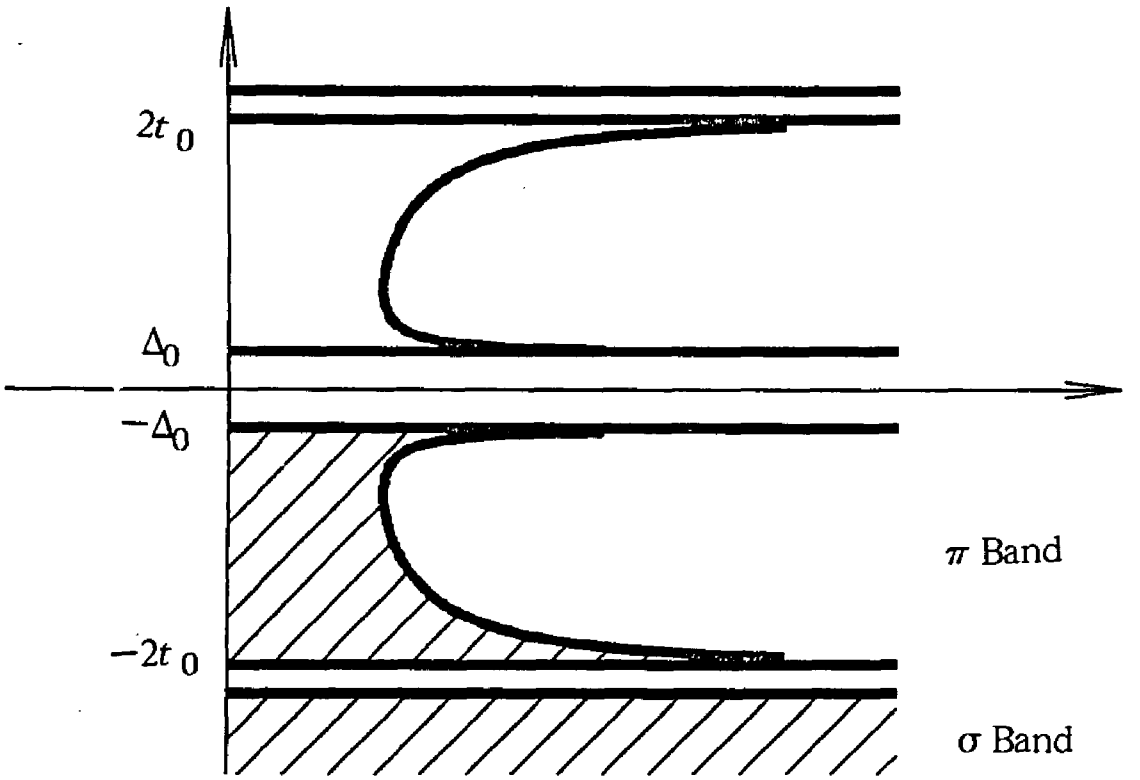

Fig. 1

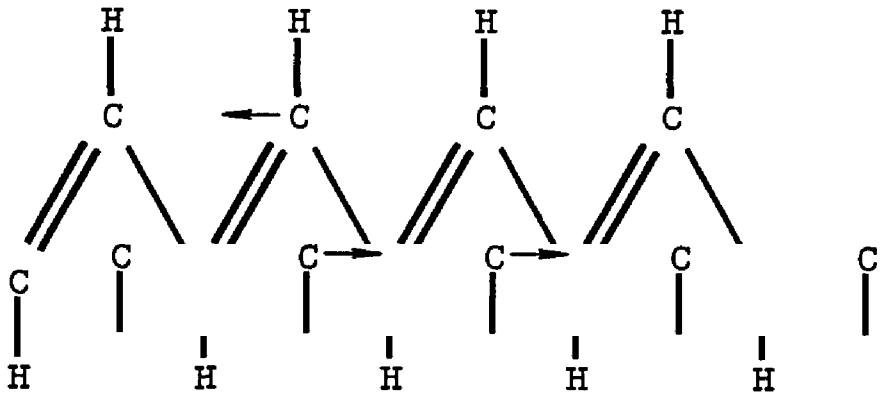

A-phase

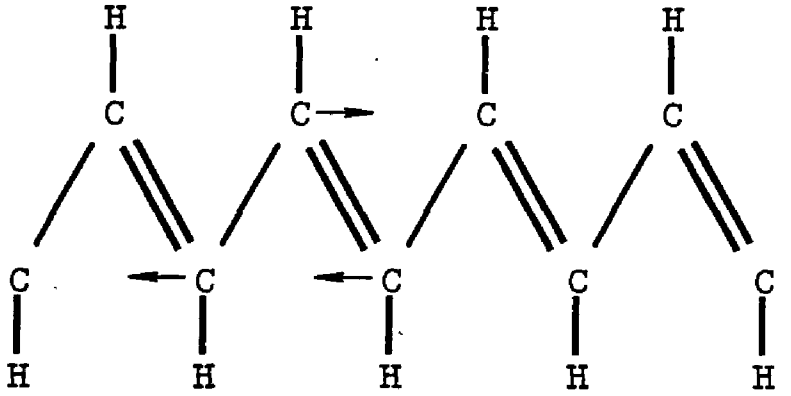

B-phase

Fig. 2

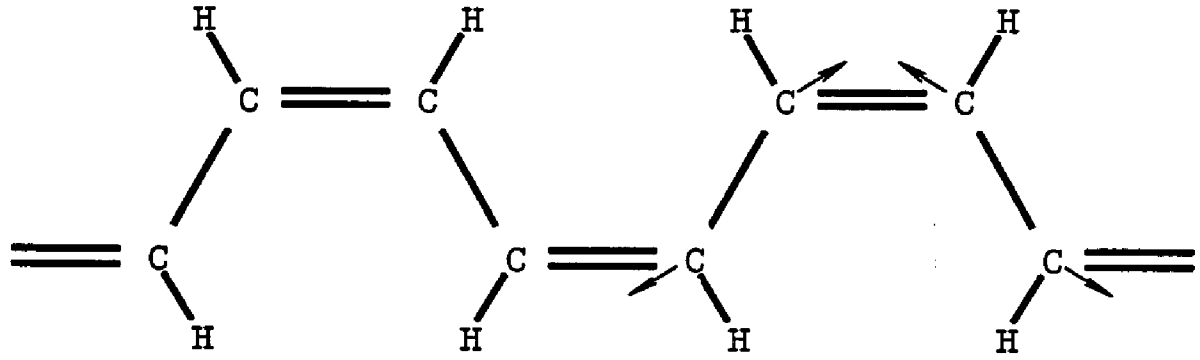

Cis-transoid Configuration

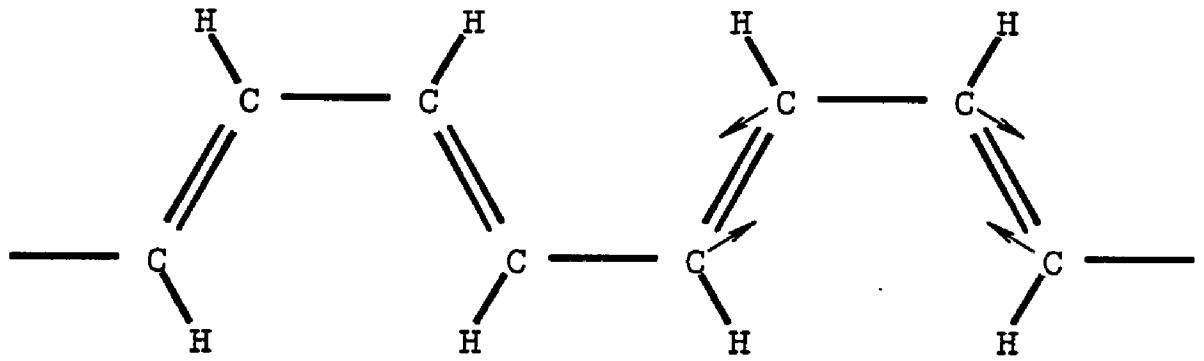

Trans-cisoid Configuration

Fig. 3

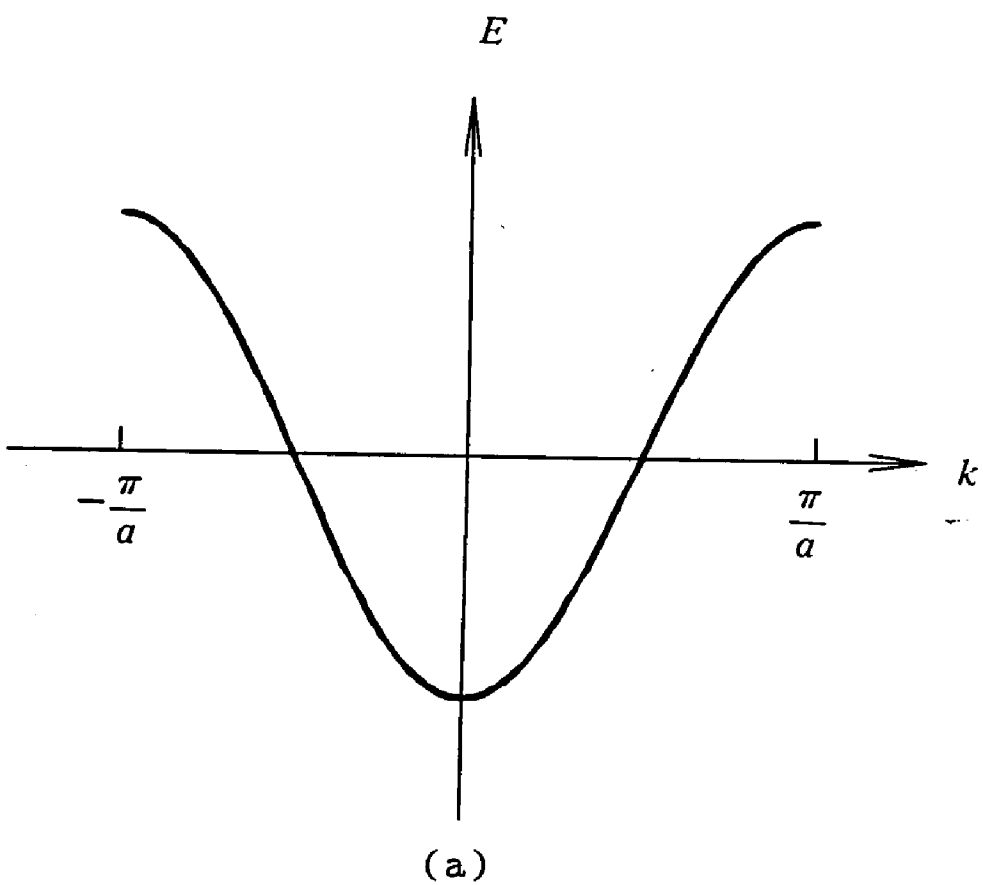

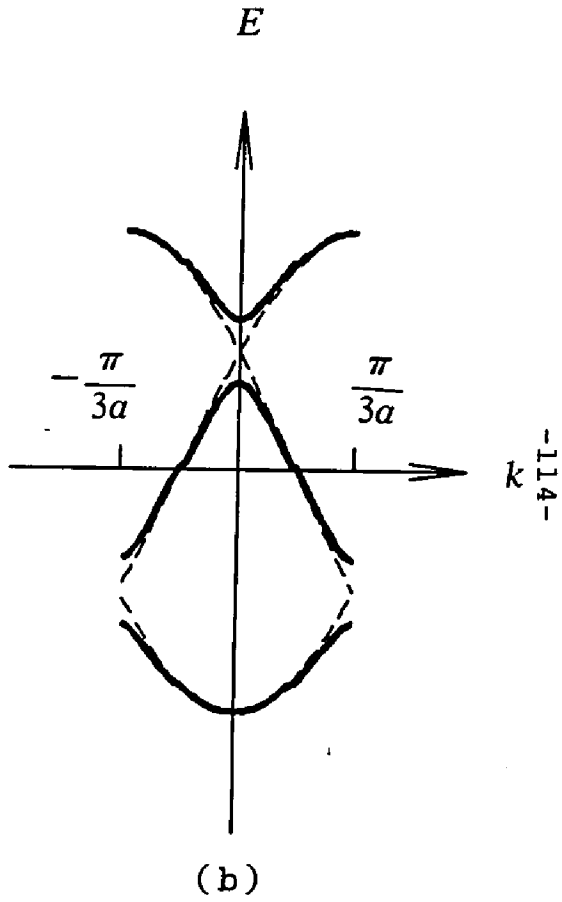

Fig. 4

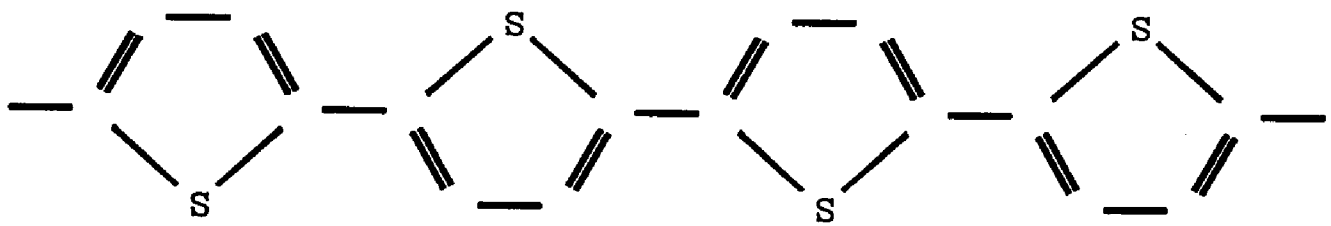

A-phase

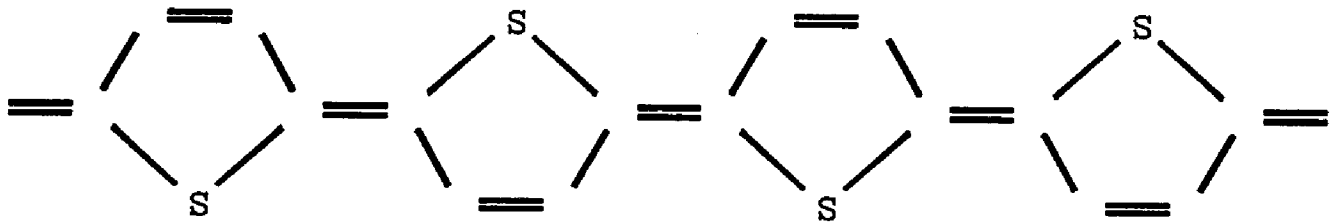

B-phase

Fig. 5

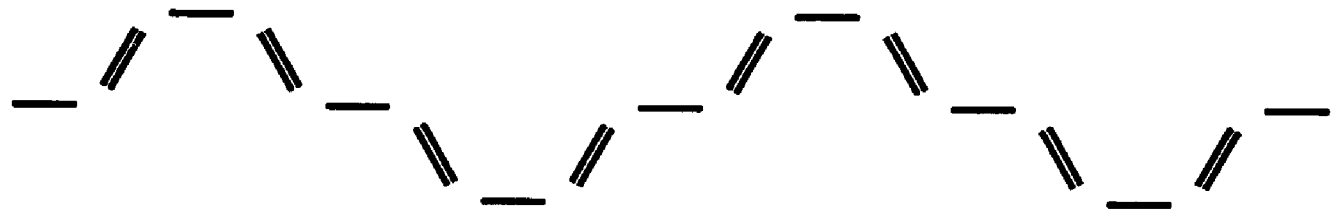

A-phase

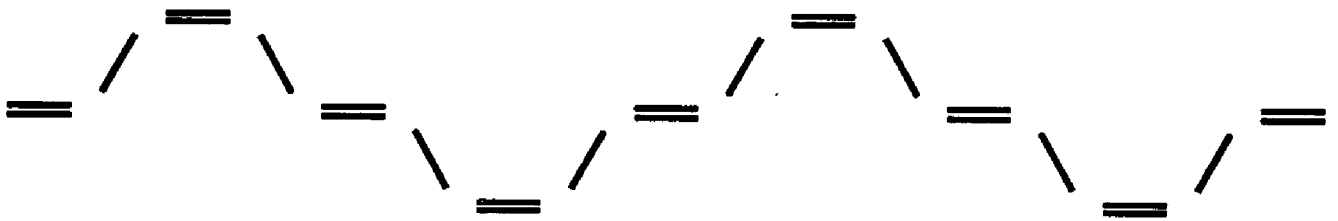

B-phase

Fig. 6

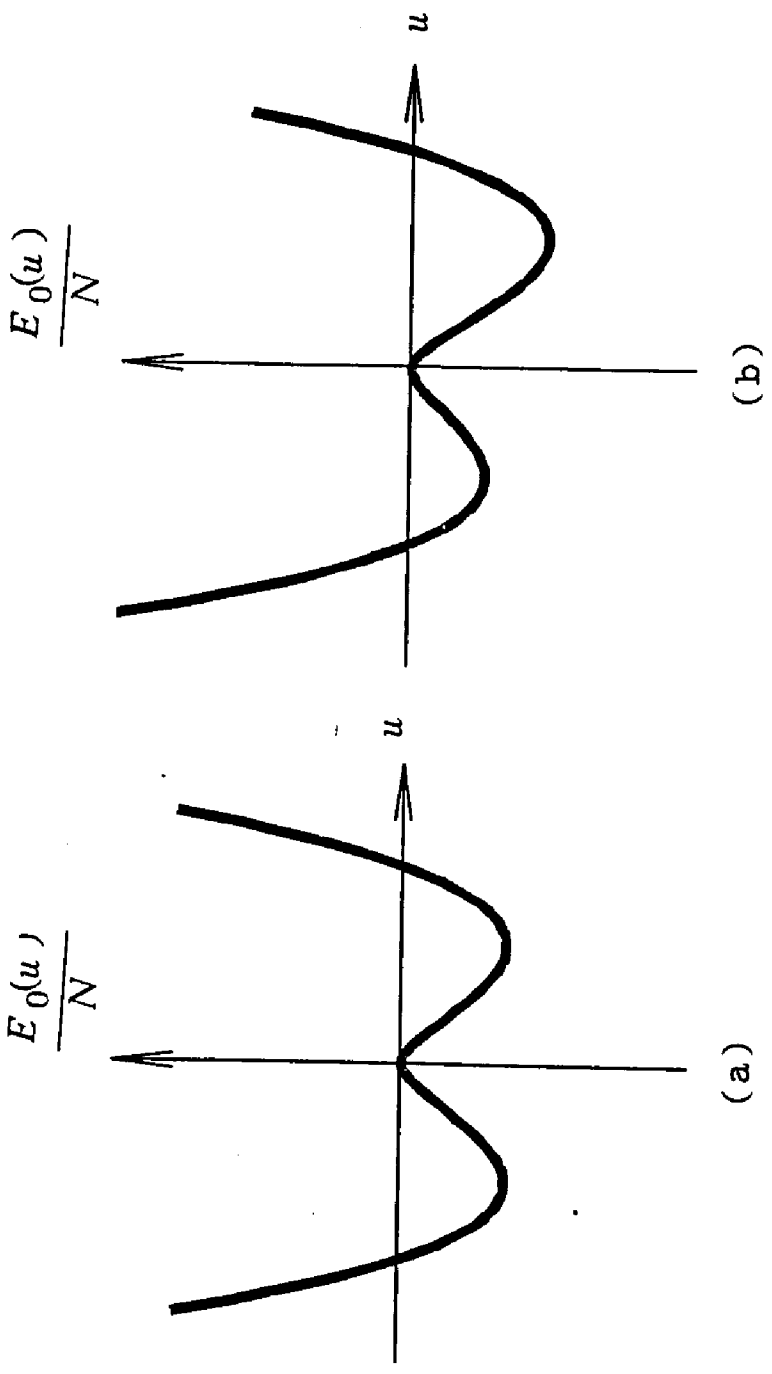

Fig. 7

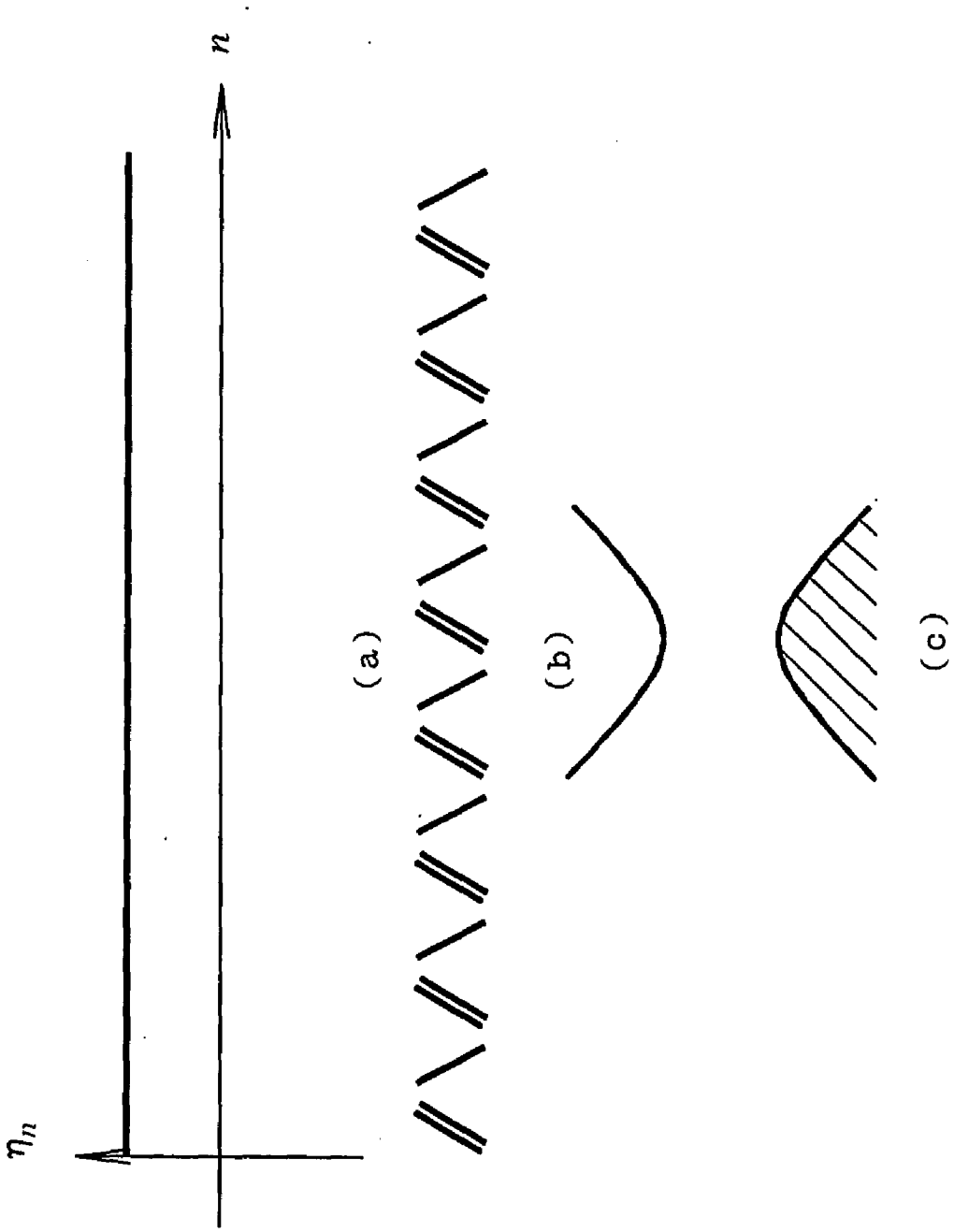

Fig. 8

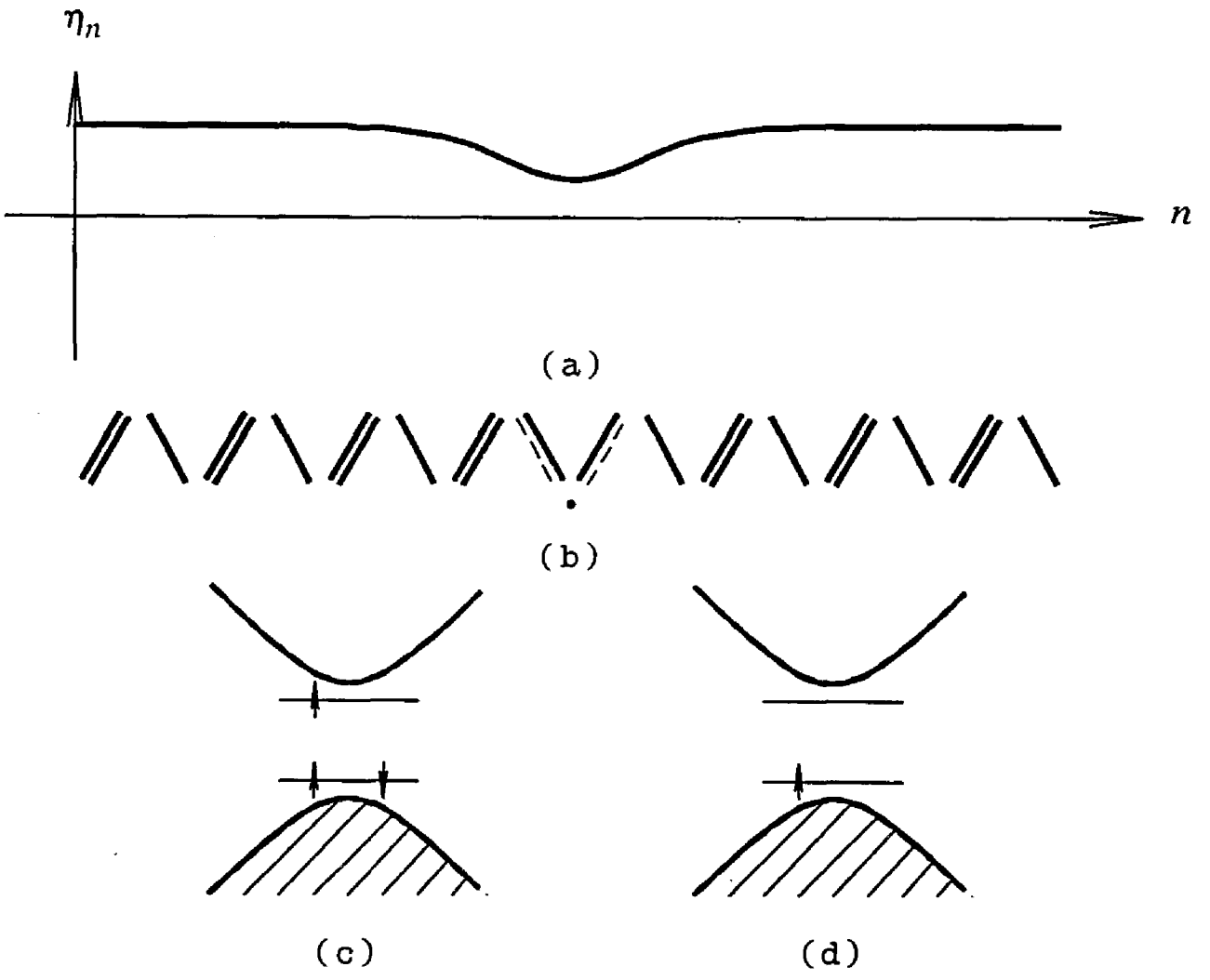

Fig. 9

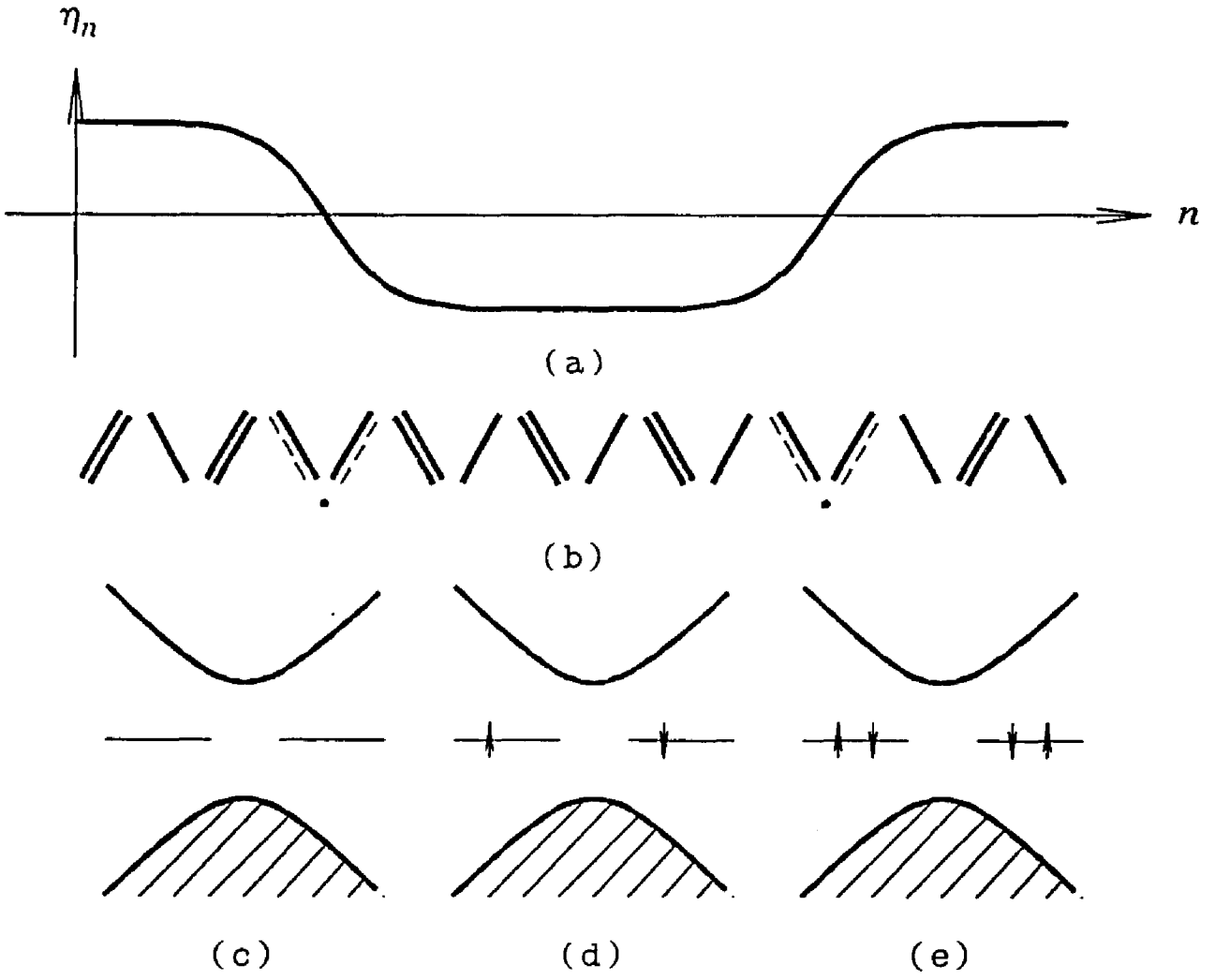

Fig. 10

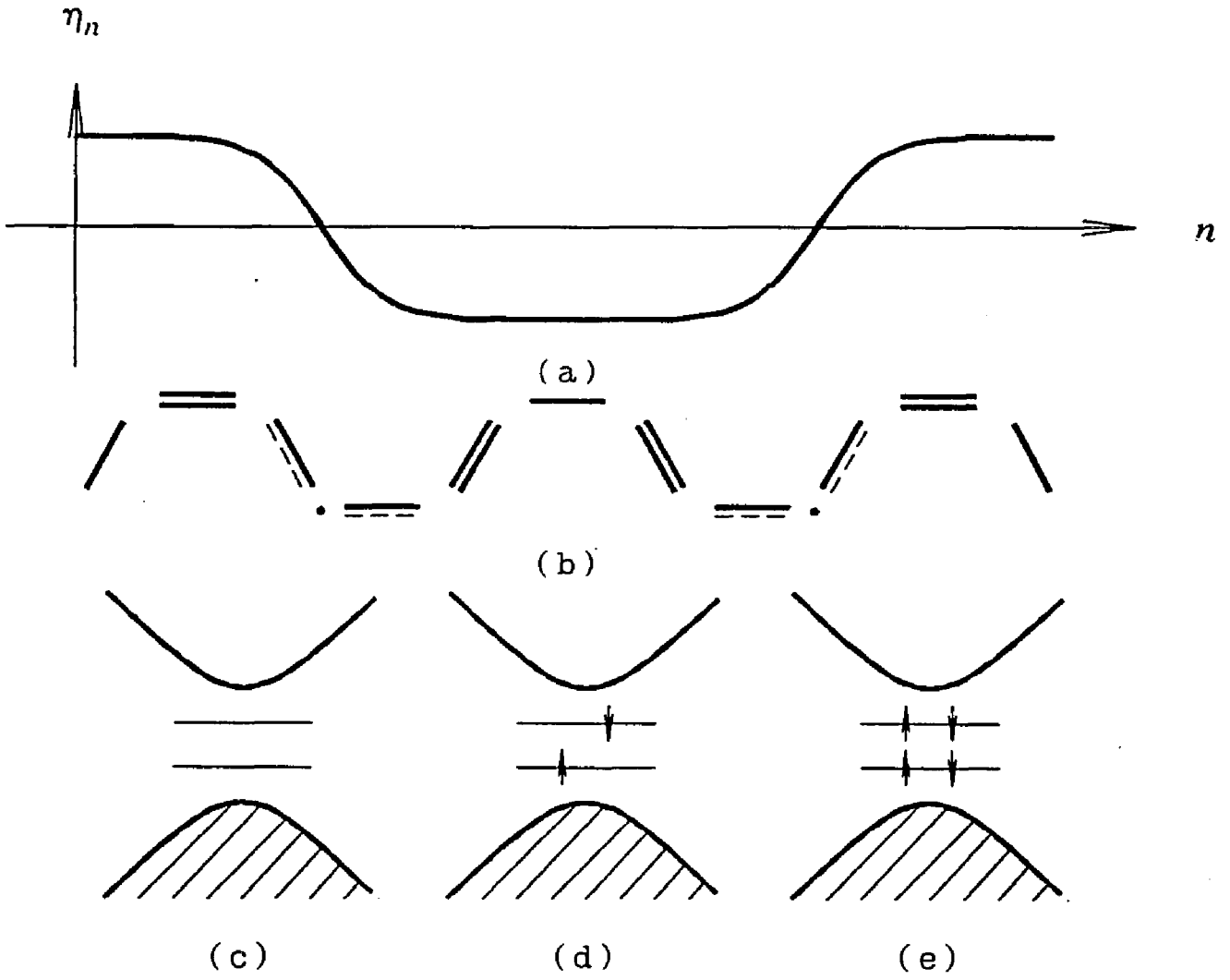

Fig. 11

(a)

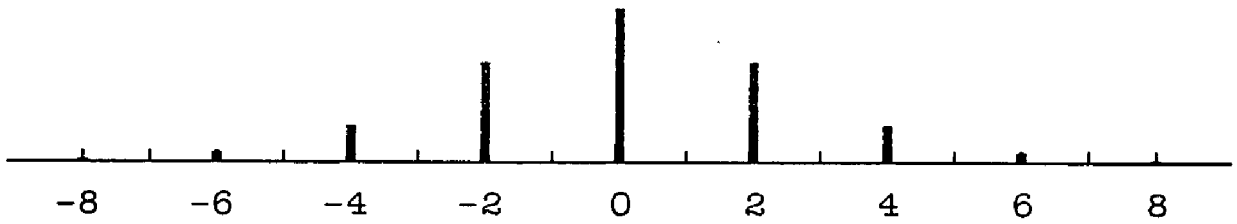

(b)

Fig. 12

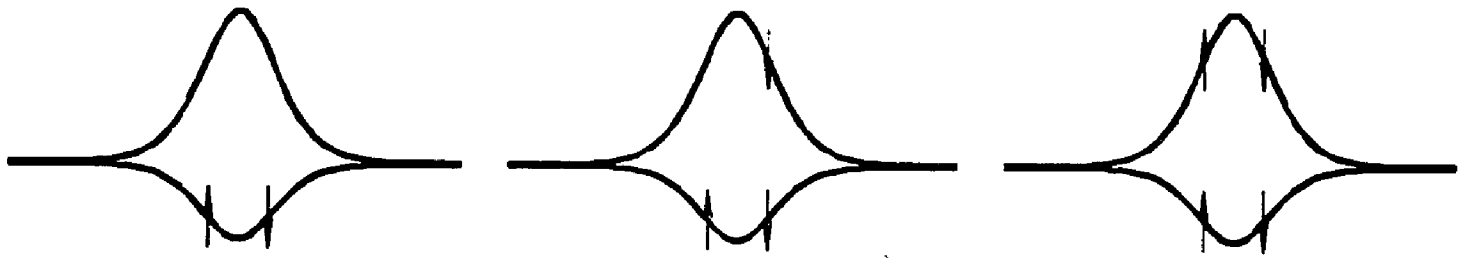

Fig. 13

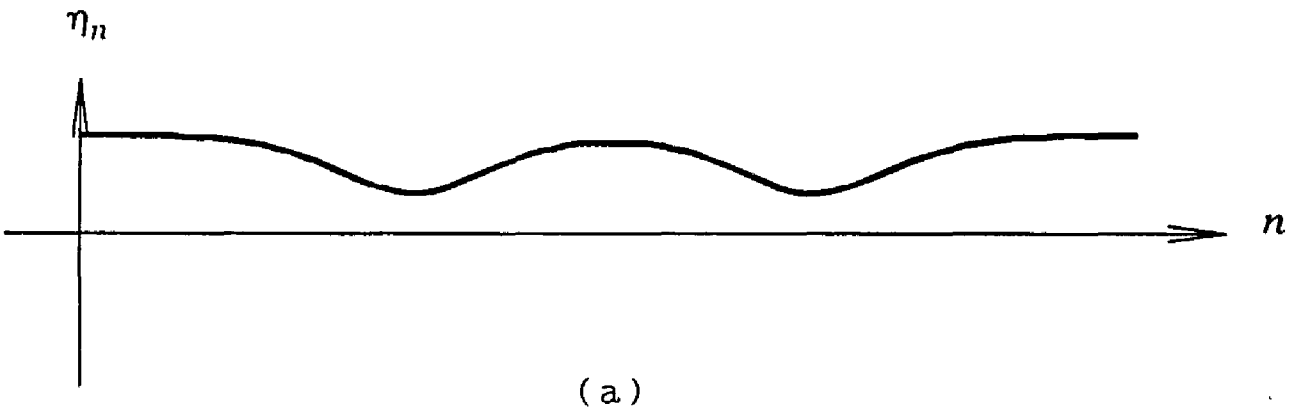

(a)

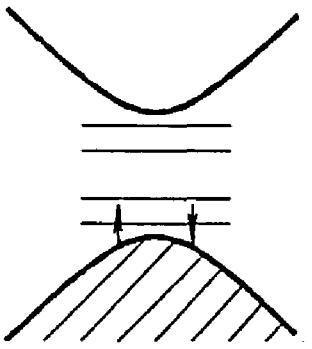

(b)

Fig. 14

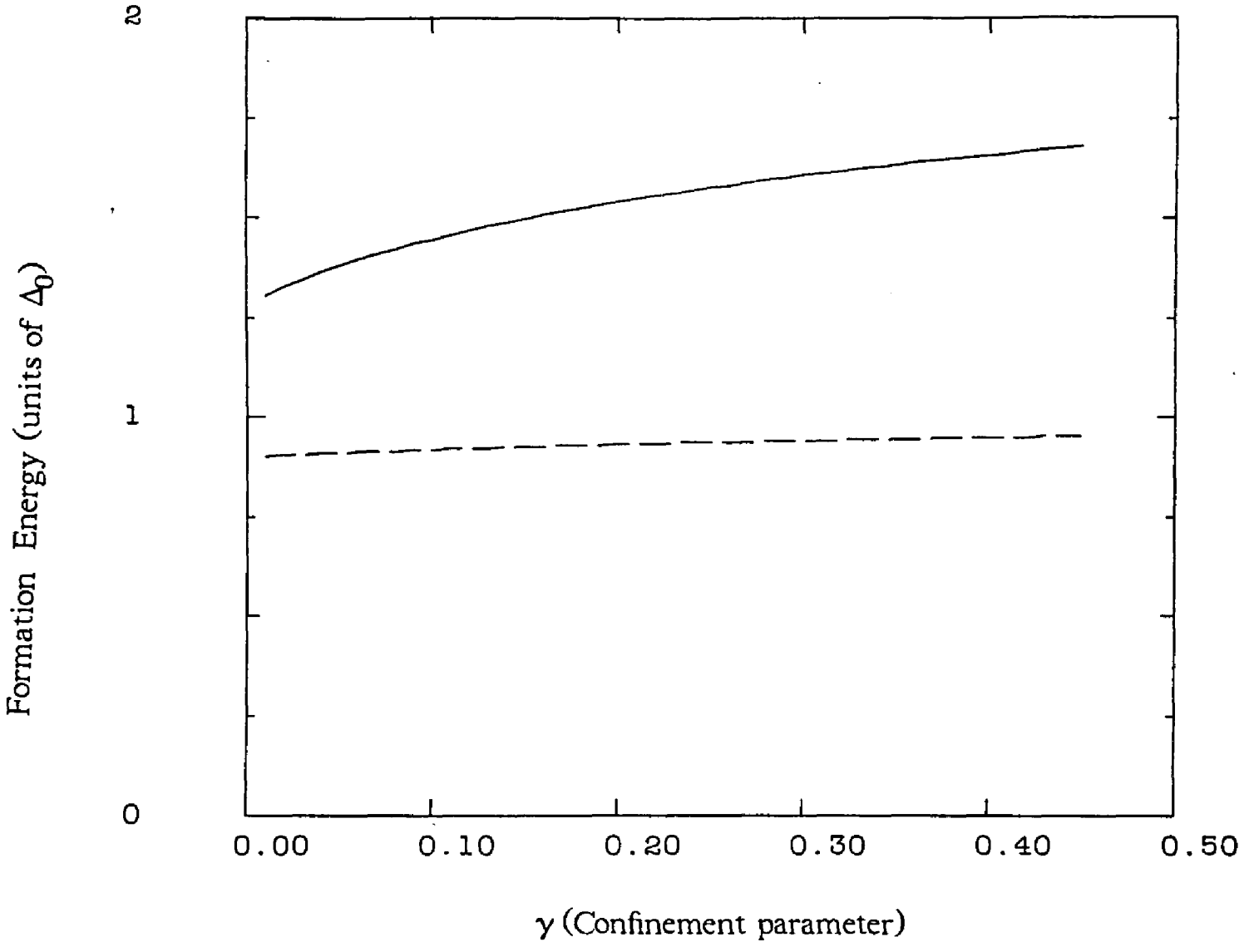
2
1
0
Formation Energy (units of Δ_0)
0.00
0.10
0.20
0.30
0.40
0.50
γ (Confinement parameter)

Fig. 15

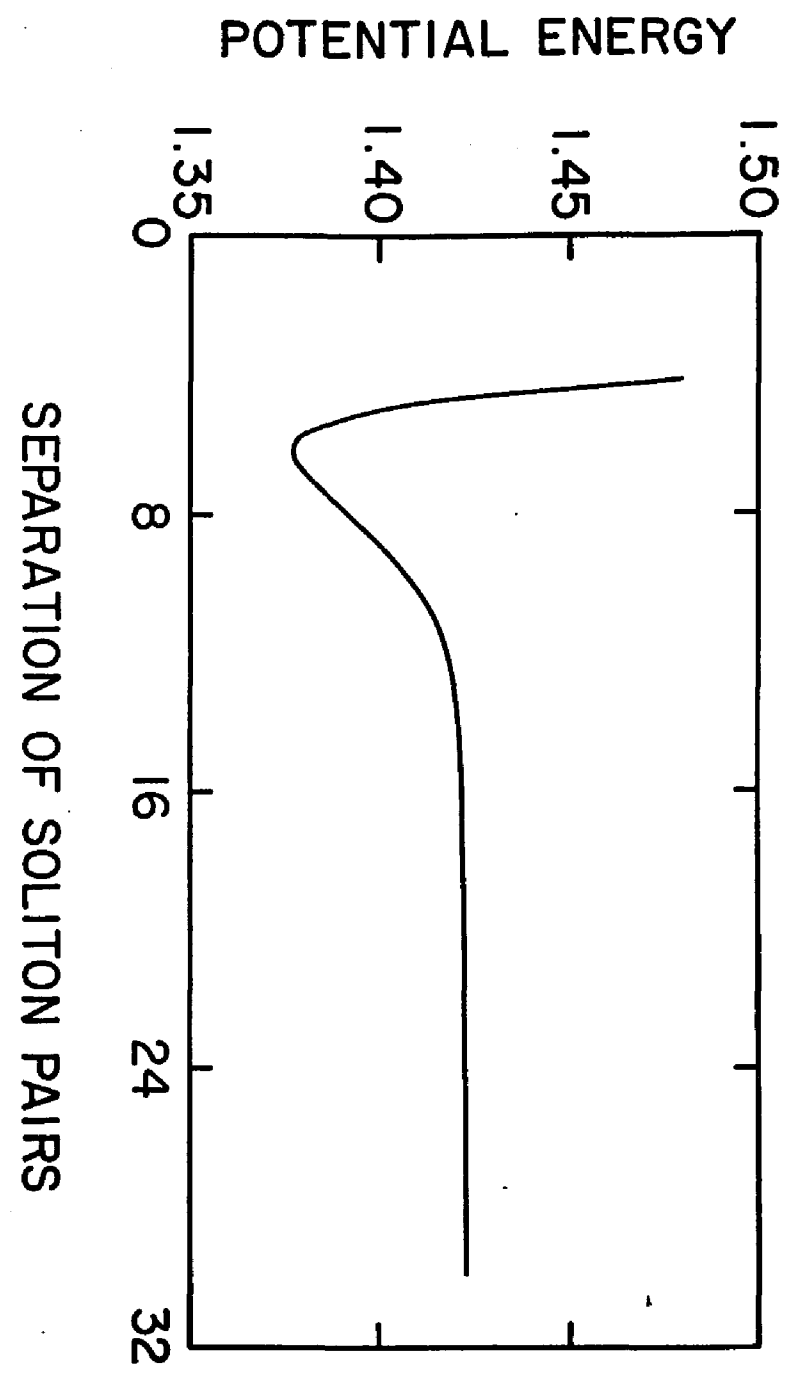
POTENTIAL ENERGY
1.35
1.40
1.45
1.50
0
8
16
24
32
SEPARATION OF SOLITON PAIRS

Fig. 16

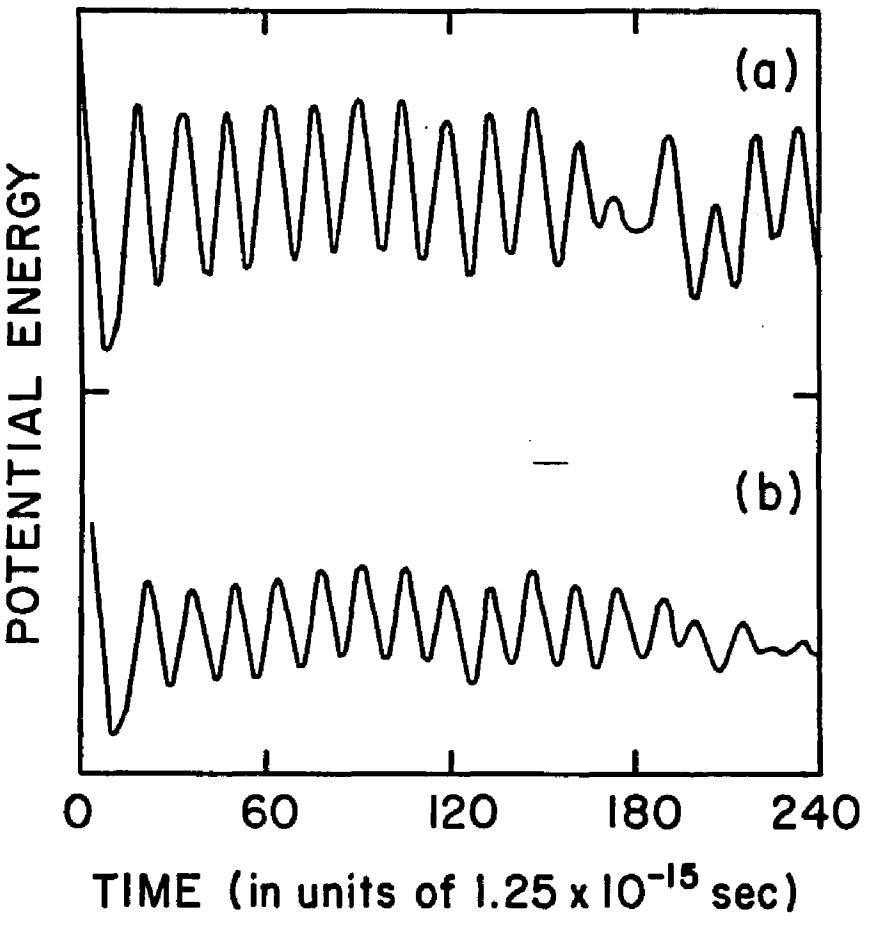
(a)
(b)
POTENTIAL ENERGY
0
60
120
180
240
TIME (in units of 1.25 x 10^-15 sec)

Fig. 17

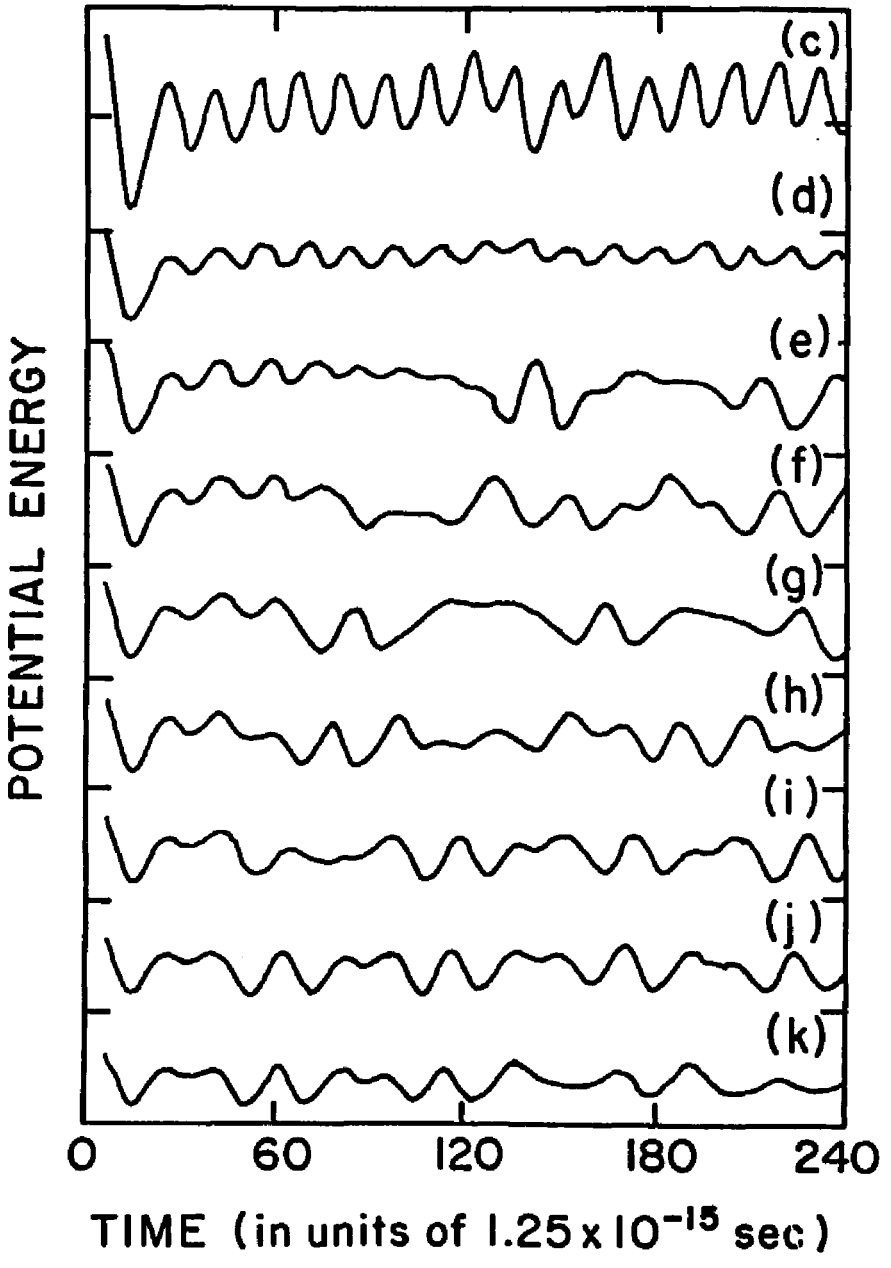
(c)
(d)
(e)
(f)
(g)
(h)
(i)
(j)
(k)
POTENTIAL ENERGY
0
60
120
180
240
TIME (in units of 1.25 x 10⁻¹⁵ sec)

Fig. 18

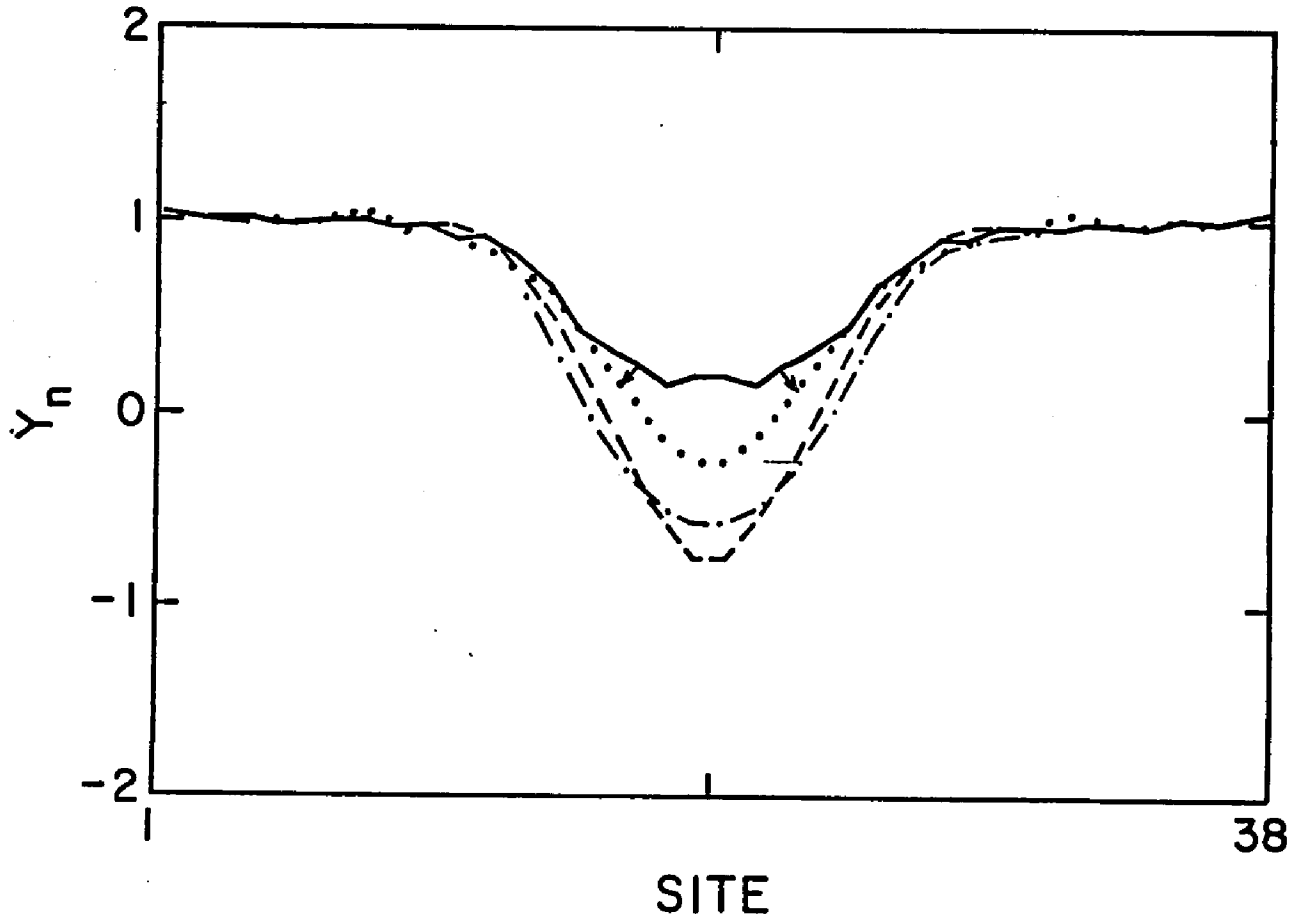

Fig. 19

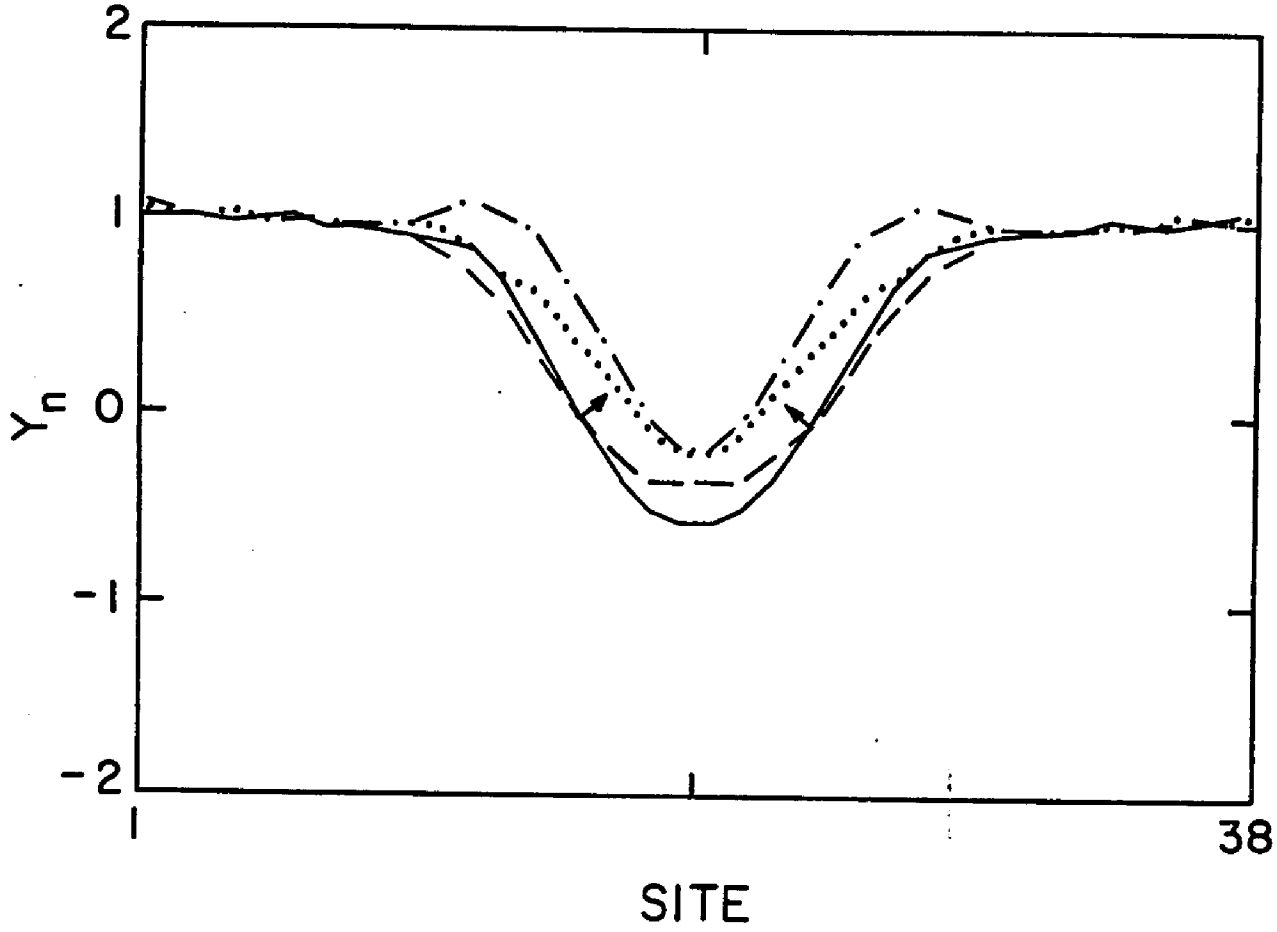

Fig. 20

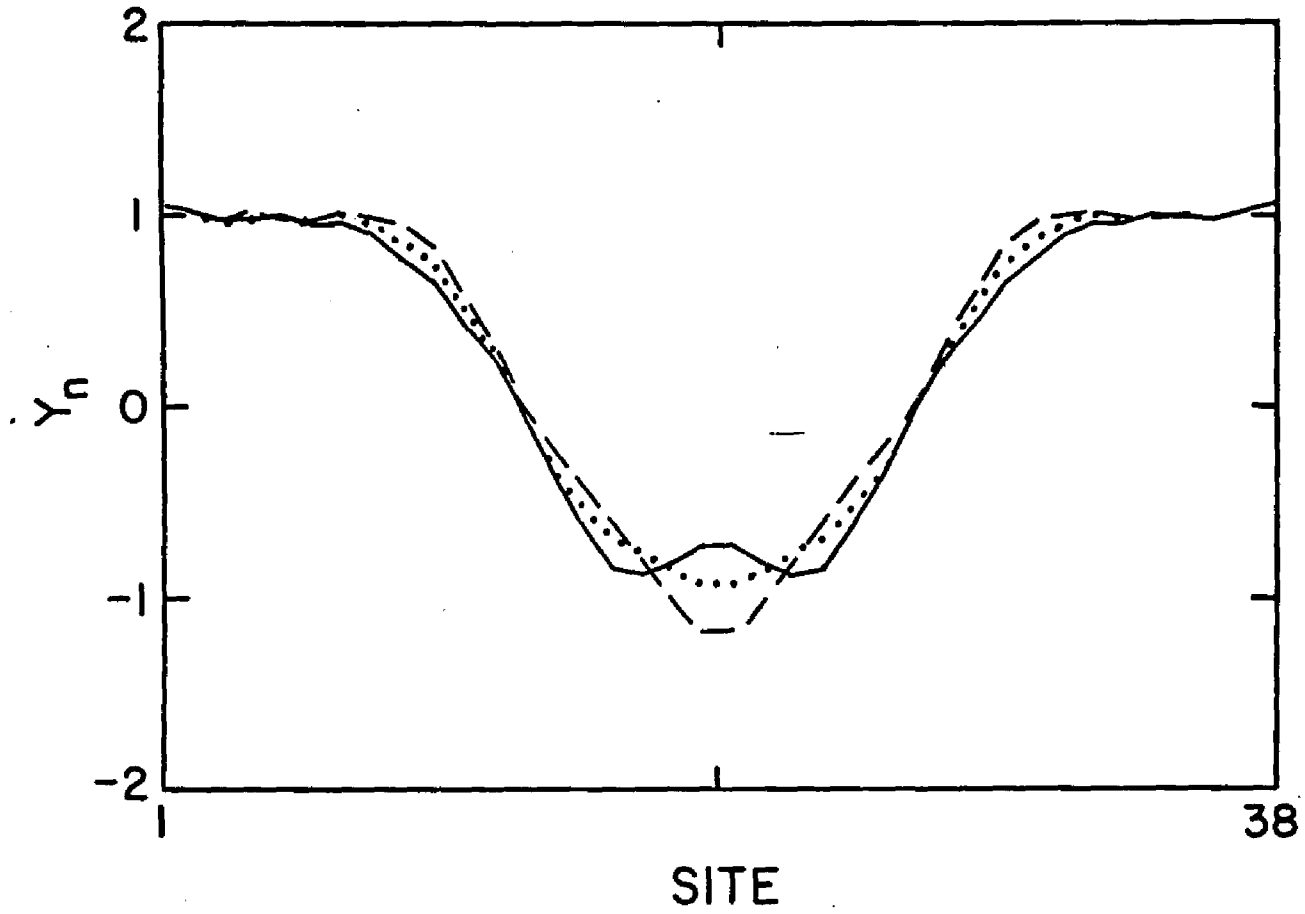

Fig. 21

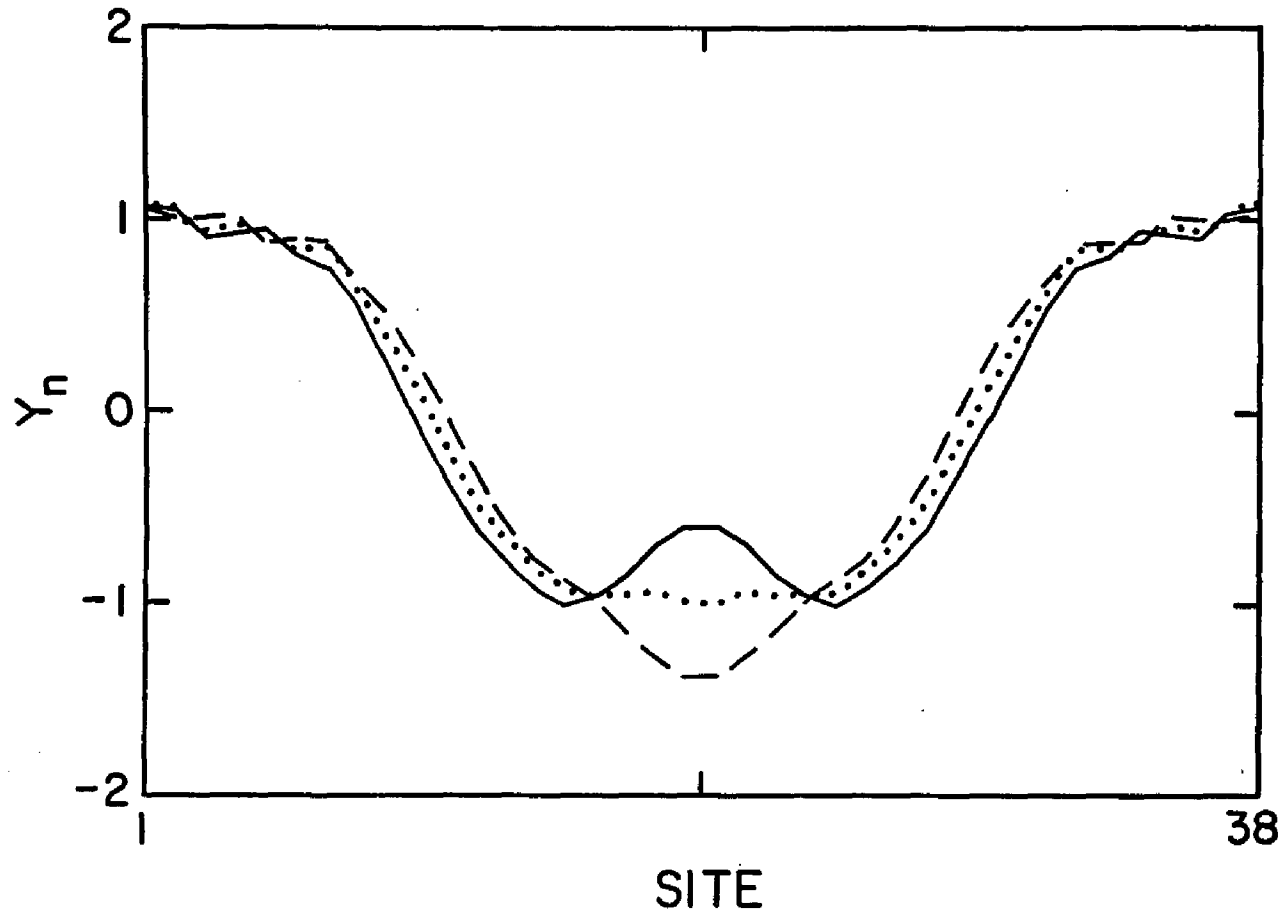

Fig. 22

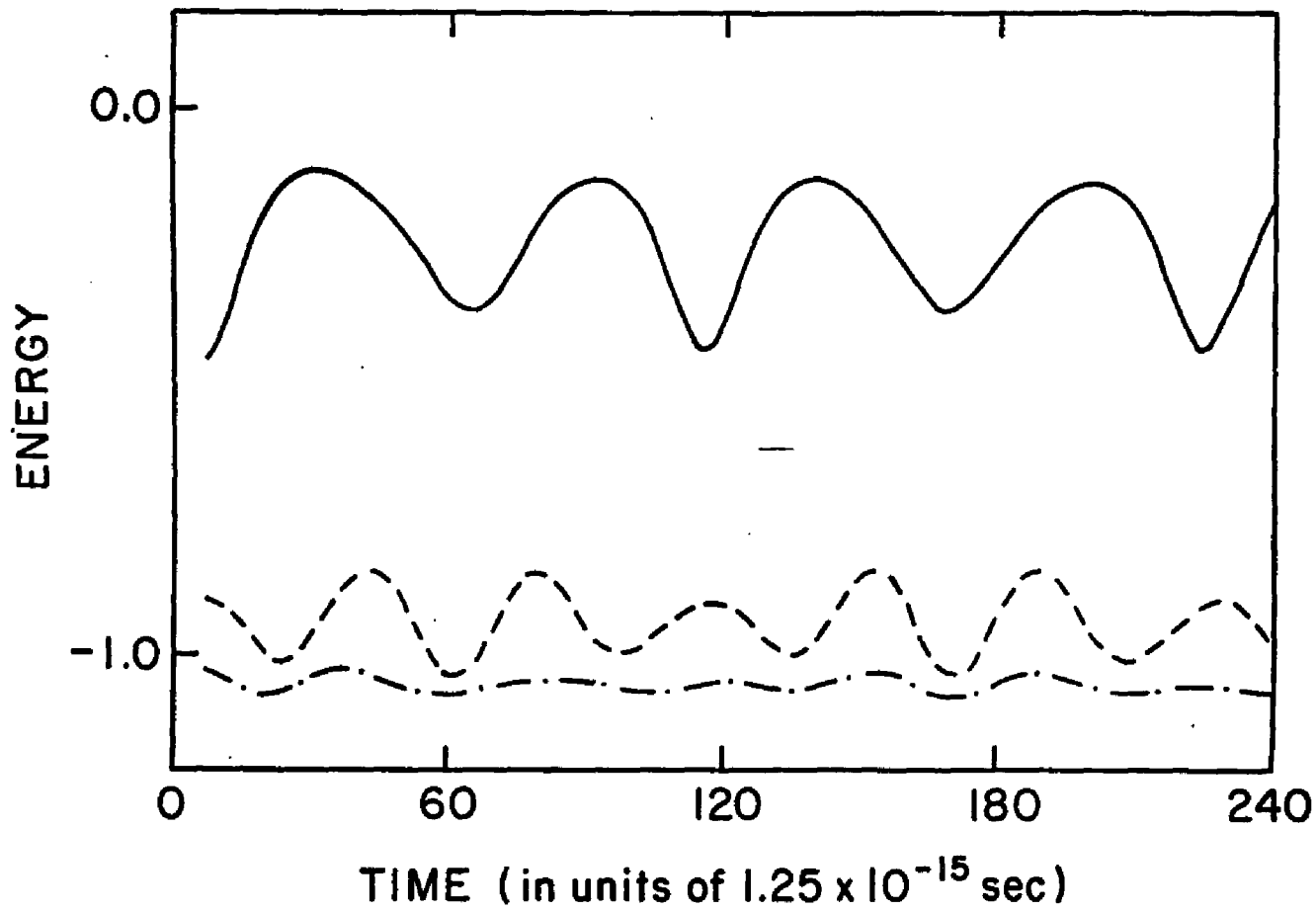

Fig. 23

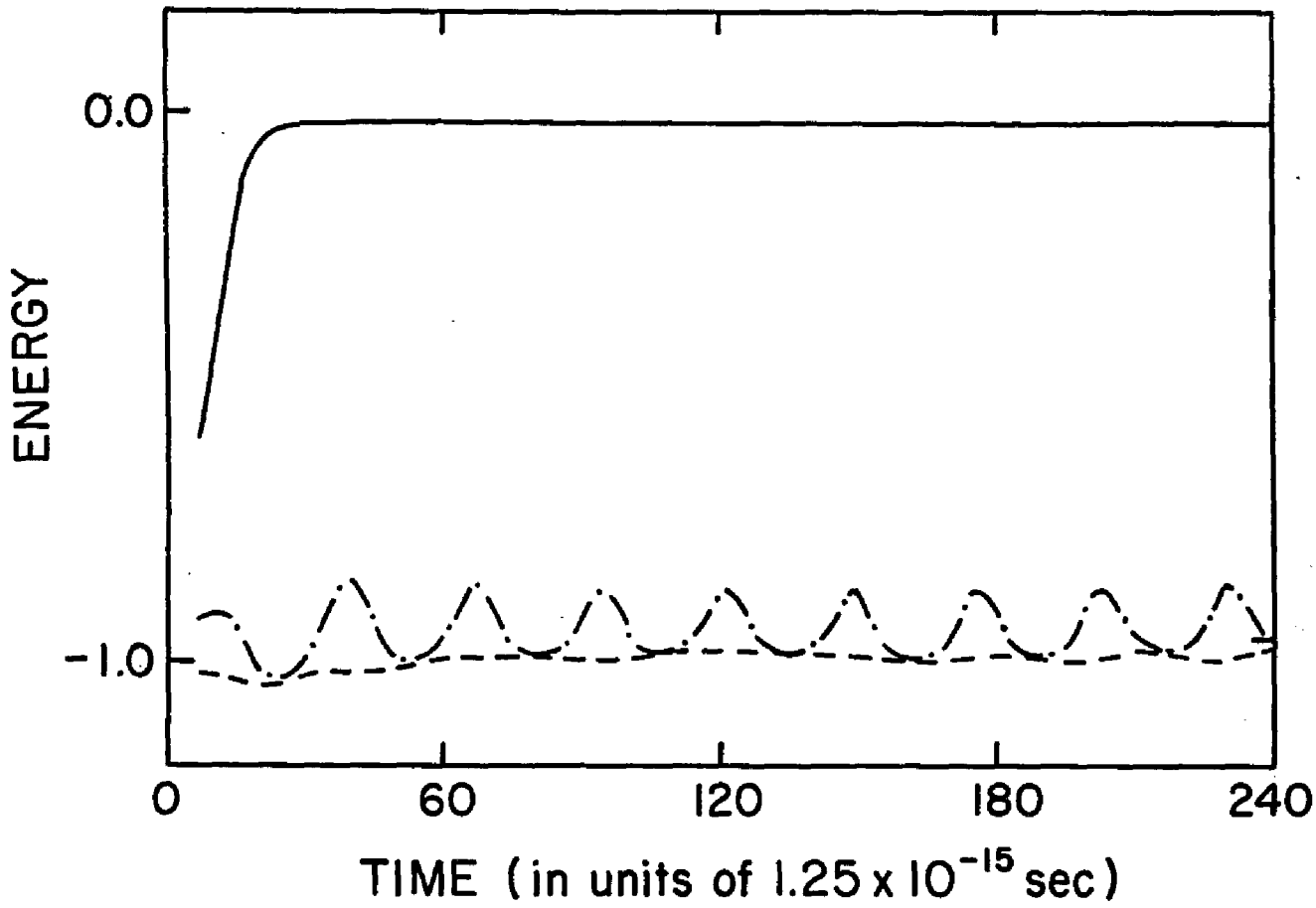

Fig. 24

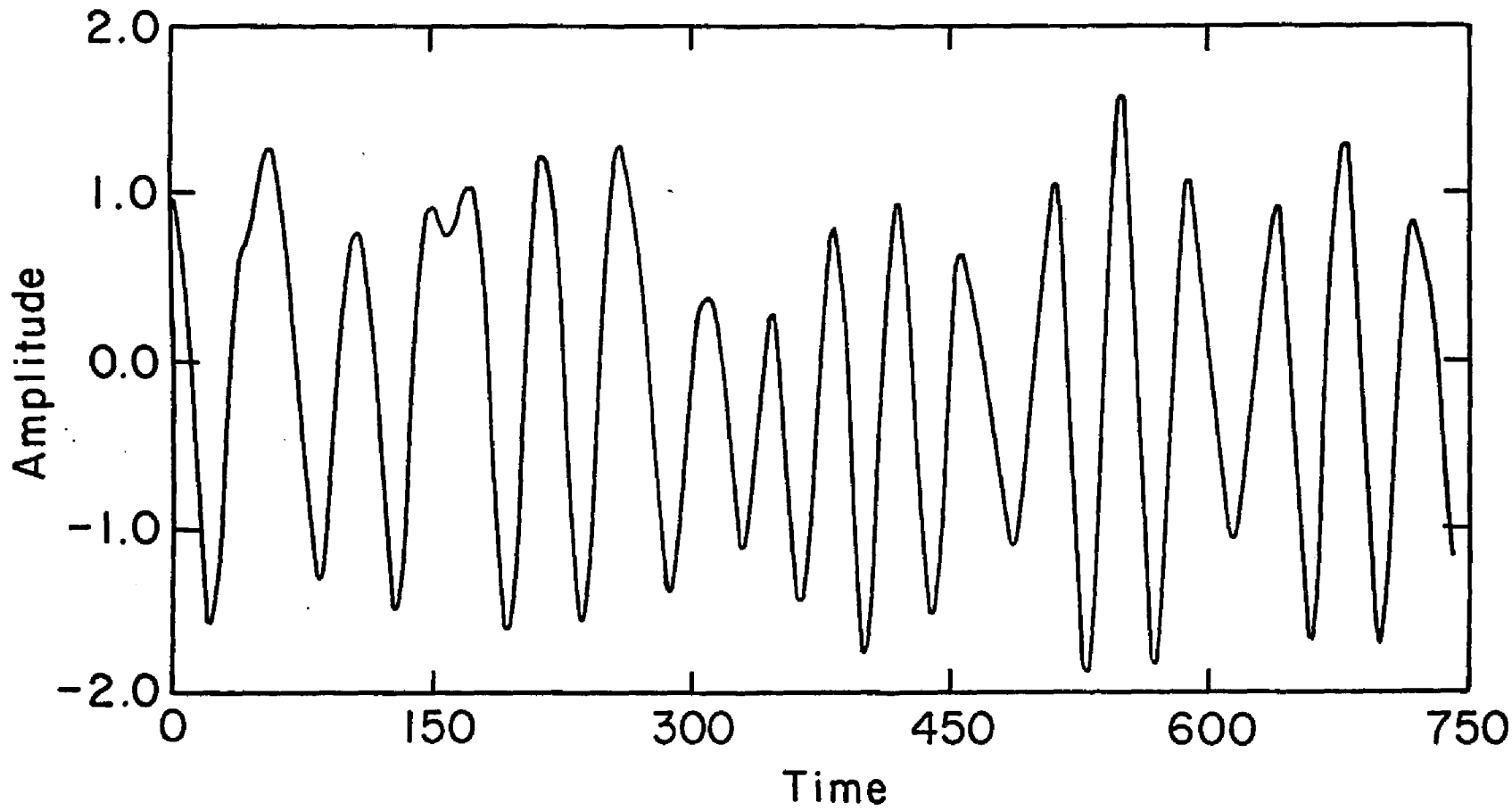

Fig. 25

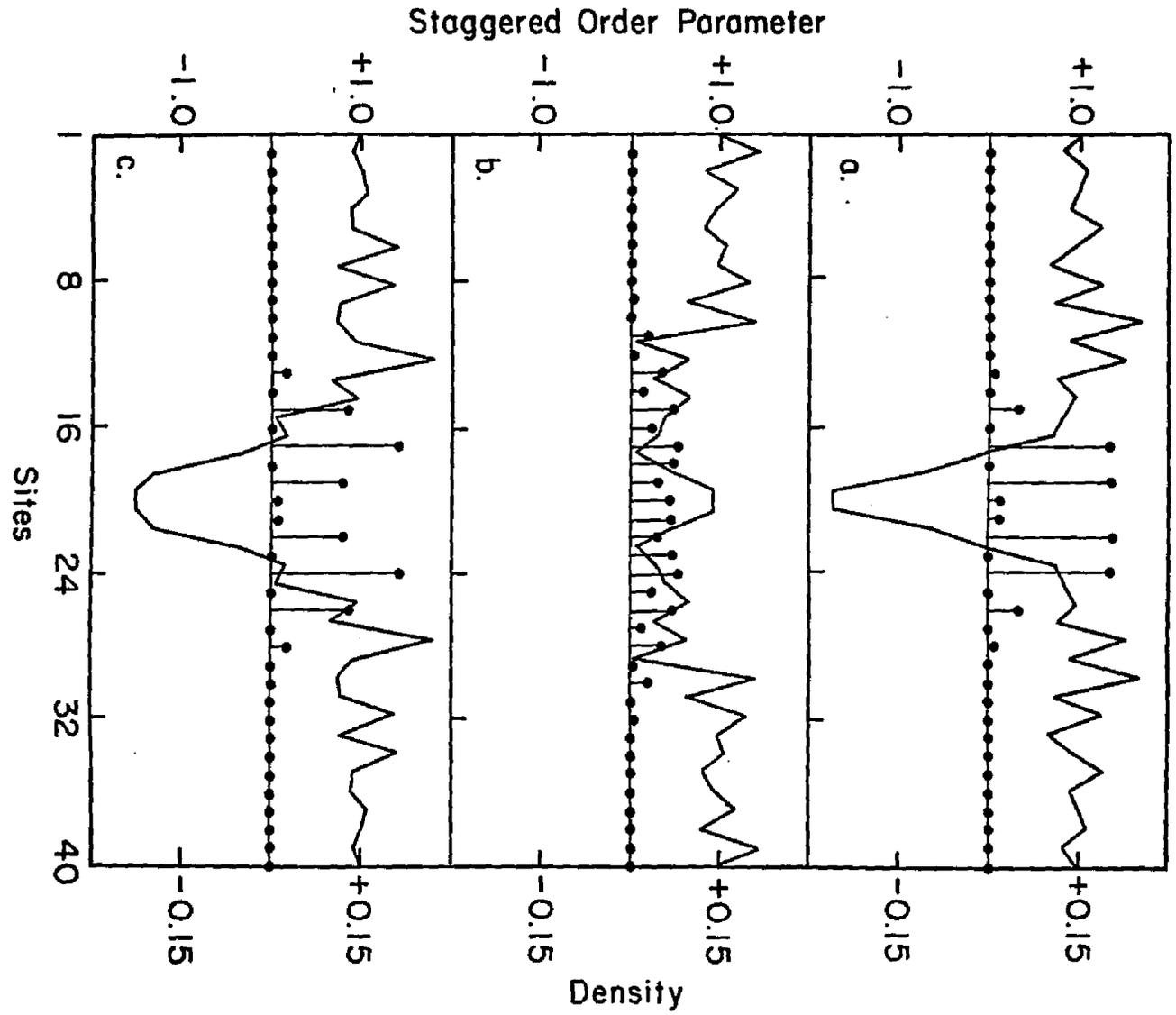
Staggered Order Parameter
+1.0
-1.0
a.
b.
c.
Sites
1
8
16
24
32
40
-0.15
+0.15
Density

Fig. 26

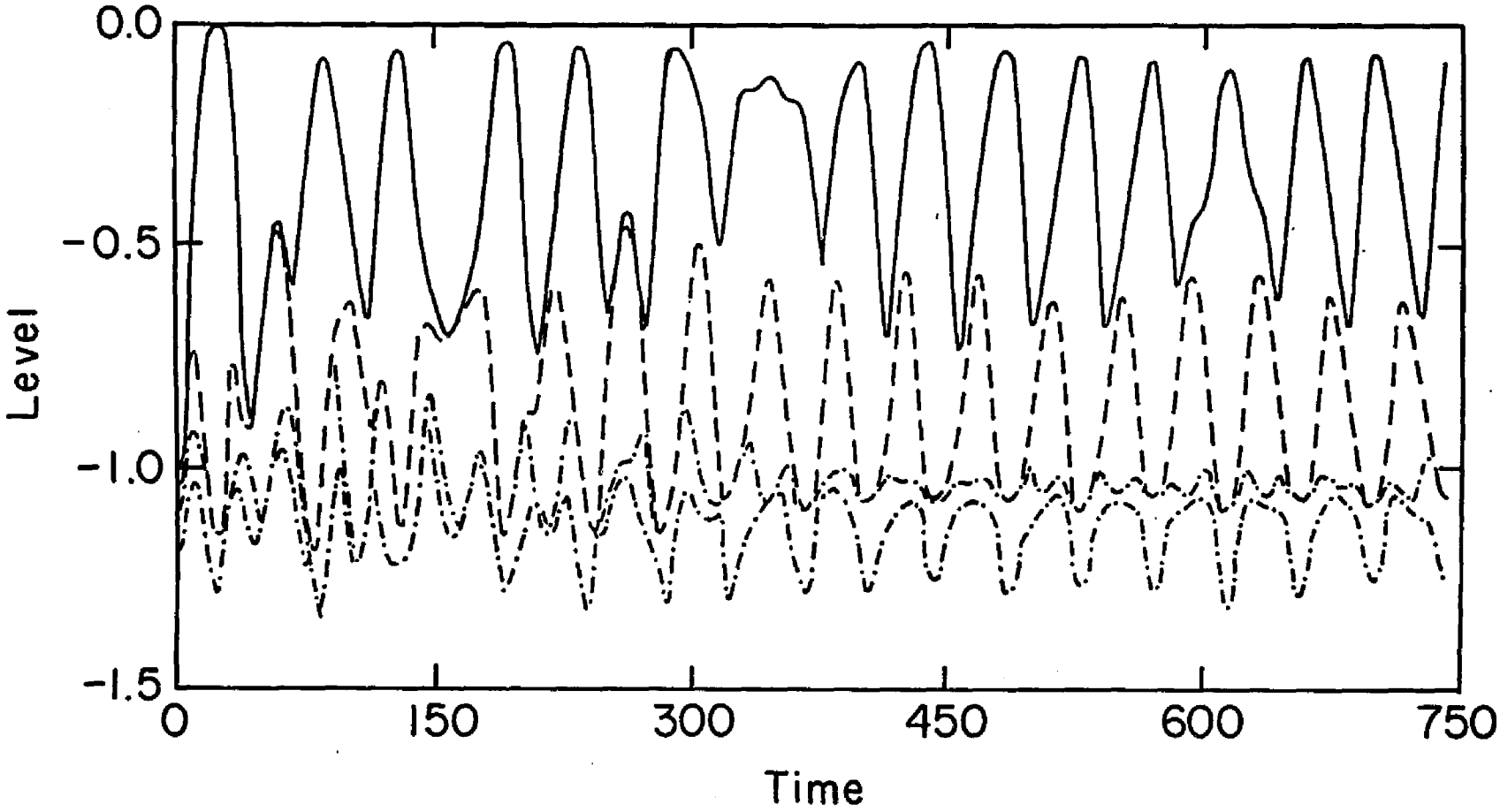

Fig. 27

References

[1] C. K. Chiang, C. R. Fincher, Jr., Y. W. Park, A. J. Heeger, H. Shirakawa, E. J. Louis, S. C. Gau, and A. G. MacDiarmid, *Phys. Rev. Lett.*, **39**, 1098(1977).

[2] J. A. Pople and S. H. Walmsley, *Mol. Phys.* 5 15(1962).

[3] B. R. Weinberger, J. Kaufer, A. J. Heeger, A. Pron, and A. G. Macdiarmid, *Phys. Rev. B*, **20**, 223(1979).

[4] J. C. Scott, H. J. Pedersen, and K. Bechgaard, *Phys. Rev. Lett.*, **45**, 2125(1980).

[5] P. J. Nigrey, A. G. MacDiarmid, and A. J. Heeger, *J. C. S. Chem. Comm.*, 594(1979).

[6] B. R. Weinberger, S. C. Gau, and Z. Kiss, *Appl. Phys. Lett.*, **38**, 555(1981).

[7] A. J. Heeger and A. G. MacDiamid ol. Cryst. Liq. Cryst. **77**, 1 (1981).

[8] W. P. Su, J. R. Schrieffer, and A. J. Heeger, *Phys. Rev. Lett.* **42**, 1698 (1979); *Phys. Rev. B* **22**, 2099 (1980); **28**, 1138(E) (1983).

[9] A. Kotani, *J. Phys. Soc. Jpn.* **42**, 408(1977); **42**, 416(1977).

[10] M. J. Rice, *Phys. Rev. Lett.* **51**, 142(1983).

[11] S. A. Brazovskii *Pis'ma Zh. Eksp. Teor. Fiz.* 28,606(1978) [*JETP Lett.* 28,606(1978)]; *JETP* **51**, 342(1980).

[12] H. Takayama, Y. R. Lin-Liu, and K. Maki, *Phys. Rev. B* **21**, 2388(1980).

[13] G. B. Blanchet, C. R. Fincher, T. C. Chung, and A. J. Heeger, *Phys. Rev. Lett.* **50**, 1938(1983).

[14] B. R. Weinberger, *Phys. Rev. Lett.* **50**, 1693(1983).

[15] G. B. Blanchet, C. R. Fincher, and A. J. Heeger, *Phys. Rev. Lett.* **51**, 2132(1983).

[16] L. Lauchlan, S. Etemad, T.-C. Chung, A. J. Heeger and A. G. MacDiarmid, *Phys. Rev. B*, 24, 3701(1981).

[17] C. L. Wang, Z. B. Su, and F. Martino, *Phys. Rev. B* **33**, 1512(1986).

[18] C. L. Wang, and F. Martino, *Phys. Rev. B*, **34**, 5540 (1986).

[19] C. R. Fincher Jr., M. Ozaki, M. Tanaka, D. Peebles, L. Lauchlan, and A. J. Heeger, *Phys. Rev. B*, **20**, 1589 (1979).

[20] T. Ito, H. Shirakawa, and S. Iketa, *J. Polym. Sci., Polym. Chem. Ed.* **12**, 11 (1974).

[21] J. Scott-Russell "*Report on waves*", *Proc. Roy. Soc. Edinburgh*, 319 (1844).

[22] C. A. Wingate, *S.I.A.M. J. Appl. Math.* **43**, 120 (1983).

[23] A. C. Scott, P. Y. F. Chu, D. W. McLaughlin, *Proc. I.E.E.E.* **61**, 1443 (1973).

[24] Z. Vardeny, E. Ehrenfreund, O. Brafman, M. Nowak, H. Schaffer, A. J. Heeger, and F. Wudl, *Phys. Rev. Lett.*, **56**, 671 (1986).

[25] A. J. Heeger, *Polymer J.* **17**, 201 (1985).

[26] R. L. Greene, and G. B. Street, *Science*, 226,651 (1984).

[27] J. D. Flood, E. Ehrenfreund, A. J. Heeger and A. G. MacDiarmid, *Solid State Commun.* **44**, 1055(1982).

[28] R. Ball, W. P. Su and J. R. Schrieffer, *J. Phys. (Paris) Colloq.* **44**, c3-429(1983).

[29] Z. B. Su and Lu Yu, *Phys. Rev. B* 27, 5199(1983).

[30] A. J. Heeger, *Comments on Solid State Physics*, **10**, 53(1981).

[31] S. Brazovskii, N. Kirova, and V. Yakovenko, *Solid State Commun.*, 55,187(1985).

[32] B. Horovitz, *Solid State Comm.* **41**, 729 (1982).

[33] S. Kivelson "*Soliton Model of Polyacetylene*", (preprint).

[34] S. A. Brazovskii and I. E. Dzyaloshinskii, *Zh. Eksp. Teor. Fiz.* **71**, 2338(1976).

[35] C. R. Fincher, C. E. Chen, A. J. Heeger, A. G. MacDiarmid, and J. B. Hastings, *Phys. Rev. Lett.* **48**, 100 (1982).

[36] M. J. Rice and I. A. Howard, *Phys. Rev. B* 28, 6089(1983).

[37] S. Stafström and K. A. Chao, *Phys. Rev. B*, 29, 7010(1984).

[38] A. J. Heeger and J. R. Schrieffer, *Solid State Commun.* 48, 207(1983).

[39] J. R. Schrieffer, *Mol. Cryst. Liq. Cryst.* 77, 209(1981).

[40] W. P. Su and J. R. Schrieffer, *Phys. Rev. Lett.*,, 46, 738 (1981).

[41] S. Kivelson and J. R. Schrieffer, *Phys. Rev. B*,, 24, 6447 (1982).

[42] H. Thomman, L. R. Dalton, Y. Tomkiewicz, N. S. Shiren, and T. C. Clarke, *Phys. Rev. Lett.* 50, 533(1983).

[43] S. Kuroda and H. Shirakawa, *Solid State Commun.* 43, 591(1982).

[44] K. R. Subbaswamy and M. Grabowski, *Phys. Rev. B* 24, 2168(1981).

[45] S. Kivelson and D. E. Heim, *Phys. Rev. B*, 26, 4278 (1982).

[46] P. Horsch, *Phys. Rev. B*, 24, 7351(1981).

[47] J. E. Hirsch, *Phys. Rev. Lett.*, 51, 296(1983).

[48] D. K. Campbell, T. A. DeGrand, and S. Masumdar, *Phys. Rev. Lett.*, 52, 1717(1984).

[49] J. Orenstein and G. L. Baker, *Phys. Rev. Lett.* 49, 1043(1982).

[50] A. J. Heeger, G. B. Blanchet, T. -C. Chung and C. R. Fincher, *Synthetic Metals*, 9,173(1984).

[51] M. Peo, S. Roth, K. Dransfeld, B. Tieeke, J. Hocker, H. Gross, A. Grupp and H. Sixl, *Solid State Commun.*, 35, 119(1980).

[52] J. C. Scott, P. Pfluger, M. T. Krounbi and G. B. Street, *Phys. Rev. B*, 28, 2140 (1983).

[53] After our paper[17] was published, we received a preprint from Dr. S. Kivelson. In that paper he also proposed a similar model to describe the non-degenerate ground state system(see Ref. 31).

[54] P. G. de Gennes, "*Superconductivity of Metals and Alloys*" (Benjamin, New York, 1966).

[55] J. M. Luttinger, *J. of Math. Phys.* 4, 1154 (1963).

[56] S. Kivelson, T. K. Lee, Y. R. Lin-Liu, I. Peschel and L. Yu *Phys. Rev. B* 25 4173(1982).

[57] S. A. Brazovskii and N. N. Kirova *Pis'ma Zh. Eksp. Teor. Fiz.* 33,6(1981) [JETP Lett. 33,5(1981)].

[58] K. Fesser, A. R. Bishop and D. K. Campbell *Phys. Rev. B* 27,4804(1983).

[59] Y. Onodera *Phys. Rev. B* 30, 775 (1984).

[60] D. K. Campbell and A. R. Bishop, *Nucl. Phys.* 200, 297(1982); *Phys. Rev. B* 24, 4859(1981).

[61] R. F. Dashen, B. Hasslacher, and A. Neveu, *Phys. Rev. D* 12, 2443 (1975).

[62] Y. Kato, *Progr. Theor. Phys. Suppl.* 55, 247 (1974).

[63] T.-C. Chung, J. H. Kaufman, A. J. Heeger and F. Wudl, *Phys. Rev. B* 30, 702 (1984).

[64] S. Etemad, A. J. Heeger, L. Lauchlan, T.-C. Chung, A. G. MacDiarmid *Mol. Cryst. & Liq. Cryst.* 77, 43 (1981).

[65] Y. Onodera and S. Okuno *J. Phys. Soc. Jpn.* 52, 2478 (1983).

[66] A. J. Heeger and J. R. Schrieffer, *Solid State Commun.* 48, 207(1983).

[67] H. Thomman, L. R. Dalton, M. Grabowski, and T. C. Clarke, *Phys. Rev. B* 31, 3141(1985).

[68] J. E. Hirsch and M. Grabowski, *Phys. Rev. Lett.* 52, 1713(1984).

[69] M. Grabowski, D. Hone and J. R. Schrieffer, *Phys. Rev. B* 31, 7850(1985).

[70] J. Orenstein, Z. Vardeny, G. L. Baker, G. Eagle, and S. Etemad, *Phys. Rev. B* 30, 786 (1984).

[71] W. P. Su and J. R. Schrieffer, *Proc. Natl. Acad. Sci. USA* 77, 5626 (1980).

[72] E. J. Mele, *Phys. Rev. B* **26**, 6901(1982).

[73] F. Guinea, *Phys. Rev. B* **30**, 1884(1984).

[74] A. R. Bishop, D. K. Campbell, P. S. Lomdahl, B. Horovitz, and S. R. Phillpot, *Phys. Rev. Lett.* **52**, 671(1984).

[75] Z. B. Su and Lu Yu, *Phys. Rev. B* **27**, 5199(1983).

[76] P. S. Lomdahl, O. H. Olsen and M. R. Samuelsen *Phys. Rev. A* **29**, 350(1984).

[77] L. Falicov and F. Yudurain, *J. Phys. C*, **8**, 147(1975).

[78] M. Nakahara and K. Maki, *Phys. Rev. B*, **25**, 7789(1982).

[79] J. P. Sethna and S. Kivelson, *Phys. Rev. B* **26**, 3513(1982).

[80] W. E. Milne, *Amer. Math. Month*, **40**, 322(1933).

[81] C. V. Shank, R. Yen, R. L. Fork, J. Orenstein, and G. L. Baker, *Phys. Rev. Lett.* **49**, 1660(1982).

[82] M. J. Rice, *Phys. Lett.* **71A**, 152 (1979).

[83] A. J. Heeger, G. B. Blanchet, T.-C. Chung and C. R. Fincher, *Synthetic Metals*, 9,173(1984).

[84] J. H. Kaufman, N. Colaneri, J. C. Scott and G. B. Street, *Phys. Rev. Lett*, **53**, 1005(1984).

[85] C. R. Fincher Jr., M. Ozaki, A. J. Heeger, and A. G. MacDiarmid, *Phys. Rev. B* **19**, 4140 (1979).

[86] T. Tanaka, *et, al Mol. Cryst. & Liq. Cryst.* **83**, 75 (1982).

[87] Z. Vardeny, J. Orenstein, and G. Baker, *Phys. Rev. Lett.* **50**, 2032 (1983).

[88] B. Horovitz, Z. Vardeny, E. Ehrenfreund, and O. Brafman, *Synth. Met.* **9**, 215 (1984).

[89] E. J. Mele, and J. C. Hicks, *Synth. Met.* **13**, 149 (1986).

[90] M. Nakahara, and K. Maki, *Phys. Rev. B* **25**, 7789 (1982).

[92] C. R. Fincher, C. E. Chen, A. J. Heeger, A. G. MacDiarmid, and J. B. Hastings, *Phys. Rev. Lett.* **48**, 100 (1982).

[91] D. Moses, A. Feldblum, E. Ehrenfreund, A. J. Heeger, T.-C. Chung, and A. G. MacDiarmid, *Phys. Rev. B* **26**, 3361 (1982).

[93] D. Baeriswyl, and K. Maki, *Phys. Rev. B* **28**, 2068 (1983).

[94] S. Kivelson, *Phys. Rev. B* **26**, 7093 (1982).

[95] S. Jeyadev, *Phys. Rev. B* **28**, 3447 (1983).

[96] R. R. Chance *et. al.* in "*Quantum chemistry of Polymers: Solid State Aspects.*" ed. by J. Ladik, and J. Andre (1984).

[97] S. Barisic *J. Physique* **44**, 185 (1983).

[98] W. K. Wu, and S. Kivelson, (preprint) "*Theory of Conducting Polymers with weak Electron Electron Interaction*".

[99] J. Solyom, *Adv. in Phys.* **28**, 201 (1979).

[100] I. Bozoric, (peprint), "*Polyacetylene: Helices, Heavy Solitons, and Hyperconductivity*".

[101] A. J. Heeger, G. Blanchet, T.-C. Chung, and C. R. Fincher, *Synth. Met.* 9, 173 (1984).